Quantum Chemical Studies of Iron Carbonyl Complexes
- Structure and Properties of $(CO)_4FeL$ Complexes -

Yu Chen

Marburg/Lahn 2000

Quantum Chemical Studies of Iron Carbonyl Complexes
- Structure and Properties of $(CO)_4FeL$ Complexes -

DISSERTATION
zur
Erlangung des Doktorgrades
der Naturwissenschaften
(Dr. rer. nat.)

dem
Fachbereich Chemie
der Philipps-Universität Marburg
vorgelegt von

Yu Chen

aus Liaoning/China

Marburg/Lahn 2000

Vom Fachbereich Chemie der Philipps-Universität Marburg als Dissertation angenommen am: 16.11.2000
Tag der mündlichen Prüfung: 29.11.2000
Erstgutachter: Prof. Dr. G. Frenking
Zweitgutachter: Prof. Dr. W. Petz

Vorwort

Die vorliegende Arbeit wurde am Fachbereich Chemie der Philipps-Universität Marburg/Lahn unter der Leitung von Herrn Prof. Dr. G. Frenking in der Zeit von Oktober 1996 bis Mai 2000 angefertigt.

Herrn Prof. Dr. G. Frenking danke ich sehr herzlich für die interessante Themenstellung, die geduldige Betreuung, anregende Diskussionen und wertvolle, ideenreiche Ratschläge sowie für hervorragende Arbeitsbedingungen.

Meinen Kollegen des AK Prof. Dr. G. Frenking möchte ich für das sehr gute Arbeitsklima und stete Hilfsbereitschaft danken. Besonderer Dank gebührt Dr. Michael Diedenhofen, dessen Hilfe am Anfang meines Aufenthaltes in Marburg für mich sehr wichtig war, Nicolaus Fröhlich für eine Vielzahl technischer Hilfen und natürlich auch für seine „10 Zwerge“. Dr. Michael Hartmann und Dr. Thomas Wagener sind dafür zu danken, sich Mühe gegeben zu haben, die Arbeit zu lesen und zu korrigieren.

Mein Dank gilt allen Mitarbeitern der Hochschulrechenzentren der Philipps-Universität Marburg, der Technischen Universität Darmstadt, der Justus-Liebig-Universität Gießen, der Universität Frankfurt, der Universität Kassel, und der Universität Stuttgart.

Für die finanzielle Unterstützung bedanke ich mich bei der Deutschen Forschungsgemeinschaft (DFG).

Schließlich danke ich meiner Ehefrau Shuhua Yan und meiner Tochter für ihre liebe Unterstützung.

Die Ergebnisse dieser Arbeit wurden bereits teilweise veröffentlicht:

(1) Chen, Y.; Petz, W.; Frenking, G. *Organometallics*, **2000**, *19*, 2698

(2) Chen, Y.; Hartmann, M.; Frenking, G. *Eur. J. Inorg. Chem.*, in press

(3) Chen, Y.; Hartmann, M.; Frenking, G. *submitted for publication*

Quantum Chemical Studies of Iron Carbonyl Complexes

- Structure and Properties of $(CO)_4FeL$ Complexes -

Table of Contents

Chapter 1. Introduction

Iron carbonyl compounds continue to be an extensively examined area of organometallic chemistry, because the simple carbonyl compounds are both inexpensive and versatile reagents.[1] It is well established[2] that the chemistry of main group organometallics is governed by the group the metal belongs to, whereas for organotransition metal compounds the nature of the ligand dominates. In this work, a thorough investigation of iron complexes with various ligands coordinated to the complex-fragment $Fe(CO)_4$ is presented, in order to enrich the understanding of iron carbonyl complexes in many different aspects.

As a starting point, the geometries, frequencies, and Fe-L bond dissociation energies of iron-carbonyl complexes are calculated at a gradient corrected DFT level and improved energies calculations are obtained using the CCSD(T) of single–point calculations. Based on the fully optimized geometries and other data, several selected topics are carefully discussed in their respective chapter of this thesis.

In trigonal bipyramidal carbonyl complexes containing a d^8-metal, two positions of a selected ligand L, namely the axial and equatorial coordinate sites, are in principle possible. This ligand site preference of $Fe(CO)_4L$ complexes is the first topic discussed in this work. After briefly introducing the computational background, the relative strengths of σ-donation and π-backdonation of different ligands that governs the ligand's favor coordination site are discussed, on the basis of NBO analysis and the CDA partitioning scheme.

Besides, the bonding situation of a full series of metal-carbon bonds TM-CR_2, TM-CR, and TM-C has been examined with the NBO partitioning scheme and the AIM topological analysis of the electron density. This gives us a deeper insight of the bonding situation in TM carbene, carbyne, and carbon complexes, having donor-acceptor bonds in contrast to their respective shared-electron isomers.

The following section of this thesis is devoted to the N_2-fixation process. Nitrogen fixation has been an attractive and challenging topics in the past decades. The

activation processes of dinitrogen and the stepwise hydrogenation are examined from both structural and energetical viewpoints.

^{13}C and ^{19}F NMR chemical shifts of fluorine substituted iron tetracarbonyl complexes and related compounds are calculated at the DFT-GIAO level, in order to provide a useful help for the characterization of the $(CO)_4FeCF_2$ complex.

Finally, a short summary was given in Chapter 7.

The complexes presented in this thesis are numbered independently in each chapter. The Cartesian coordinates of all iron complexes and selected free ligand molecules are given in Appendix.

Chapter 2. The Theoretical Background

The aim of *ab initio* molecular orbital theory[3] is to predict the properties of atoms and molecules. It is based on the fundamental laws of quantum mechanics using a variety of mathematical transformations and approximation-techniques to solve the equations that build up this theory. In order to gain the best efficiency/cost ratio at a suitable level of theory and to comment and interpret the results from such calculations, reviewing the historical background is essential.

2.1 Molecular Energy

2.1.1 The Schrödinger Equation

In quantum mechanics, the state of a system is fully described by the wave function $\Phi(r,t)$, where r are spatial coordinates of the particles that constitute the system and t is the time. The product of Φ with its complex conjugate is defined as the probability distribution of the particle, i.e. the probability of finding a particle in its volume element dr around its point r at the time t. The dynamical evolution of the wave function with time is described by the time-dependent Schrödinger equation[4]

$$i\hbar \frac{\partial \Phi(r,t)}{\partial t} = \hat{H}\,\Phi(r,t) = E\Phi(r,t) \tag{2.1}$$

where $\hat{H}$ is the Hamiltonian operator for the system, corresponding to the total energy.

In most cases, time-dependent interaction of atoms and molecules can be neglected. The Schrödinger equation is thus separated into equations for time and space variation of the wave function using the variable separation $\Phi(r,t) = \Phi(r)\Phi(t)$. The time-independent Schrödinger equation is therefore given as:

$$\hat{H}\,\Phi(r) = E\Phi(r) \tag{2.2}$$

where

$$\hat{H} = -\sum_{i=1}^{N} \frac{1}{2} \nabla_i^2 - \sum_{A=1}^{M} \frac{1}{2M_A} \nabla_A^2 - \sum_{i}^{N} \sum_{A}^{M} \frac{Z_A}{r_{iA}} + \sum_{i}^{N} \sum_{j>i}^{N} \frac{1}{r_{ij}} + \sum_{A=1}^{M} \sum_{B>A}^{M} \frac{Z_A Z_B}{R_{AB}} \tag{2.3}$$

Here i and j are indices of electrons whereas A and B are indices of atomic nuclei. M_A is the ratio of the mass of nucleus A to an electron, and Z_A is the atomic number of nucleus A. The distance between the ith and the jth electron is r_{ij}; the distance between the Ath nucleus and the Bth nucleus is R_{AB}; r_{iA} specifies the distance between electron i and nucleus A. The first and second terms in Eq. 2.3 are the kinetic energy operators of the electrons and the nuclei, respectively. The third term is the electron-nucleus attraction energy operator, whereas the fourth and fifth terms represent the repulsion energy operator of the electron-electron and the nucleus-nucleus repulsion, respectively.

Note that $\hat{H}\Phi(r) = E\Phi(r)$ is a non-relativistic description of the system which is not valid when the velocities of particles approach the speed of light. The mass of a moving particle m increases with its velocity v according to

$$m = m_0 \left[1 - (v/c)^2\right]^{-1/2} \tag{2.4}$$

where m_0 and c are the rest mass and the speed of light, respectively. Thus, time-independent Schrödinger equation does not give an accurate description of the core electrons in large nuclei. Relativistic effect must be considered for the heaviest elements of the periodic table, but is neglected throughout this thesis since only Fe-carbonyl complexes are considered.

Because of the large difference between the mass of the electrons and that of the nuclei, the electrons can respond almost instantaneously to a displacement of the nuclei. Therefore it is reasonable to regard the nuclei as fixed and to solve the Schrödinger equation only for the electrons in the static electronic potential arising from these nuclei. This, the so-called Born-Oppenheimer approximation[5], is very reliable for electronic ground states. The set of solutions obtained in different arrangements of nuclei is used to construct the potential energy surface (PES) of a polyatomic species.

For an isolated N-electron atomic or molecular system within the Born-Oppenheimer, nonrelativistic approximation, the electronic Schödinger equation is given by

$$\hat{H}_{elec}\Phi_{elec} = E_{elec}\Phi_{elec} \tag{2.5}$$

where $E_{elec} = E_{elec}(\{R_A\})$ is the electronic energy, $\Phi_{elec} = \Phi_{elec}(\{r_i\};\{R_A\})$ is the wave function which describes the motion of the electrons and *explicitly* depends on the electronic coordinates but depends *parametrically* on the nuclear coordinates, as does the electronic energy. $\hat{H}_{elec}$ is the electronic Hamiltonian operator:

$$\hat{H}_{elec} = -\sum_{i=1}^{N}\frac{1}{2}\nabla_i^2 - \sum_{i}^{N}\sum_{A}^{M}\frac{Z_A}{r_{iA}} + \sum_{i}^{N}\sum_{j>i}^{N}\frac{1}{r_{ij}} \tag{2.6}$$

The total energy E_{tot} is the electronic energy E_{elec} including the nucleus repulsion energy according to

$$E_{tot} = E_{elec} + \sum_{A=1}^{M}\sum_{B>A}^{M}\frac{Z_A Z_B}{R_{AB}} \tag{2.7}$$

2.1.2 The Hartree-Fock Approximation[6]

Because electrons are ferminons, Φ also must be antisymmetric with respect to the interchange of the coordinates (both space and spin) of any two electrons. That is:

$$\Phi(x_1,\ldots,x_i,\ldots x_j,\ldots x_N) = -\Phi(x_1,\ldots,x_j,\ldots x_i,\ldots x_N) \tag{2.8}$$

This requirement is a general statement of the familiar Pauli exclusion principle[7] introducing the concept of spin orbitals. A spin orbital χ_i is a product of a spatial orbital wave function ψ and a spin function. For different spins, α and β are used to refer s = 1/2 and –1/2, respectively. Suppose now that Ψ is approximated as an

antisymmetrized product of orthonormal spin orbitals χ_i, the Slater[8] determinant for a system has the following form:

$$\Psi(x_1, x_2, ..., x_N) = \frac{1}{\sqrt{N!}} \begin{vmatrix} \chi_i(x_1) & \chi_j(x_1) & ... & \chi_k(x_1) \\ \chi_i(x_2) & \chi_j(x_2) & ... & \chi_k(x_2) \\ . & . & & . \\ . & . & & . \\ . & . & & . \\ \chi_i(x_N) & \chi_j(x_N) & ... & \chi_k(x_N) \end{vmatrix} \tag{2.9}$$

with the diagonal elements written as:

$$\Psi(x_1, x_2, ..., x_N) = \left| \chi_i(x_1)\chi_j(x_2)...\chi_k(x_N) \right\rangle \tag{2.10}$$

On the basis of the variation theory,[9] the lowest value of E is indicated as E_0 identified as the electronic energy for the selected nuclear configuration.

$$E_0 = \frac{< \Psi_0 \mid \hat{H} \mid \Psi_0 >}{< \Psi_0 \mid \Psi_0 >} \qquad \text{where} \qquad \Psi_0 = \mid \chi_1, \chi_2, ..., \chi_N > \tag{2.11}$$

On the one hand, each spin orbital must be obtained by solving an equation including the Fock operator $\hat{f}$, e.g. for coordinate 1

$$\hat{f}_i(1) \;\; \chi_i(1) = \varepsilon_i \;\; \chi_i(1) \tag{2.12}$$

where the Fock operator is the sum of the one-electron operator $\hat{h}_{core}$ and the two-electron operators $\hat{J}_j$, $\hat{K}_j$.

$$\hat{f}(1) = \hat{h}_{core}(1) + \sum_j 2\hat{J}_j(1) - \hat{K}_j(1) \tag{2.12a}$$

On the other hand, however, this operator depends on the spin orbitals of all other N-1 electrons, because $\upsilon^{HF}(i)$ is the average potential experienced by the *i*th electron due to

the presence of the other electrons, which is constituted by the Coulomb operator $\hat{J}_j(1)$ and the non-classical exchange operator $\hat{K}_j(1)$.

$$\hat{J}_j(1) = \int |\chi_j(2)|^2 \frac{1}{r_{12}} dx_2 \tag{2.12b}$$

$$\hat{K}_j(1) = \int \chi_j^*(2) P_{12} \chi_j(2) \frac{1}{r_{12}} dx_2 \tag{2.12c}$$

It appears that to set up the HF equations, one must already know the solution beforehand. It is therefore necessary to adopt an iterative process to solve these equations. By using a self-consistent procedure, a trial set of spin orbitals is formulated and used to formulate the Fock operator, then the HF equation are solved to obtain a new set of spin orbitals which are then used to build up a refined Fock operator. These cycles are repeated until the chosen convergence criteria are satisfied.

The HF equations might be solved numerically according to the suggestion of Roothaan and Hall.[10] A set of known spatial basis functions (for example, atomic orbital basis functions) is introduced and the unknown molecular orbitals are expanded in the linear expansion.

$$\psi_i = \sum_{\mu}^{K} C_{i\mu} \phi_\mu \tag{2.13}$$

If the set of ϕ_μ is complete, the expansion would be exact. The problem of calculating the HF molecular orbitals is then reduced to the problem of calculating a set of expansion coefficients. Substituting Eq. 2.13 into the HF equation 2.12 therefore gives

$$\mathbf{FC} = \mathbf{SC}\boldsymbol{\varepsilon} \tag{2.14}$$

where **F**, **S**, **C**, and **ε** are Fock matrix, overlap matrix, square matrix of the expansion coefficients, and the diagonal matrix of the orbital energies ε_i, respectively. An explicit expression for the Fock matrix element is

$$F_{\mu\nu} = H_{\mu\nu}^{core} + \sum_{\lambda\sigma} \rho_{\lambda\sigma} \left[(\mu\nu \mid \sigma\lambda) - \frac{1}{2} (\mu\lambda \mid \sigma\nu) \right] \tag{2.14a}$$

and depends on the elements of the core-Hamiltonian matrix H, the density matrix ρ, and the two-electron integrals.

In SCF calculations it is common to use restricted HF (RHF) wave functions in which the spatial components of the spin orbitals are identical for each member of a pair of electrons. For open-shell states of atoms and molecule two procedures are used instead. One is the restricted open shell HF (ROHF) approch, in which all the electrons except those that occupy open-shell orbitals are forced to occupy the same spatial orbitals. Another method considers unrestricted open-shell HF (UHF) wavefunction, where the constraint of pairwise occupied orbitals is relaxed. Generally, a lower variational energy is predicted for UHF than for RHF. However, one disadvantage of the UHF approach is that such a function is not an eigenfunction of S^2.

2.1.3 Electron Correlation Methods

The motion of the electrons is correlated since the wave function must be antisymmetric with respect to the interchange of any two electrons. The difference between the exact nonrelativistic energy and the Hartree-Fock energy in a given basis set is called the electron correlation energy. Electron correlation based on electron with opposite spin is sometimes called Coulomb correlation, while electron correlation based on the repulsion of electron having the same spin is called Fermi correlation.

The HF method determines the best one-determinant wave function in a given basis set. It is therefore obvious that in order to improve on HF results, the starting point must be a trial wave function which contain more than one Slater-Determinant.

$$|\Phi\rangle = c_0 |\Psi_0\rangle + \sum_{ra} c_a^r |\Psi_a^r\rangle + \sum_{\substack{a<b \\ r<s}} c_{ab}^{rs} |\Psi_{ab}^{rs}\rangle + \sum_{\substack{a<b<c \\ r<s<t}} c_{abc}^{rst} |\Psi_{abc}^{rst}\rangle + \ldots \tag{2.15}$$

By replacing occupied MOs in the HF determinant by unoccupied MOs, a whole series of determinants may be generated. These can be denoted according to how many occupied HF-MOs have been replaced, thus leading to Slater determinants which are singly, doubly, triply, quadruply etc. excited relative to the HF determinant. These determinants are often referred to as Singles (S), Doubles (D), Triples (T), Quadruples (Q) with a maximum excitation of N electrons (N- multiple).

Limiting the number of determinants to only those which can be generated by exciting the valence electrons is known as the frozen core approximation. The contributions of the correlation from core electrons is a constant factor and drops out when calculating relative energies.

There are three main methods for calculating electron correlation: Configuration Interaction (CI), Many Body Perturbation Theory (MBPT) and Coupled Cluster (CC) Theory. The latter two methods are discussed separately in next two sections.

The trial wave functions for CI approach is written as a linear combination of determinants with the expansion coefficients determined under the requirement that the energy should be a minimum (or at least stationary). The MOs used for building the excited Slater determinants are taken from a HF calculation and are held fixed. Inclusion of all possible determinants yields the full CI wave function. This is the best possible wave function within the limitations of the chosen basis set. However, the number of determinants grows significantly with the size of the basis set, and it makes the full CI method infeasible for all but the very smallest systems.

As a systematic procedure for going beyond the HF approximation, Configuration Interaction (CI) has the important advantage that it is variational (i.e., at each it gives an upper bound to the exact energy), but it has the disadvantage that it is only size consistent when all possible excitations are incorporated into the trial function (i.e., full CI). All forms of truncated CI such as CISD are not size consistent.

2.1.3.1 Many-Body Perturbation Theory (MBPT)

A different systematic procedure for evaluating the correlation energy, which is not variational in the sense that it does not in general give energies that are upper bounds to the exact energy but is size consistent at each level, is perturbation theory (PT).

The application of PT to a system composed of many interacting particles is generally called many-body perturbation theory (MBPT). This perturbation method is based on a partitioning of the full Hamiltonian into two pieces,

$$\hat{H} = \hat{H}_0 + \lambda \hat{H}' \tag{2.16}$$

Because $\hat{H}'$ is a small perturbation to $\hat{H}_0$, the perturbed wave function and energy can be expressed as a power series in terms of the parameter λ

$$\begin{aligned} \Psi &= \Psi_0 + \lambda\Psi^{(1)} + \lambda^2\Psi^{(2)} + \ldots \\ E &= E_0 + \lambda E^{(1)} + \lambda^2 E^{(2)} + \ldots \end{aligned} \tag{2.17}$$

The perturbed wave functions and energies are substituted back into the Schrödinger equation. After expanding the products, the coefficients on each side of the equation for each power of λ can be calculated leading to a series of relations representing successively higher orders of perturbation.

To find the correlation energy for the ground state, the zero-order Hamiltonian from the Fork operators of the HF-SCF method is adopted according to the Møller-Plesset[11] perturbation theory (MPPT). $\hat{H}_0$ is defined as the sum of the one electron Fock operator,

$$\hat{H}_0 = \sum_i \hat{f}(i) \tag{2.18}$$

E_0 is the sum of the orbital energies ε_i

$$E_0 = \sum_i \varepsilon_i \tag{2.19}$$

A correction of the electron correlation energy is only achieved, if at least a 2nd order perturbation is considered. The inclusion of such a second-order energy correction is designated as MP2.

For $E^{(2)}$:

$$E^{(2)} = \sum_s \frac{|< \Psi^{(0)} \mid \hat{H}' \mid \Psi^{(0)} >|^2}{E_0 - E_s} \tag{2.20}$$

where

$$\begin{aligned} \hat{H}' = \hat{H} - \hat{H}_0 &= \sum_{i=1}^{N} \hat{h}(i) + \sum_{i=1}^{N} \sum_{j>i}^{N} r_{ij}^{-1} - \sum_{i=1}^{N} \hat{f}(i) \\ &= \sum_{i=1}^{N} \sum_{j>i}^{N} r_{ij}^{-1} - \sum_{i=1}^{N} \upsilon^{HF}(i) \end{aligned} \tag{2.21}$$

The last term is just the sum of the HF coulomb and exchange potentials. Because E_0 is the lowest energy eigenvalue of the unperturbed system the value of $E^{(2)}$ will always be negative. The explicit formula for MP2 is

$$E^{(2)} = \sum_{i<j}^{occ} \sum_{a<b}^{virt} \frac{[< \chi_i \chi_j \mid \chi_a \chi_b > - < \chi_i \chi_j \mid \chi_b \chi_a >]^2}{\varepsilon_i + \varepsilon_j - \varepsilon_a - \varepsilon_b} \tag{2.22}$$

The low cost compared to CI methods makes MP2 calculations to one of the most economical methods for including electron correlation. If MPPT is extended to include third- and fourth-order energy correction, the procedures are referred to as MP3 and MP4, and the algebra involved becomes more and more complicated.

2.1.3.2 Density Functional Theory (DFT)

Density function theory has its roots in the work of Thomas and Fermi in the 1920s.[12] It became a complete and accurate theory only due to the publications in the early 1960s of Hohenberg, Kohn, and Sham.[13,14] This theory allows one to replace the complicated N-electron wave function Ψ and the associated Schrödinger equation by much simpler electron density $\rho(r)$ and its associated calculational schemes. This is the reason that DFT has been growing in popularity over the past decade. Unfortunately, the form of the functional dependence of the energy on the density $E[\rho(r)]$ is not given by the Hohenberg-Kohn theorem[13], it is confirmed that such a functional exists.

Following the work of Kohn and Sham,[14] the approximate functionals employed by current DFT methods partition the electronic energy into several terms:

$$E = E_T + E_V + E_J + E_{XC} \tag{2.23}$$

where E_T is the kinetic energy term arising from the motion of the electrons. E_V includes terms describing the potential energy of the nuclear-electron attraction and of the repulsion between pairs of nuclei. E_J is the electron-electron repulsion term, also described as the coulomb self-interaction of the electron density, and E_{XC} is the exchange-correlation term and includes the remaining part of the electron-electron interactions, that is (1) the exchange energy arising from the antisymmetry of the quantum mechanical wave function, and (2) the dynamic correction of the motions of individual electrons. Note that all terms except the nuclear-nuclear repulsion are functionals of the electron density ρ.

E_{XC} is further divided into exchange and correlation functionals, corresponding to "same-spin" and "mixed-spin" interactions, respectively:

$$E_{XC}(\rho) = E_X(\rho) + E_C(\rho) \tag{2.24}$$

Both components on the right side of the equation can be of two distinct types: local functionals depend only on the electron density ρ, while gradient-corrected functionals depend on both ρ and its gradient, $\nabla\rho$.

The local exchange functionals (e.g. LDA) were developed to deduce the exchange energy of a uniform electron gas and thus has its shortcoming in describing molecular system. In 1988 Becke[15] therefore formulated the gradient-corrected exchange functional based on the LDA exchange functional. It succeeds in remedying many of the LDA functional's deficiencies. Similarly, local (e.g. Vosko, Wilk, and Nusair[16]) and gradient-corrected (Perdew[17]) correlation functionals exist and are widely used. Pure DFT methods are defined by pairing an exchange functional with a correlation functional. For example, BP86[15,17], BLYP[15,18] .

In practice, self-consistent Kohn-Sham DFT calculations are performed in an iterative manner analogous to the SCF procedure described for HF. The density may be approximately written in terms of a set of auxiliary one-electron functions, so-called Kohn-Sham orbitals, as

$$\rho(r) = \sum_{i}^{N} |\psi_i|^2 \tag{2.25}$$

The Kohn-Sham equations have the form

$$\hat{h}_{KS}\psi_i = \varepsilon_i\psi_i \tag{2.26}$$

where the operator

$$\hat{h}_{KS} = -\frac{1}{2}\nabla_1^2 - \sum_A \frac{Z_A}{r_{1A}} + \int \frac{\rho(2)}{r_{12}} dr_2 + v_{XC}(1) \tag{2.27}$$

is similar to the Fock operator in the HF-approach. The corresponding potential $v_{XC}(1)$ is given by a derivative of the energy E_{XC} with respect to the density ρ

$$v_{XC}(1) = \frac{\partial E_{XC}[\rho]}{\partial\rho(r)} \tag{2.28}$$

HF theory also includes an exchange term as part of its formulation. According to the Gaussian user's reference, a Becke[19]-style three-parameter functional (B3LYP) may be defined via the following expression:

$$E_{XC}^{B3LYP} = E_X^{LDA} + c_0(E_X^{HF} - E_X^{LDA}) + c_X E_X^{B88} + E_C^{VWN3} + c_C(E_C^{LYP} - E_C^{VWN3}) \quad (2.29)$$

Here the parameter c_0 allows any mixture of HF and LDA local exchange. In addition, Becke's gradient correction to the LDA exchange is also included, scaled by the parameter c_X. Similarly, the VWN3 local correction functional is used, and it may be optionally corrected by the LYP correlation correction via the parameter c_C. In the formulation of the B3LYP functional, the parameters were determined by fitting them to the atomization energies in the G1 molecule set, the values are: c_0=0.20, c_X=0.72 and c_C=0.81. Note, however, that LDA densities and PerdewWang91[20] correlation functional rather than VWN3[16] and LYP[18] are used in original paper[19].

E_{XC} can not be evaluated analytically for DFT methods, so it is computed via numerical integration. Thus, in order to perform the numerical integration a grid of points in space must be employed. A crucial point in comparing different DFT-result based on the same functional is the quality of the chosen integration grid. But for the whole system in this thesis, the quality of grids does not play an important role.

2.1.3.3 Coupled Cluster(CC) Theory

Perturbation methods add all types of excitations (S, D, T, Q etc.) to the reference wave function to a given order (2, 3, 4 etc.). The idea in Coupled Cluster (CC)[21] methods is to include all corrections of a given type to infinite order. The coupled cluster wave function is written as

$$\Psi_{CC} = e^{\hat{T}}\Psi_0 \quad (2.30)$$

$$e^{\hat{T}} = 1 + \hat{T} + \frac{1}{2}\hat{T}^2 + \frac{1}{6}\hat{T}^3 + \ldots = \sum_{k=0}^{\infty}\frac{1}{k!}\hat{T}^k \quad (2.31)$$

where the cluster operator T is given by

$$\hat{T} = \hat{T}_1 + \hat{T}_2 + \hat{T}_3 + \ldots + \hat{T}_N \quad (2.32)$$

The $\hat{T}_i$ operator acting on a HF reference wave function generates all i th excited Slater determinants.

$$\hat{T}_1 \Psi_0 = \sum_{i}^{occ} \sum_{a}^{vir} t_i^a \Psi_i^a \tag{2.33a}$$

$$\hat{T}_2 \Psi_0 = \sum_{i<j}^{occ} \sum_{a<b}^{vir} t_{ij}^{ab} \Psi_{ij}^{ab} \tag{2.33b}$$

The expansion coefficients t is called amplitudes.

From Eqs. (2.31) and (2.32) the exponential operator may be written as

$$e^{\hat{T}} = 1 + \hat{T}_1 + (\hat{T}_2 + \frac{1}{2}\hat{T}_1^2) + (\hat{T}_3 + \hat{T}_2\hat{T}_1 + \frac{1}{6}\hat{T}_1^3) + \ldots \tag{2.34}$$

The first term generates the reference HF and the second all singly excited states. The first term in parenthesis generates all doubly excited states. The second parenthesis generates all triply excited states.

Truncated coupled cluster methods are used due to the limitations of computational resources. Including only the $\hat{T}_1$ operator does not yield any improvement over HF, as matrix element between the HF and singly excited states are zero. The lowest level of approximation is therefore $\hat{T} = \hat{T}_2$, referred to as CCD. Using $\hat{T} = \hat{T}_1 + \hat{T}_2$ gives the CCSD model. The triples contribution may be evaluated by perturbation theory and added to the CCSD results thus resulting in a method abbreviated as CCSD(T).

If all cluster operators up to $\hat{T}_N$ are included in $\hat{T}$, all possible excited determinants are generated and the coupled cluster wave function is equivalent to full CI.

2.2 Basis set and Effective Core Potentials (ECPs)

Historically, quantum chemical calculations for atoms and molecules were performed as linear combination of atomic orbitals-molecular orbitals (LCAO-MO).

$$\psi_i = \sum_{\mu}^{n} c_{i\mu} \varphi_{i\mu} \tag{2.35}$$

where ψ_i is the i-th molecular orbital, $c_{i\mu}$ are the coefficients of linear combination, $\varphi_{i\mu}$ is the u-th atomic orbital, and n is the number of atomic orbitals.

Atomic orbitals (AO) are solutions of the HF equations for the atoms. This term may also be replaced by "basis functions". An example for such function are Slater Type Orbitals (STO's)[22], that were used due to their similarity to the atomic orbitals of the hydrogen atom. They are described by a function depending on spherical coordinates:

$$\varphi(\zeta, n, l, m; r, \theta, \phi) = N r^{n-1} e^{-\zeta r} Y_{lm}(\theta, \phi) \tag{2.36}$$

where N is a normalization constant, ζ is called "exponent", r, θ and ϕ are spherical coordinates, Y_{lm} is the angular momentum and n, l and m are the principal-, angular momentum-, and magnetic quantum numbers, respectively.

Unfortunately, functions of this kind are not suitable for a convenient and fast evaluation of the two-electron integrals. That is why the Gaussian type orbitals (GTO's)[23] were introduced. One can approximate the shape of the STO function by summing up a number of GTOs with different exponents and coefficients. The GTO is expressed as:

$$g(\alpha, n, l, m; x, y, z) = N x^l y^m z^n e^{-\alpha r^2} \tag{2.37}$$

where N is a normalization constant, α is the "exponent", x, y and z are cartesian coordinates and l, m and n are simply integral exponents in cartesian coordinates,

which are completely different from the same notations used in STO's due to $r^2 = x^2 + y^2 + z^2$.

For quantum chemical calculations, a linear combination of gaussian primitives is usually used as basis functions. Such functions will have their coefficients and exponents fixed. The contractions are sometimes called Contracted Gaussian Type Orbitals (CGTO). Obviously, the best results could be obtained if all coefficients in such gaussian expansions were allowed to vary during molecular calculations. However, the CPU time requirements are more acute.

The first gaussian contractions were obtained by a least square fit to Slater-type atomic orbitals. In the minimal basis set (i.e. SZ; the numbers of zeta ζ is $N_\zeta = 1$) only one basis function (contraction) per Slater-type atomic orbital is used. DZ sets ($N_\zeta = 2$) have two basis functions per orbital, etc. Since valence orbitals of atoms are more affected by forming a bond than the inner (core) orbitals, more basis functions were assigned to describe valence orbitals. This prompted the development of split-valence (SV) basis sets, i.e., basis sets in which more contractions are used to describe valence orbitals than core orbitals. Frequently, the core orbitals are extensive contractions consisting of many primitive gaussians to represent the "cusp" of s-type functions at the position of the nucleus reasonably well. The "zeta" terminology is often augmented with a number of polarization (P) functions. Thus, DZP means double-zeta plus polarization, TZP stands for triple-zeta plus polarization, etc. Occasionally the number of polarization functions is given explicitly, e.g. TZDP, TZ2P, TZ+2P stands for triple-zeta plus double polarization. The letter “V” denotes split valence basis sets, e.g., DZV represents basis set with only one contraction for inner orbitals, and two contractions for valence orbitals.

The notation adopted by Pople and co-workers emphasizes also on the nature of split valence basis sets (SV), resulting in the general notation-scheme n-ijG or n-ijkG, which can be decoded as: n-number of primitives for the inner shells, ij or ijk-numbers of primitives for contractions in the valence shell. Pople's basis sets can also be augmented with d-type polarization functions on heavy atoms only (n-ijG(d) or n-ijkG(d)) or on all atoms, with additional p-functions on hydrogen (n-ijG(d,p) or n-ijkG(d,p)). The polarization functions are important for reproducing chemical bonds.

Basis sets are also frequently augmented with diffuse functions. Such Gaussian function have very small exponents and decay slowly with the distance from the nucleus. Diffuse functions are necessary for a correct description of anions and weak bonds (e.g. hydrogen bonds) and are frequently used for calculations of various properties (e.g. dipole moments, polarizabilities, etc.). The notation is widely used: n-ij+G, or n-ijk+G when 1 diffuse s-type or p-type function is added to a standard basis set on heavy atoms. In this case the s- and p-type function have the same exponents.

It was well known for a long time that core (inner) orbitals are in most cases not affected significantly by changes of chemical bonds. This prompted the development of Effective Core Potential (ECP) approaches, which treat inner shell electrons as if they were some averaged potential rather than actual particles. ECP's are not orbitals but modifications to a Hamiltonian, and as such are very efficient computationally. In addition, it is very easy to incorporate relativistic effects into ECPs, whereas all-electron relativistic computations are very expensive. The relativistic effects are very important in describing heavier atoms, and ECP's simplify calculations and at the same time make them more accurate with popular non-relativistic *ab initio* packages. The core potentials are usually specified for shells that are filled, while basis functions are provided for the rest of electrons (i.e. valence electrons).

The core electrons are replaced by a linear combination of Gaussian functions, called potential functions, which are parameterized using data from all-electron atom calculations as a reference. The Phillips-Kleinman[24] operator is a starting point for the valence-only approximation. The atomic orbitals are partitioned into valence orbitals φ_V and core orbital φ_C, which are eigenfunctions of the respective Fock-operator:

$$\hat{f}\,\varphi_V = \varepsilon_V \varphi_V \quad \text{and} \quad \hat{f}\,\varphi_C = \varepsilon_C \varphi_C \tag{2.38}$$

The pseudo-orbital for valence electrons is then

$$\chi_V = \varphi_V + \sum_C b_{VC}\varphi_C \tag{2.39}$$

The nodeless pseudo-orbital is orthogonal to the core orbitals. And the equation for pseudo-orbital is

$$(\hat{f} + \sum_C (\varepsilon_V - \varepsilon_C) \mid \varphi_C >< \varphi_C \mid \ )\chi_V = \varepsilon_V \chi_V \quad \text{or}$$

$$(\hat{f} + v^{PK})\chi_V = (\hat{f}^V + v^{PP})\chi_V = \varepsilon_V \chi_V \tag{2.40}$$

where the Phillips-Kleinman-potential v^{PP} has the form of

$$v^{PP} = -\frac{Z - N_V}{r} + \sum_k^{N_C/2} (2\hat{J}_k^C - \hat{K}_k^C) + \sum_k^{N_C/2} (\varepsilon_j^V - \varepsilon_k^C) \mid \chi_k >< \chi_k \mid \tag{2.41}$$

or

$$v^{PP} = \sum_{l=0}^{l_{\max}} \sum_{m=-l}^{l} \sum_k A_{lk} r^{nlk} e^{-B_{lk} r^2} \mid Y_{lm} >< Y_{lm} \mid \tag{2.42}$$

The finally produced ECP are usually tabulated in the literature as parameters of the following expansion:

$$ECP(r) = \sum_{i=1}^{M} d_i r^{n_i} e^{-\zeta_i r^2} \tag{2.43}$$

It is necessary to specify the number of core electrons that are substituted by ECPs for a given atomic center, the largest angular momentum quantum number included in the potential, and number of terms M in the polynomial expansion shown above. For each term in this expansion one need to specify: coefficient d_i, power n_i of the distance from nucleus r and exponent ζ_i of the gaussian function. Since only functions for valence electrons are required the number of necessary basis functions is reduced drastically. Thus, in many cases it would simply be impossible to perform calculations on systems involving heavier elements without ECP's.

The core size and the number of basis functions of the valence orbitals play the most important role among the various parameters needed for calculations of geometries and bond energies. For transition metal complexes, the small core ECP was recommended.

Although ECPs do not have the correct nodal structure for the valence orbitals, it benefits from the reduction of the size of the basis set. The most important point is that

there is no significant difference in accuracy between the ECP and the model potential if basis sets of the same quality are used. The latter potential is proposed and developed by Huzinaga and co-workers[25].

To get the parameters for the pseudopotentials and the pseudo-orbitals, several methods are used by different groups. In the group of Stoll and Preuss[26], the difference in atomic excitation energies between the calculated values with ECP and all-electron results was minimized to get optimized parameters, while the principle of shape consistency is adopted from Hay and Wadt[27].

2.3 Geometry Optimization and Characterization of Stationary Point

Geometry optimizations usually attempt to locate minima on the potential energy surface, therefore predicting equilibrium structures of molecular systems. For minima as well as for saddle points, the first derivative of the energy (i.e. the gradient) is zero.

For N atoms, the energy is a function of $3N-6$ (or $3N-5$) degrees of freedom. The energy E of a molecular system obtained on the basis of the Born-Oppenheimer approximation is a parametric function of the nuclear coordinates denoted as $X^+ = (X_1, X_2, ..., X_{3N})$. Moving from $E(X)$ to $E(X_1)$, where $q = (X_1 - X)$, the energy may be expanded in a Taylor series about X as follows:

$$E(X_1) = E(X) + q^+ f(X) + \frac{1}{2} q^+ H(X) q^+ + ... \qquad (2.44)$$

where the gradient is $f_i = \partial E(X) / \partial X_i$ and the Hessian is $H_{ij} = \partial^2 E(X) / \partial X_i \partial X_j$

Energy calculations and geometry optimizations ignore the vibrations in molecular systems. In reality, however, the nuclei in molecules are constantly in motion. In equilibrium states these vibrations are regular and predictable since molecular frequencies depend on the second derivative of the energy with respect to the nuclear positions, and molecules can be identified by their characteristic spectra.

The zero-point vibration and thermal energy corrections to the total energies can be obtained through harmonic frequency calculations.

Another purpose of the frequency calculations is to identify the nature of stationary point on the potential energy surface found by a geometry optimization. A structure which has *n* imaginary frequencies is an *n*th order saddle point. Ordinary transition structures are usually characterized by one imaginary frequency since they are first-order saddle points. Whenever a structure yield an imaginary frequency, it means that there is some geometric distortion for which the energy of the system is lower than it is at the current structure. In order to fully understand the nature of a saddle point, one must determine the nature of this deformation by looking at the normal mode corresponding to the imaginary frequency. A further steps towards characterizing a transition state fully is by running intrinsic reaction coordinate (IRC) calculations. Only on the basis of such calculation it can be shown that the transition state connects reactants and products.

2.4. Methods for Electronic Structure Analysis

2.4.1 Topologic Analysis of Electron Density

The purpose of the "atoms in molecules" (AIM) concept developed by Bader[28] is to relate molecular properties to those of its constituent atoms by means of a topological analysis of its electron density.

According to Bader's theory, the quantum subsystems (atoms or atomic groups) are open systems defined in real space, their boundaries being determined by a particular property of the electronic charge density.

$$\rho(1) = N\int \psi^{*}(1,2,...,N)\psi(1,2,...,N)dr_2 dr_3 ...dr_N$$
$$= N\int |\psi(1,2,...,N)|^2 d\tau' \qquad (2.45)$$

where $d\tau'$ denotes the spin coordinates of all the electrons and the cartesian coordinates of all electrons but one. The charge density, ρ, has a definite value at each point of

space. It is a scalar field defined over three dimensional space. Each topological feature of ρ is associated with a point in space called a critical point r_C where the first derivatives $\nabla\rho(r_C)$ of ρ vanish, i.e. $\nabla\rho(r_C) = 0$. The second derivative $\nabla^2\rho(r_C)$ of the charge density function at this point determines whether it is a maximum, a minimum or a saddle point. It is also called the Laplacian of charge density, which is invariant to the choice of coordinates axes.

The critical point is labeled using the set of values (ω, r), where ω is equal to the number of non-zero curvatures of ρ at the critical point and r is the algebraic sum of the sign of the values. The critical points of charge distributions for molecules at or in the neighborhood of energetically stable nuclear configurations are all of rank three (ω = 3) while a critical point with ω < 3 is degenerate or unstable. For rank three there are four possible signature values (see Table 2.1) .

Table 2.1 Four possible critical points of rank three

(ω, r)	Properties of the critical point
(3, -3)	Nucleus region
(3, -1)	Bond critical point
(3, +1)	Ring critical point
(3, +3)	Cage critical point

The properties of the electron density at a bond critical point (3, -1) characterize the interaction defined by its associated trajectories. When $\nabla^2\rho(r_C) < 0$ and is large in magnitude, $\rho(r_C)$ is also large, and electronic charge is concentrated in the nuclear region, the result is a sharing of electronic charge by both nuclei, as it is found for interactions usually characterized as covalent or polar (shared interactions). For closed-shell interactions, as found in ionic, hydrogen-bonded, van der Waals and repulsive interactions, $\rho(r_C)$ is relatively low in value and the value of $\nabla^2\rho(r_C)$ is positive. A another quantity used to determine the nature of the interaction is the energy density at the critical point H_b. It is found that H_b has to be negative for all interactions which result from the accumulation of electron density at the bond critical point. The charge density of an interatomic surface attains its maximum value at the bond critical point

and the two associated curvatures of ρ at r_C denoted by λ_1 and λ_2 are negative. In a bond with cylindrical symmetry $\lambda_1 = \lambda_2$. If two curvatures are not of equal magnitude, λ_2 may be referred to as the value of the curvature of smallest magnitude. The quantity $\varepsilon = [\lambda_1 / \lambda_2 - 1]$ is then called the ellipticity of the bond, which provides a measure of the content to which charge is preferentially accumulated in a given plane.

The qualitative associations of topological features of the electron density with elements of the molecular structure can be viewed by using its associated gradient vector field, which is represented through a display of the trajectories traced out by the $\nabla\rho(r, X)$ for a given molecular geometry. All trajectories terminate at core critical points (3, -3), which behave as a point attractor. The basin of the attractor is defined as the region of space traversed by all trajectories that terminate at the attractor. The "atomic surface" of atom A is the boundary of its basin. The "zero-flux" surface condition is the boundary condition: $\nabla\rho(r) \bullet n(r) = 0$ for every point on the interatomic surface $S(r)$ where $n(r)$ is the unit vector normal to the surface at r.

2.4.2 Natural Bond Orbital (NBO) Analysis

The natural bond orbital (NBO) analysis developed by Weinhold *et al.* [29, 30] consists of a sequence of transformations from the input basis set such as atomic orbitals (AOs), to various *localized* basis sets: natural atomic orbitals (NAOs), natural hybrid orbitals (NHOs), natural bond orbitals (NBOs), and natural localized molecular orbitals (NLMOs). The localized sets may be subsequently transformed to *delocalized* natural orbitals (NOs) or canonical molecular orbitals (MOs).

$$\text{AOs} \rightarrow \text{NAOs} \rightarrow \text{NHOs} \rightarrow \text{NBOs} \rightarrow \text{NLMOs} \rightarrow \text{NOs or MOs}$$

The initial transformation from the one-center basis AOs to NAO is generally non-unitary since basis-AOs are generally nonorthogonal. The subsequent transformations are, however, unitary. Each set of one-center (NAO, NHO) and two-center (NBO, or NLMO) orbitals constitute a complete, orthonormal "chemist's basis set" which is in close correspondence to the picture of localized bonds and lone pairs as basis units of the molecular structure.

1. NOs Conventional natural orbitals are introduced originally by Löwdin[31], which were derived from properties of the one-particle density operator $\hat{\Gamma}$

$$\hat{\Gamma} = N\int \psi(1,2,...,N)\psi^*(1',2,...,N)d\tau_2...d\tau_N \tag{2.46}$$

and its associated matrix representation Γ in an AO basis $\{\chi_i\}$

$$(\Gamma)_{ij} = \int \chi_i^*(1)\hat{\Gamma}\chi_j(1')d\tau_1 d\tau_1' \tag{2.47}$$

The eigenorbitals of $\hat{\Gamma}$ are $\{\phi_i^{NO}\}$,

$$\hat{\Gamma}\phi_i^{NO} = \nu_i\phi_i^{NO} \tag{2.48}$$

which are hence "natural" to the *N*-electron wave function ψ itself. The corresponding eigenvalues are occupation numbers ν_i. The orbitals transform as irreducible representations of the full symmetry point group of the molecule and are therefore completely delocalized.

2. AO→NAO's The first step for the construction of NAOs is the diagonalization of the one-center angular symmetry blocks $\Gamma^{(Alm)}$ of the density matrix. This leads to a set of "pre-NAOs", an orthonormal set of orbitals for each atom which are optimal for the atom in its molecular binding environment. On the basis of occupancy these pre-NAOs can be divided into two sets: (1) the "minimal" set $\{\phi_{im}\}$, corresponding to all atomic (*n*, *l*) subshells of non-zero occupation in the atomic ground state electronic configuration, and (2) the "Rydberg" set $\{\phi_{ir}\}$ consisting the remaining (formal unoccupied) orbitals. The pre-NAOs of one-center overlap those of other centers so that the occupancies of these orbitals can not be used directly to assess the atomic charge.

In the second step, the interatomic overlap is removed. By using the occupancy-weighted symmetric orthogonalization (OWSO) procedure, higher weight is given to

preserving the forms of strongly occupied orbitals than of those that play little or no role in describing the atomic electron density. The OWSO procedure is performed on all the minimal functions $\{\phi_{im}\}$. For the Rydberg sets $\{\phi_{ir}\}$, the Schmidt transformation is carried out before OWSO.

$$\{\phi_{im}\} = W_{OWSO}\{\tilde{\phi}_{im}\} \tag{2.49a}$$

$$\{\tilde{\phi}_{ir}{}^{S}\} = S_{Schmidt}\{\tilde{\phi}_{ir}\} \tag{2.49b}$$

$$\{\phi_{ir}\} = W_{OWSO}\{\tilde{\phi}_{ir}{}^{S}\} \tag{2.49c}$$

The final NAOs may also be divided into two sets. The NAOs $\{\phi_{i,NMB}\}$ of the minimal set are the "natural minimal basis"(NMB), whereas those $\{\phi_{i,NRB}\}$ of the Rydberg set will be referred as "natural Rydbegr basis"(NRB).

The OWSO procedure is done as follows: Non-orthogonal AOs $\{\tilde{\phi}_i\}$ are transformed to corresponding orthonormal AOs $\{\phi_i\}$ according to:

$$W_{OWSO}\{\tilde{\phi}_i\} = \{\phi_i\} \tag{2.50a}$$

$$\langle \phi_i | \phi_j \rangle = \delta_{ij} \tag{2.50b}$$

The transformation matrix W_{OWSO} has the property of minimizing the occupancy-weighted, mean-squared deviations of the ϕ_i from the parent non-orthogonal $\tilde{\phi}_i$

$$\min\left\{\sum_i w_i \int |\phi_i - \tilde{\phi}_i|^2 d\tau\right\} \tag{2.51}$$

where the weighting factor w_i is the expectation value of the density operator $\hat{\Gamma}$.

$$w_i = \langle \tilde{\phi}_i | \hat{\Gamma} | \tilde{\phi}_i \rangle \tag{2.52}$$

3. Natural population analysis (NPA) The natural population $q_i^{(A)}$ of orbital $\phi_i^{(A)}$ on atom A is the diagonal density matrix element in the NAO basis

$$q_i^{(A)} = \left\langle \phi_i^{(A)} \middle| \hat{\Gamma} \middle| \phi_i^{(A)} \right\rangle \tag{2.53}$$

which may be summed to give the total number of electrons

$$q^{(A)} = \sum_i q_i^{(A)} \tag{2.54}$$

and the natural charge $Q^{(A)}$ on atom A with atomic number $Z^{(A)}$

$$Q^{(A)} = Z^{(A)} - q^{(A)} \tag{2.55}$$

The populations automatically satisfy the Pauli principle $(0 \le q_i^{(A)} \le 2)$ and sum to the total number of electrons.

$$N_{electron} = \sum_A^{atoms} q^{(A)} \tag{2.56}$$

4. NHOs and NBO Once the density matrix has been transformed to the NAOs basis, the NBO program will begin the search for an optimal natural Lewis structure. Firstly, NAOs of high occupancy (>1.999e) are removed as unhybridized core orbitals (C_A). The next step is to search for lone-pair eigenvectors L_A, which occupancy exceeds a preset pair threshold ($\rho_{threshold}$ =1.90) in one-center blocks $\Gamma^{(A)}$. The density matrix is depleted of eigenvectors satisfying this threshold, and the program then cycles over all two center blocks $\Gamma^{(AB)}$ searching for bond vector b_{AB} whose occupancy exceeds $\rho_{threshold}$. The search may be further extended to three-center bonds if an insufficient number of electron pairs were found in the one- and two-center searches. The set of localized electron pairs $(C_A)^2(L_A)^2(b_{AB})^2$ formed in this manner constitutes a "natural Lewis structure" to describe the system. The best NBO structure is that corresponding to the largest overall ρ_{Lewis} and is generally formed to agree with the pattern of bonds and lone pairs of the chemist's standard Lewis formula.

Each bond-type b_{AB} may be decomposed into its constituent normalized atomic hybrids ($\tilde{h}^{(A)}, \tilde{h}^{(B)}$) and polarization coefficients ($c^{(A)}, c^{(B)}$).

$$b_{AB} = c^{(A)}\tilde{h}^{(A)} + c^{(B)}\tilde{h}^{(B)} \tag{2.57}$$

Because of possible overlap of an initial bond orbital $\phi^{(AB)}$ with other bond orbitals $\phi^{(AC)}$, the hybrids are systematically reorthogonalized to produce the final set of NHOs ($h^{(A)}, h^{(B)}$).

5. NLMOs The semi-localized NLMOs are obtained by slightly modifying the NBOs. The corresponding unitary transformation is found by zeroing the off-diagonal block $\Gamma_{ij}^{(AB)}$ of $\Gamma^{(AB)}$ by a Jocobi transformation, where A is strongly occupied (core, lone pairs, bonds) and B weakly occupied (antibond, Rydberg, etc.) in the NBO. The magnitudes of the NLMO mixing coefficients give a quantitative measure of the "resonance" delocalization leading to departures from a strictly localized "Lewis structure" NBO picture.[32]

2.4.3 Charge Decomposition Analysis (CDA)

The charge decomposition analysis (CDA)[33] constructs the wave function of the complex in terms of the linear combination of the donor and acceptor fragment orbitals (LCFO). Three terms are then calculated for each LCFO orbital of the complex: (i) the charge donation d given by the mixing of the occupied orbitals of the donor and the unoccupied orbitals of the acceptor; (ii) the back donation b given by the mixing of the occupied orbitals of the acceptor and the unoccupied orbitals of the donor; (iii) the charge depletion from the overlapping area (charge polarization) r given by mixing of the occupied orbitals of donor and acceptor. The sum of the three contributions gives the total amount of donation, back donation and charge polarization in the complex.

For example, for a molecule AB with properly chosen fragments A and B, the charge donation d_i from fragment A to fragment B can then be defined as

$$d_i = \sum_{k}^{occ,A} \sum_{n}^{vcc,B} m_i c_{ki} c_{ni} < \phi_k \mid \phi_n > \tag{2.58}$$

where the functions ϕ are atomic orbitals or any other basis set. For every orbital of the molecule, summation of d_i leads to the overall charge donation from A to B. In a similar manner, back donation b_i can be written as

$$b_i = \sum_{l}^{occ,B} \sum_{m}^{vcc,A} m_i c_{li} c_{mi} < \phi_l \mid \phi_m > \tag{2.59}$$

The closed shell interaction of the two fragments is then defined by

$$r_i = \sum_{k}^{occ,A} \sum_{l}^{occ,B} m_i c_{ki} c_{li} < \phi_k \mid \phi_l > \tag{2.60}$$

The r_i term is calculated from the overlap of the occupied region of the fragment orbitals and the sum of the r_i term is always negative. That is, interactions between filled orbitals are repulsive. We can also call this term the charge polarization because it seems that r_i gives the amount of electronic charge which is removed from the overlap of the occupied MOs into the nonoverlapping regions.

Chapter 3. Ligand Site Preference in Iron Tetracarbonyl Complexes

3.1 Introduction

The nature of the metal–CO bond in transition metal carbonyl and related complexes is commonly described by the Dewar-Chatt-Duncanson (DCD) model of synergistic CO→metal σ-donation and CO←metal π-back donation (Figure 3.1).[34] This conceptual framework has been widely accepted in inorganic[35] and organometallic[2] chemistry and many properties of complexes with CO and other ligands can be easily classified or even predicted in terms of σ-donor/π-acceptor interactions.[36]

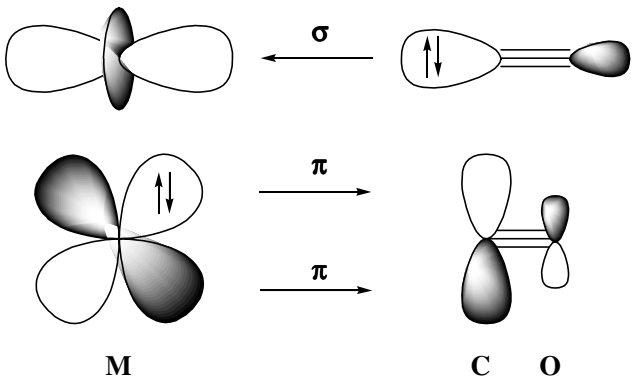

Figure 3.1 Schematic representation of the dominant orbital interactions of transition metal carbonyls in terms of CO→M σ-donation (top) and CO←M π-back donation (bottom).

Quite recently, it was shown that the use of quantum chemical calculations in conjunction with charge partitioning schemes like the charge decomposition analysis (CDA)[33] or Weinhold's natural bond orbital (NBO) approach[29] support this model even at a more quantitative level.[37-39] For example, it was shown that in a series of isoelectronic complexes $M(CO)_6$ (M = Hf^{2-}, Ta^{-}, W, Re^{+}, Os^{2+}, and Ir^{3+}) the C–O stretching frequencies decrease with the extent of OC ← metal π-back donation.[39] In addition, it was also pointed out that the metal–CO bond length of carbonyl coordinated in trans position to various ligands L of $M(CO)_5L$ (M = Cr, Mo, W) complexes is lengthened with increasing L ← metal π-back donation.[37] Charge back donation is, however, not the only factor that determines stretching frequencies and

bond lengths to coordinated ligands. This is best illustrated by non-classical transition metal carbonyl complexes[40] in which the wavenumbers of the C–O stretching mode is larger for coordinated than for isolated CO. It was shown that this behaviour is not due to donor-acceptor interactions but due to polarizing effects exerted from the positively charged metal on coordinated CO.[41]

Whereas the actual virtue of charge partitioning schemes lies in the possibility of comparing σ-donor/π-acceptor strengths of various ligands *relative* to each other, it does not predict which of these contributions is more important for the actual metal–ligand binding energy. Numerous earlier theoretical studies showed that in transition metal carbonyl complexes, CO←M π-back donation is indeed more important for the binding energy than OC→M σ-donation.[42-44] However, quite recently it was pointed out that the interaction energy between metal carbonyl and CO fragments correlates with the increase of the stabilizing orbital interaction of these fragments, which in turn is dominated by their HOMO-LUMO contributions.[39b] In the aforementioned series of isoelectronic hexacarbonyl complexes of Hf^{2-}, Ta^{-}, W, Re^{+}, Os^{2+} and Ir^{3+} it was shown that the HOMO and the LUMO of the corresponding metal pentacarbonyl fragments are lowered on going from Hf^{2-} to Ir^{3+}. Thus pentacarbonyl fragments with relatively high lying HOMOs (*e.g.* $Hf(CO)_5^{2-}$, $W(CO)_5$) imply that π-back donation is more important for the M–CO binding energy, whereas σ-donation dominates for those fragments with low lying LUMOs (*e.g.* Ir^{3+}).[39b]

Beside the aforementioned consequences of σ-donation and π-back donation another effect of varying donor-acceptor strengths originated in a generally applied rule for predicting the structures of transition metal carbonyls. Experimental evidence and qualitative molecular orbital considerations suggest that strong π-accepting ligands prefer the equatorial position of trigonal bipyramidal complexes containing d^8 metals, while σ-donor ligands prefer axial coordination sites.[45,46] This model is supported by a limited number of quantum chemical studies of complexes $Fe(CO)_4L$ (L = N_2,[47] η^2-C_2H_4,[48] H_2,[49] PR_3[50] and η^2-C_2H_2[51]). However, no systematic and comparative theoretical work with respect to a wider range of such complexes has been published so far. Moreover, the reason for the ligand site preference was not included. In the present study, a detailed and thorough examination of the bonding situation and the relative stability of complexes of the general type $Fe(CO)_4L$ (L =

CO, CS, N_2, NO^+, CN^-, NC^-, η^2-C_2H_4, η^2-C_2H_2, CCH_2, CH_2, CF_2, η^2-H_2, NH_3, NF_3, PH_3, PF_3) is therefore carried out. In particular, energetic and structural differences between axially and equatorially coordinated ligands L are focused on and requisites leading to their preferred coordination site are addressed.

3.2 Theoretical Methods

Geometry optimizations and energy calculations were performed using Becke's three-parameter hybrid-functional in combination with the correlation functional according to Lee, Yang and Parr (B3LYP).[52] A non-relativistic small-core effective core potential and a (441/2111/41) split-valence basis set were used for Fe[27c] and an all-electron 6-31G(d) basis set was chosen for first- and second-row elements.[53] An additional polarization function was used for the hydrogens in $Fe(CO)_4H_2$.[54] This combination of basis sets is further denoted as basis set II.[55] All stationary points found on the potential energy surface were further characterized by numerical frequency analyses. An improved estimate for bond dissociation energies is obtained by single-point energy calculations on the B3LYP/II geometries using coupled-cluster theory with singles and doubles and a non-iterative estimate of triple substitution (CCSD(T)).[21] All calculations used the program packages Gaussian 94/98,[56] ACES II[57] and MOLPRO 96/2000.[58] Metal-ligand donor-acceptor interactions were examined in terms of charge donation, back donation and repulsive polarization using the program CDA 2.1[59] and Weinhold's NBO analysis[29] as implemented in Gaussian98.[56b]

3.3 Results and Discussion

Figure 3.2 shows the optimized geometries of the complexes $Fe(CO)_5$ (**1**), singlet and triplet $Fe(CO)_4$ (**2a**, **2b**) and $Fe(CO)_4L$ where L is CS (**3a**, **3b**), N_2 (**4a**, **4b**), NO^+ (**5a**, **5b**), CN^- (**6a**, **6b**), NC^- (**7a**, **7b**), η^2-C_2H_4 (**8a**, **8b**), η^2-C_2H_2 (**9a**, **9b**), CCH_2 (**10a**, **10b**), CH_2 (**11a**, **11b**), CF_2 (**12a**, **12b**), η^2-H_2 (**13a**, **13b**), NH_3 (**14a**, **14b**), NF_3 (**15a**, **15b**), PH_3 (**16a**, **16b**) or PF_3 (**17a**, **17b**) coordinated either at an axial or equatorial site (Scheme 3.1).

Table 3.1 Calculated Relative Energies E_{rel}[a] and Bond Dissociation Energies D_e and D_o with Respect to Singlet $Fe(CO)_4$ and Singlet L (L = CO, CS, N_2, NO^+, CN^-, NC^-, η^2-C_2H_4, η^2-C_2H_2, CCH_2, CH_2[b], CF_2, η^2-H_2, NH_3, NF_3, PH_3, PF_3).

			B3LYP/II//B3LYP/II		CCSD(T)/II//B3LYP/II	
molecule		sym.	E_{rel}	D_e (D_o)	E_{rel}	D_e (D_o)[c]
$Fe(CO)_4CO$	**1**	D_{3h}		41.8 (39.0)		47.9(45.1)
$Fe(CO)_4CS$(ax)	**3a**	C_{3v}	0.0	58.4 (55.8)	0.0	66.8(64.2)
$Fe(CO)_4CS$(eq)	**3b**	C_{2v}	0.2	58.1 (55.4)	-0.1	66.9(64.2)
$Fe(CO)_4N_2$(ax)	**4a**	C_{3v}	0.0	18.7 (16.5)	0.0	25.1(22.9)
$Fe(CO)_4N_2$(eq)	**4b**	C_{2v}	1.2	17.5 (15.3)	0.5	24.6(22.4)
$Fe(CO)_4NO^+$(ax)	**5a**	C_{3v}	0.0	81.1 (79.2)	0.0	86.7(84.8)
$Fe(CO)_4NO^+$(eq)	**5b**	C_{2v}	-13.6	94.7 (92.4)	-20.7	107.4(105.1)
$Fe(CO)_4CN^-$(ax)	**6a**	C_{3v}	0.0	89.6 (87.0)	0.0	99.1(96.5)
$Fe(CO)_4CN^-$(eq)	**6b**	C_{2v}	6.1	83.5 (81.0)	6.7	92.4(89.9)
$Fe(CO)_4NC^-$(ax)	**7a**	C_{3v}	0.0	72.8 (70.7)	0.0	80.7(78.6)
$Fe(CO)_4NC^-$(eq)	**7b**	C_{2v}	6.8	66.0 (64.2)	6.3	74.5(72.7)
$Fe(CO)_4(\eta^2$-$C_2H_4)$(ax)	**8a**	C_s	0.0	21.3 (18.3)	0.0	33.6(30.6)
$Fe(CO)_4(\eta^2$-$C_2H_4)$(eq)	**8b**	C_{2v}	-7.6	28.9 (25.9)	-8.6	42.2(39.2)
$Fe(CO)_4(\eta^2$-$C_2H_2)$(ax)	**9a**	C_s	0.0	18.8 (16.9)	0.0	28.8(26.9)
$Fe(CO)_4(\eta^2$-$C_2H_2)$(eq)	**9b**	C_{2v}	-8.8	27.6 (25.4)	-10.7	39.5(37.3)
$Fe(CO)_4CCH_2$(ax)	**10a**	C_s	0.0	68.6 (64.7)	0.0	79.6(75.7)
$Fe(CO)_4CCH_2$(eq)	**10b**	C_{2v}	-6.2	74.8 (70.3)	-8.7	88.3(83.8)
$Fe(CO)_4CH_2$(ax)	**11a**	C_s	0.0	74.3 (69.1)	0.0	84.8(79.6)
$Fe(CO)_4CH_2$(eq)	**11b**	C_{2v}	-6.5	80.8 (75.1)	-8.3	93.1(87.4)
$Fe(CO)_4CF_2$(ax)	**12a**	C_s	0.0	55.1 (52.2)	0.0	62.7(59.8)
$Fe(CO)_4CF_2$(eq)	**12b**	C_{2v}	-3.0	58.2 (55.2)	-4.6	67.3(64.3)
$Fe(CO)_4(\eta^2$-$H_2)$(ax)	**13a**	C_s	0.0	15.0 (10.3)	0.0	21.2(16.5)
$Fe(CO)_4(\eta^2$-$H_2)$(eq)	**13b**	C_{2v}	-2.0	17.1 (12.8)	-1.6	22.8(18.5)
$Fe(CO)_4NH_3$(ax)	**14a**	C_s	0.0	33.7 (29.9)	0.0	42.9(39.1)
$Fe(CO)_4NH_3$(eq)	**14b**	C_s	6.6	27.1 (23.7)	6.4	36.5(33.1)
$Fe(CO)_4NF_3$(ax)	**15a**	C_s	0.0	16.9 (15.3)	0.0	25.1(23.5)
$Fe(CO)_4NF_3$(eq)	**15b**	C_s	3.4	13.5 (12.2)	3.0	22.2(20.9)
$Fe(CO)_4PH_3$(ax)	**16a**	C_{3v}	0.0	30.2 (26.8)	0.0	42.3(38.9)
$Fe(CO)_4PH_3$(eq)	**16b**	C_s	1.1	29.1 (25,9)	2.7	39.7(36.5)
$Fe(CO)_4PF_3$(ax)	**17a**	C_{3v}	0.0	36.6 (34.1)	0.0	47.6(45.2)
$Fe(CO)_4PF_3$(eq)	**17b**	C_s	-0.3	36.9 (34.5)	1.0	46.5(44.1)

All energies are in kcal mol^{-1}. [a] relative to the axial isomer and without zero-point energy (ZPE) correction. [b] triplet CH_2. [c] ZPE correction obtained at the B3LYP/II level of theory.

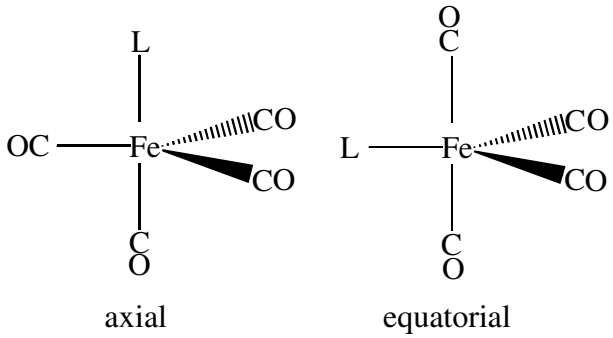

Scheme 3.1 Schematic representation of the axial (left) and equatorial isomer (right) of $(CO)_4FeL$.

Relative energies and $(CO)_4Fe–L$ bond dissociation energies without and with zero-point energy corrections (D_e and D_o, respectively) are summarized in Table 3.1. These values are calculated using total energies E_{total} without and with zero-point energy corrections obtained either at the B3LYP/II//B3LYP/II or CCSD(T)/II//B3LYP/II level of theory (eq 3.1). Due to the interest in spin-allowed dissociation processes, these values were derived only with respect to the singlet ground states of $Fe(CO)_4$ and ligands L.[60]

$$D_{e/o} = E_{total}[Fe(CO)_4] + E_{total}[L] – E_{total}[Fe(CO)_4L] \qquad (3.1)$$

Frequency analyses show that iron tetracarbonyl complexes with the axial ligands ethylene (**8a**), acetylene (**9a**), vinylidene (**10a**), carbene (**11a**) and difluorcarbene (**12a**) are transition states on their respective potential energy surface rather than local minima. A direct comparison between these complexes and their corresponding equatorial isomers, particularly with respect to the $(CO)_4Fe–L$ bond dissociation energies, therefore does not seem appropriate.

According to the calculations (B3LYP/II//B3LYP/II) side-on (η^2) coordination of the diatomic ligands CS, N_2, and NO^+ result in complexes that are significantly less stable than their respective end-on counterparts. These structures are thus not discussed in detail. Furthermore, with the exception of cyanide and isocyanide complexes, only the energetically most stable linkage isomers of complexes containing potential ambidentate ligands are focused on.

Unless otherwise noted, only the bond dissociation energies D_o obtained at the highest level of theory, namely CCSD(T)/II//B3LYP/II, are referred to. Bond dissociation energies are not corrected for the basis set superposition error (BSSE).[61]

3.3.1 Charge Partitioning Schemes

Table 3.2 Results of the CDA and NBO Analysis for Complexes $Fe(CO)_4$ L (L = CO, CS, N_2, NO^+, CN^-, NC^-, η^2-C_2H_4, η^2-C_2H_2, CCH_2, CH_2, CF_2, η^2-H_2, NH_3, NF_3, PH_3, PF_3).

		CDA				NBO		
molecule		d[a]	b[b]	r[c]	Δ[d]	q($Fe(CO)_4$)[e]	q(σ)L[f]	q(π)L[g]
$Fe(CO)_4CO$(ax)	**1**	0.51	0.28	-0.33	0.00	-0.17	0.49	0.32
$Fe(CO)_4CO$(eq)	**1**	0.47	0.29	-0.31	0.01	-0.07	0.39	0.33
$Fe(CO)_4CS$(ax)	**3a**	0.45	0.34	-0.41	0.00	-0.06	0.55	0.49
$Fe(CO)_4CS$(eq)	**3b**	0.42	0.36	-0.37	0.00	0.06	0.47	0.53
$Fe(CO)_4N_2$(ax)	**4a**	0.28	0.14	-0.25	-0.02	-0.08	0.25	0.17
$Fe(CO)_4N_2$(eq)	**4b**	0.22	0.14	-0.25	0.01	0.00	0.18	0.18
$Fe(CO)_4NO^+$(ax)	**5a**	0.24	0.44	-0.30	0.01	0.66	0.31	0.97
$Fe(CO)_4NO^+$(eq)	**5b**	0.19	0.42	-0.31	0.03	0.77	0.21	0.98
$Fe(CO)_4CN^-$(ax)	**6a**	0.66	0.06	-0.33	-0.04	-0.53	0.60	0.07
$Fe(CO)_4CN^-$(eq)	**6b**	0.62	0.08	-0.26	-0.03	-0.47	0.54	0.07
$Fe(CO)_4NC^-$(ax)	**7a**	0.57	0.01	-0.27	-0.06	-0.39	0.40	0.01
$Fe(CO)_4NC^-$(eq)	**7b**	0.53	0.02	-0.21	-0.03	-0.33	0.34	0.01
$Fe(CO)_4(\eta^2$-$C_2H_4)$(ax)	**8a**	0.47	0.20	-0.36	-0.02	-0.09	-	-
$Fe(CO)_4(\eta^2$-$C_2H_4)$(eq)	**8b**	0.44	0.27	-0.38	-0.02	0.07	-	-
$Fe(CO)_4(\eta^2$-$C_2H_2)$(ax)	**9a**	0.48	0.21	-0.36	-0.01	-0.08	-	-
$Fe(CO)_4(\eta^2$-$C_2H_2)$(eq)	**9b**	0.51	0.30	-0.41	0.00	0.10	-	-
$Fe(CO)_4CCH_2$(ax)	**10a**	0.52	0.33	-0.41	0.01	-0.04	0.61	0.57
$Fe(CO)_4CCH_2$(eq)	**10b**	0.53	0.38	-0.37	0.01	0.11	0.52	0.63
$Fe(CO)_4CH_2$(ax)	**11a**	0.51	0.32	-0.38	0.01	-0.01	0.69	0.68
$Fe(CO)_4CH_2$(eq)	**11b**	0.48	0.40	-0.32	0.00	0.13	0.65	0.78
$Fe(CO)_4CF_2$(ax)	**12a**	0.56	0.26	-0.31	-0.01	-0.15	0.48	0.33
$Fe(CO)_4CF_2$(eq)	**12b**	0.55	0.30	-0.29	0.00	0.02	0.38	0.40
$Fe(CO)_4(\eta^2$-$H_2)$(ax)	**13a**	0.44	0.19	-0.23	0.00	-0.19	-	-
$Fe(CO)_4(\eta^2$-$H_2)$(eq)	**13b**	0.43	0.25	-0.21	0.00	-0.09	-	-
$Fe(CO)_4NH_3$(ax)	**14a**	0.33	-0.01	-0.24	-0.01	-0.27	0.40	0.13
$Fe(CO)_4NH_3$(eq)	**14b**	0.26	-0.01	-0.18	-0.01	-0.20	0.32	0.12
$Fe(CO)_4NF_3$(ax)	**15a**	0.30	0.09	-0.20	-0.01	-0.12	0.28	0.16
$Fe(CO)_4NF_3$(eq)	**15b**	0.24	0.09	-0.19	0.00	-0.03	0.18	0.15
$Fe(CO)_4PH_3$(ax)	**16a**	0.43	0.15	-0.39	0.01	-0.36	0.52	0.16
$Fe(CO)_4PH_3$(eq)	**16b**	0.40	0.14	-0.37	-0.03	-0.25	0.40	0.15
$Fe(CO)_4PF_3$(ax)	**17a**	0.58	0.18	-0.31	-0.03	-0.38	0.58	0.20
$Fe(CO)_4PF_3$(eq)	**17b**	0.56	0.19	-0.29	-0.04	-0.26	0.46	0.20

[a] L→$Fe(CO)_4$ σ-donation. [b] L←$Fe(CO)_4$ π-back donation. [c] L↔$Fe(CO)_4$ repulsive polarization. [d] residual term Δ. [e] partial charge of $Fe(CO)_4$. [f] charge donation involving valence σ-orbitals of the ligand. [g] charge-back donation expressed as the natural occupancy of the valence p-π orbitals of ligand L.

Within the CDA partitioning scheme, the donor-acceptor strengths of the various ligands L are classified by the relative amounts of L → $Fe(CO)_4$ σ-donation (d), L ← $Fe(CO)_4$ π-back donation (b) and L ↔ $Fe(CO)_4$ charge repulsion (r) between the ligand L and the remaining complex fragment $Fe(CO)_4$. These charge contributions together with the residual term Δ are summarized in Tables 3.2 and 3.3. Note, that Δ ≈ 0 holds for all complexes considered in this study indicating that the interpretation of the $(CO)_4$Fe–L bonds in terms of σ-donor/π-acceptor interactions is indeed justified.[38,62] Furthermore, it should be emphasized that more complete basis sets like TZ2P or 6-31G(d,p) do not change the *relative* ratio of the charge components significantly.[33] Under certain circumstances, however, the known basis set dependence of the CDA may yield inconsistent results and the use of this partitioning scheme as a 'black-box' tool is not advisable at this stage.[51]

The results of the NBO analyses are summarized in Table 3.2. The charge-back donation q(π)L of ligand L is expressed as the difference of the p(π) populations between the coordinated and isolated ligand with frozen complex geometry. The difference between q(π)L and the partial charge of the complex fragment $Fe(CO)_4$ is then used as a measure of the charge-donation q(σ)L.

3.3.2 $Fe(CO)_5$ (1) and $Fe(CO)_4$ (2)

The equatorial Fe–CO distance of $Fe(CO)_5$ (**1**) is found to be shorter than the axial one (Fig 3.2.1). The respective bond lengths of 1.805 Å and 1.819 Å are in very good agreement with X-ray crystallographic data.[63] Similarly, the C–O bond lengths of 1.151 Å and 1.147 Å found for axial and equatorial CO are also in accord with the experiment.[63] Due to contradictory experimental[64-67] and theoretical results[44,68-73] an unequivocal assignment of the relative Fe–CO bond lengths of $Fe(CO)_5$ is, however, still somewhat ambiguous.

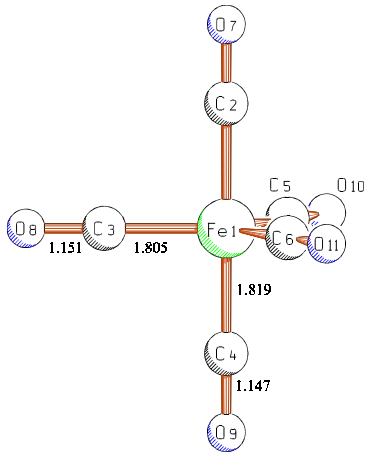

1

Figure 3.2.1 Optimized geometries (B3LYP/II) of $Fe(CO)_5$. Bond lengths are given in Å.

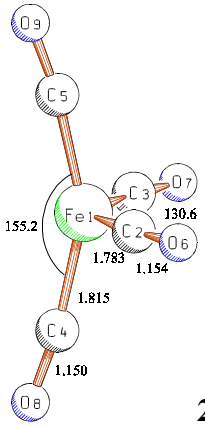

2a

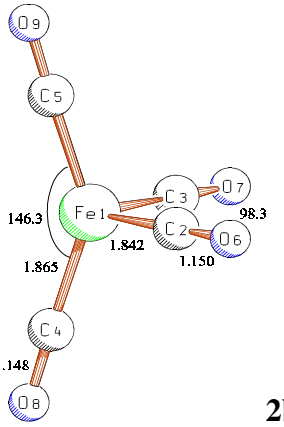

2b

Figure 3.2.2 Optimized geometries (B3LYP/II) of $Fe(CO)_4$, singlet (**2a**) and triplet (**2b**). Bond lengths are given in Å , bond angles in degree.

The first bond dissociation energy D_o of CO for **1** is calculated to be 45.1 kcal mol^{-1}. Although this value does not differ significantly from the previous estimate[70] it converges nicely to the experimental value of 41±2 kcal mol^{-1} [74] and is also in line with other calculations.[44,47,69]

The total amount of OC→$Fe(CO)_4$ σ-donation and OC←$Fe(CO)_4$ π-back donation obtained from CDA and NBO analysis clearly show that CO is a stronger σ-donor than π-acceptor with respect to the charge transferred between complex fragment $Fe(CO)_4$ and the carbonyl ligand. The ability of CO to act as a σ-donor is slightly more pronounced when it is coordinated in an axial position, whereas its π-

acceptor capabilities are almost independent from the coordination site. Table 3.3 shows the partitioning of the electronic interaction between $Fe(CO)_4$ and CO into explicit orbital contributions. It is evident that $OC\rightarrow Fe(CO)_4$ σ-donation occurs *via* orbitals of a_1' and a_2'' symmetry suggesting the main charge transfer from occupied CO(σ) to vacant Fe(d), Fe(s) and Fe(p) orbitals. On the other hand, $OC\leftarrow Fe(CO)_4$ π-back donation is dominated by orbitals of e' and e" symmetry implying charge transfer from occupied Fe(d) into vacant $CO(\pi^*)$ orbitals. Interestingly, there is also a substantial amount of $OC\leftrightarrow Fe(CO)_4$ repulsive polarization involving orbitals of a_2'' (axial CO) and - to a lesser extend - e' and e" (equatorial CO) symmetry.

Table 3.3 CDA-Partitioning of the Electronic Interaction between $Fe(CO)_4$ and CO into Explicit Orbital Contributions.

Orbital	d[a]	b[b]	r[c]	Δ[d]
$\sum A_1'$	0.273	-0.005	0.002	-0.008
$\sum A_2'$	0.000	0.000	0.000	0.000
$\sum A_2''$	0.227	-0.021	-0.263	0.004
$\sum E'$	0.008	0.131	-0.035	0.002
$\sum E''$	0.004	0.174	-0.038	0.002
$\sum$	0.511	0.280	-0.332	0.000

[a] $OC\rightarrow Fe(CO)_4$ σ-donation. [b] $OC\leftarrow Fe(CO)_4$ π-back donation. [c] $OC\leftrightarrow Fe(CO)_4$ repulsive polarization. [d] residual term.

3.3.3 $Fe(CO)_4CS$ (3)

The thiocarbonyl iron tetracarbonyl complex $Fe(CO)_4CS$ was first synthesized by Petz and co-workers and has been extensively studied by this group since that time.[75] The Fe–CS bond length of axial (**3a**) and equatorial (**3b**) thiocarbonyl are calculated to be 1.787 Å and 1.779 Å, respectively. The C–S bond lengths of coordinated thiocarbonyl are 1.551 Å (**3a**) and 1.559 Å (**3b**) and thus slightly longer than the corresponding value of isolated thiocarbonyl, which is calculated to be 1.548 Å. The closely related complex $Fe(CO)_2(PPh_3)_2CS$ has Fe–CS and C–S bond lengths of 1.768 Å and 1.563 Å,[76] respectively, in reasonable agreement with the calculated values.

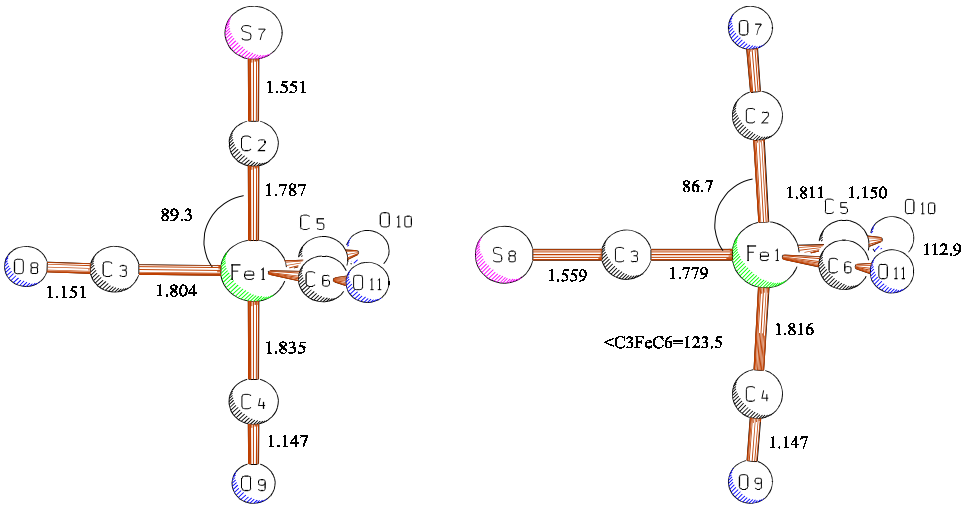

3a **3b**

Figure 3.2.3 Optimized geometries (B3LYP/II) of $(CO)_4FeCS$, axial (**3a**) and equatorial (**3b**) isomers. Bond lengths are given in Å , bond angles in degree.

The $(CO)_4Fe–CS$ bond dissociation energy of 64.2 kcal mol^{-1} is the same for the axial (**3a**) and equatorial (**3b**) isomer. This situation is reflected by IR and NMR data[75a] suggesting that experimentally observed $Fe(CO)_4CS$ is indeed a mixture of the two isomers. The comparison between the experimental and theoretical frequencies values is shown for **3a** and **3b** in Table 3.4. Two C-S bands of 1320 and 1305 cm^{-1} in IR spectrum are observed. [75a] The higher frequency is assigned to **3a**. The lower one must belong to C-S for **3b**. The calculated frequencies of 1341 for **3a** and 1324 cm^{-1} for **3b** are in excellent agreement with experimental results. The C-O bands are also comparable between calculated and measured data. It is noteworthy that the bond dissociation energy of **3** is significantly increased compared to the $(CO)_4Fe–CO$ bond strength of **1.** Other arrangements of the thiocarbonyl ligand were found to be energetically highly unfavourable.[77]

According to the CDA results, thiocarbonyl is a slightly stronger σ-donating than π-accepting ligand. The difference of these charge contributions is, however, small and with regard to the negligible energy difference of 0.1 kcal mol^{-1} between isomers **3a** and **3b**, one could conclude that there is no distinct ligand site preference of CS due to almost equal amounts of σ-donation and π-back donation. Although the NBO analysis deviates sporadically from this results (*e.g.* in **3b** CS is predicted to be

a slightly better π-acceptor than σ-donor), this does not change the indecisive character of CS with respect to the coordination site. Both partitioning approaches thus agree in that CS is a better π-acceptor than CO.

Table 3.4 Vibrational Frequencies γ (cm $^{-1}$) and IR intensity (km mol $^{-1}$) for $Fe(CO)_4CS$ (**3a** and **3b** isomers)

3a				**3b**			
	mode	Exp.[a,b] γ	Calc. γ(IR Int.)		mode	Exp.[a,b] γ	Calc. γ(IR Int.)
A_1	[CO]		2167(446)	A_1	[CO]		2173(241)
	[CO]		2121(332)		[CO]		2118(370)
	[CS]	1320	1341(818)		[CS]	1305	1324(818)
	[δMCO]		611(168)		[δCMC]		659(174)
	[MC]	465 [c]	458(14)		[δMCO]		475(4)
	[MC]		429(6)		[MC]	465 [c]	466(28)
	[MC]		377(0)		[δMCO]		425(3)
	[δMCO]		108(0)		[MC]		384(0)
A_2	[δMCO]		371(0)		[δMCO]		104(0)
E	[CO]		2096(1113)		[δCMC]		62(0)
	[δMCO]		651(121)	A_2	[δMCO]		566
	[δMCO]		547(1)		[δMCO]		369
	[δMCO]		485(1)		[δCMC]		95
	[δMCO]		420(11)	B_1	[CO]		2100(1067)
	[δMCS]		355(4)		[δCMC]		662(120)
	[δMCO]		102(0)		[δMCO]		482(7)
	[δMCS]		84(0)		[δMCS]		407(1)
	[δCMC]		44(0)		[δMCS]		330(3)
					[δCMC]		100(0)
					[δMCS]		31(0)
				B_2	[CO]		2121(1282)
					[MC]		611(111)
					[δMCO]		555(0)
					[δMCS]		461(9)
					[δMCS]		347(5)
					[δMCO]		105(0)
					[δMCS]		79(0)

[a] see ref 75a [b] C-O: 2103, 2100, 2000 cm $^{-1}$ [c] Fe-C: 465 cm $^{-1}$ is listed here for both isomers for comparison.

3.3.4 $Fe(CO)_4N_2$ (4)

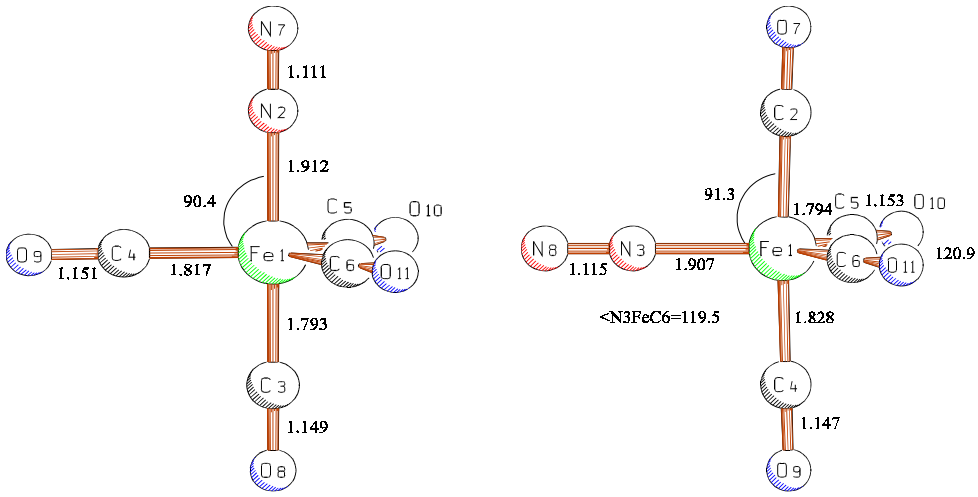

Figure 3.2.4 Optimized geometries (B3LYP/II) of $(CO)_4Fe\,N_2$, axial (**4a**) and equatorial (**4b**) isomers . Bond lengths are given in Å , bond angles in degree.

The structures of axial (**4a**) and equatorial (**4b**) dinitrogen iron tetracarbonyl $Fe(CO)_4N_2$ show Fe–N_2 bond lengths of 1.912 Å and 1.907 Å, respectively.[78] This contrasts the results of Radius *et al.*,[47] who predict that the Fe–N_2 bond length of axial N_2 is shorter than of equatorial N_2. The small energy difference of 0.5 kcal mol^{-1} between **4a** and **4b**, is in favour of the axial isomer, again opposite to the trend suggested by the same group, which is based on bond dissociation *enthalpies*.[47] Although, the reaction of $Fe(CO)_5$ with N_2 in polyethylene film implies that N_2 *may* occupy an equatorial rather an axial coordination site,[79] photolysis experiments of $Fe(CO)_5$ in nitrogen-containing matrices[60a,c] show an opposite behaviour, that is a more stable axial than equatorial isomer. The calculated energy difference is, however, too small to provide a reasonable and conclusive solution to these contradictory experimental results.

Mössbauer spectra of several dinitrogen complexes,[80] suggest that N_2 is a stronger π-acceptor than σ-donor. Whereas this is certainly true for complexes $M(CO)_5N_2$ (M = Cr, Mo, W), it does not apply for $Ni(CO)_3N_2$.[37] In the present case, the CDA and NBO results both yield a consistent trend predicting the extend of N_2←$Fe(CO)_4$ π-back donation to be somewhat smaller than N_2→$Fe(CO)_4$ σ-donation. The difference in the extend of σ-donation and π-back donation is, however,

negligible and in conjunction with the very small energy difference between the isomers, there is no pronounced tendency of N_2 to coordinate either into an axial or equatorial coordination site. For the equatorial isomer **4b** the NBO method even gives exactly the same numerical value for σ-donation and π-back donation.

3.3.5 $Fe(CO)_4NO^+$ (5)

It is found that axial $Fe(CO)_4NO^+$ (**5a**) is considerably less stable than its equatorial isomer (**5b**) by 20.7 kcal mol^{-1} indicating a strong preference of coordination at the equatorial rather than axial site. The Fe–NO^+ bond length of equatorial $Fe(CO)_4NO^+$ (**5b**) is calculated to be 1.695 Å and compared to its Fe–CO bond lengths of 1.879 Å and 1.869Å shorter by approximately 0.2 Å. This difference and the absolute bond lengths are in good agreement with experimental findings of the closely related $Fe(CO)_2(NO)_2$ complex: the deviations are less than 0.014 Å.[81] The Fe-NO^+ bond dissociation energy D_o is 105.1 kcal mol^{-1} indicating the strongest Fe–L bond of all complexes studied in this work.[82]

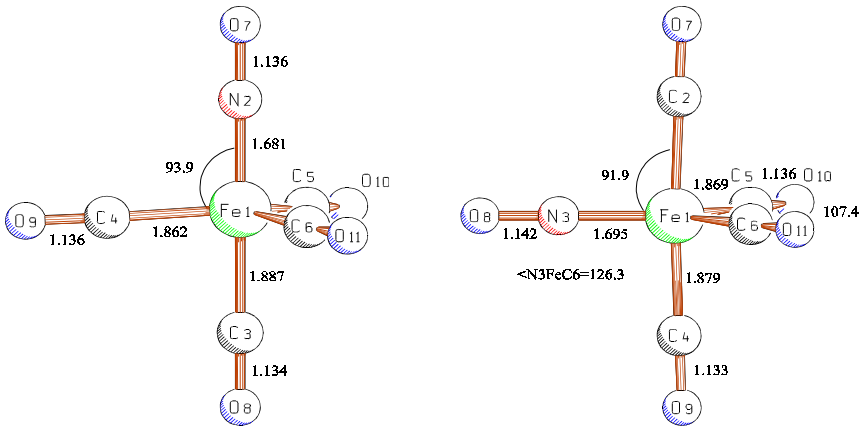

5a **5b**

Figure 3.2.5 Optimized geometries (B3LYP/II) of $(CO)_4Fe\ NO^+$, axial (**5a**) and equatorial (**5b**) isomers. Bond lengths are given in Å, bond angles in degree.

The results from both charge partitioning approaches show that NO^+ is a very poor σ-donor but at the same time an excellent π-acceptor. In fact, the NBO data even suggest the extent of π-back donation to be almost five times larger than the

extent of σ-donation. The reason is clear that the positive charge of the ligand lowers its orbital energies, which in turn alleviates π-backdonation significantly (Scheme 3.2). In conjunction with the large energy difference between **5a** and **5b** this convincingly demonstrates a pronounced tendency to coordinate in an equatorial coordination site.

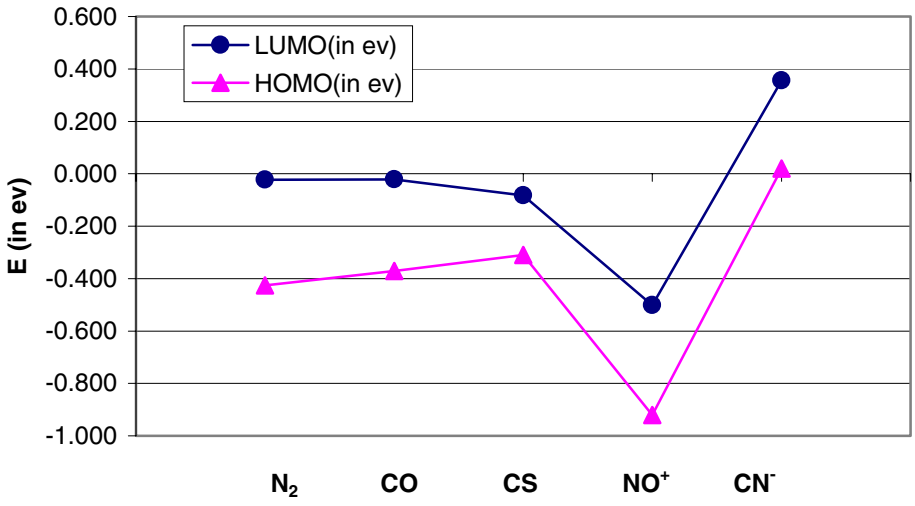

Scheme 3.2 Schematic representation of the relative energy for HOMO and LUMO in free two-atom ligand molecules at the B3LYP/II level.

3.3.6 $Fe(CO)_4CN^-$ (6) and $Fe(CO)_4NC^-$ (7)

In a previous paper, it was reported that M–CN^- and M–NC^- bonds are rather strong for transition metals of group 6 and 10.[37] The extension of these studies to analogous iron complexes shows that Fe–CN^- and Fe–NC^- bonds also have remarkably high bond dissociation energies ranging from 72.7 to 96.5 kcal mol^{-1}. Except for axial $Fe(CO)_4CN^-$ (**6a**), the bond dissociation energies are, however, smaller than those of corresponding $Fe(CO)_4NO^+$ isomers. This is also reflected by the Fe–CN^- and Fe–NC^- bonds, which are significantly elongated by 0.3 Å compared

to their corresponding NO^+ analogues. Note, that the bond dissociation energy is always higher for Fe–CN^- than for Fe–NC^-.

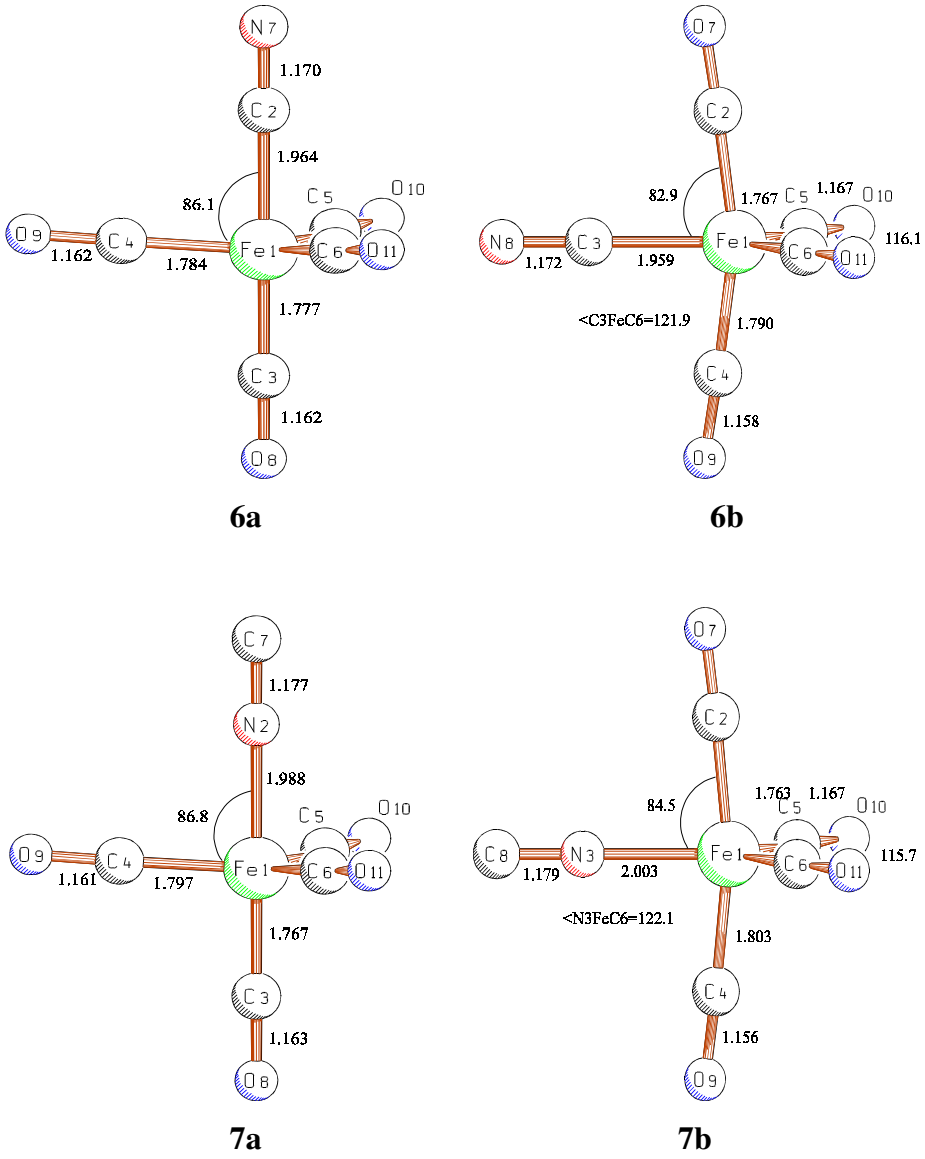

Figure 3.2.6 Optimized geometries (B3LYP/II) of $(CO)_4FeCN^-$ and $(CO)_4FeNC^-$, axial (**6a**, **7a**) and equatorial (**6b**, **7b**) isomers. Bond lengths are given in Å , bond angles in degree.

For the linkage isomers $Fe(CO)_4CN^-$ (**6a** and **6b**) and $Fe(CO)_4NC^-$ (**7a** and **7b**) only axially coordinated cyanide/isocyanide leads to the energetically most favoured complex. The energy differences favouring the axial isomers are 6.7 kcal mol^{-1} for the cyanide and 6.3 kcal mol^{-1} for the isocyanide complex. For the cyanide complex,

this relative stability is supported by the crystallographic data of $[Fe(CO)_4CN][N(P(C_6H_5)_3)]$ in which the $[Fe(CO)_4CN]^-$ moiety forms a distorted trigonal bipyramid.[83] As expected, the calculated bond lengths of the Fe–CN bond and of the axial and equatorial Fe–CO bonds are somewhat larger compared to their corresponding values measured in a *crystal* environment. The differences are, however, in an acceptable range of 0.02 to 0.05 Å.

With respect to the cyanide/isocynaide donor-acceptor strength, CDA and NBO results present a consistent picture indicating that CN^- as well as NC^- show an opposite behaviour compared with NO^+. Thus, an extremely pronounced extend of σ-donation combined with an almost vanishing amount of π-back donation is predicted for these ligands. The remarkable site preference, which governs the ligands in axial coordination sites of pentacoordinated iron complexes is nicely resembled by the energy difference that favours the axial isomers **6a** and **7a** over the equatorial isomers **6b** and **7b**, respectively.

3.3.7 $Fe(CO)_4(\eta^2\text{-}C_2H_4)$ (8) and $Fe(CO)_4(\eta^2\text{-}C_2H_2)$ (9)

The bond dissociation energy D_o of the equatorial $Fe(CO)_4(\eta^2\text{-}C_2H_4)$ isomer **8b** is 39.2 kcal mol^{-1} and close to the experimental value of 37.2 kcal mol^{-1} [84] and other theoretical data. [48] The calculated $Fe–C_{ethylene}$ bond lengths of 2.145 Å resembles the experimental value of 2.117 Å based on microwave spectra reasonably well.[85] Other structural parameters like the axial and equatorial Fe–CO bond lengths or the ethylenic C–C bond lengths of coordinated ethylene are in particular good agreement with experimental data and differ by less than 0.015 Å.[85]

The corresponding acetylene complex **9b** has a calculated bond dissociation energy D_o of 37.3 kcal mol^{-1}. The $Fe–C_{acetylene}$ bond lengths is 2.097 Å which is in line with the experimental value of 2.048 Å reported for the related $Fe(CO)_2(POMe_3)(\eta^2\text{-}C_2Ph_2)$ complex.[86] The same holds for the bond length of the acetylenic C–C bond, which is calculated to be 1.259 Å (exp. 1.263 Å).[86] At the B3LYP/II level, we find that the C–C triple bond is slightly lengthened upon complex formation by about 0.06 Å implying a decrease in its bond order.

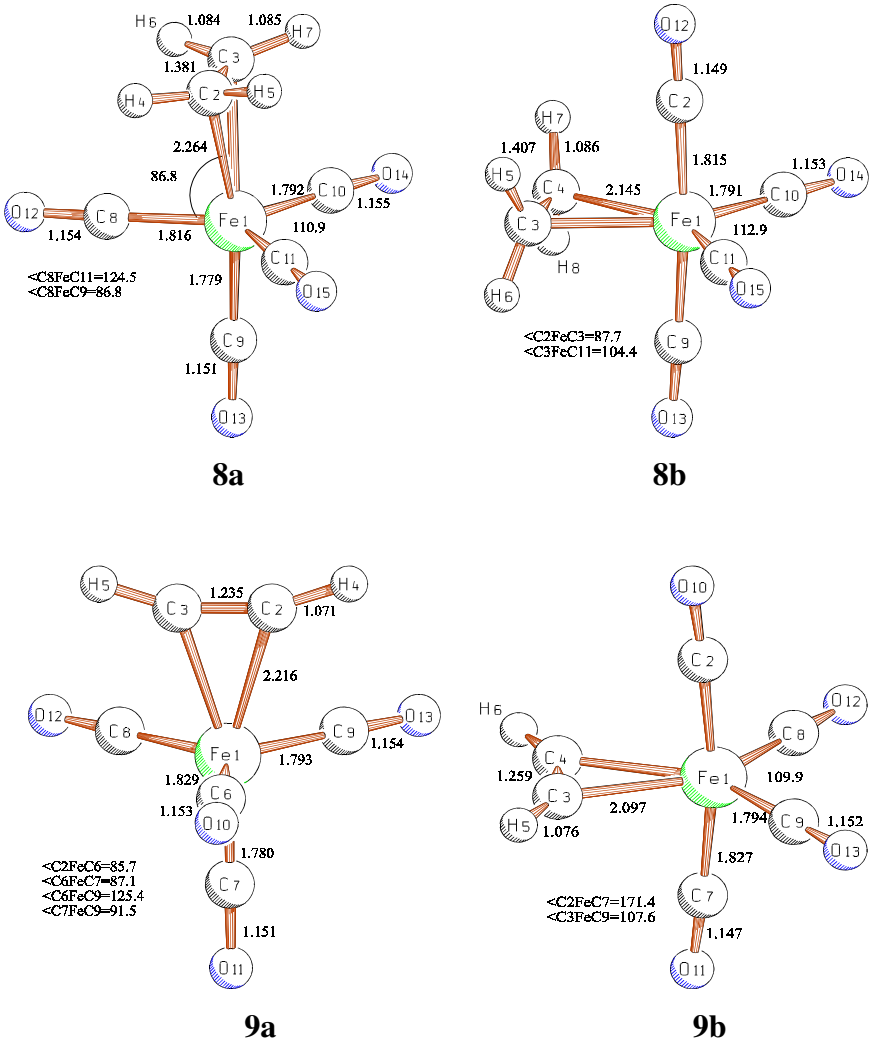

Figure 3.2.7 Optimized geometries (B3LYP/II) of $(CO)_4Fe(C_2H_4)$ and $(CO)_4Fe(C_2H_2)$, axial (**8a** , **9a**) and equatorial (**8b** , **9b**) isomers. Bond lengths are given in Å , bond angles in degree.

For ethylene and acetylene it is found that σ-donation dominates over π-back donation, which is consistent with previous theoretical results.[38,51] Surprisingly, this trend objects the generally applied rule for predicting the site preference of ligands that are strong σ-donors.[45,46] According to this, ethylene as well as acetylene should prefer an axial rather than an equatorial coordination site. We find, however that the axial isomers $Fe(CO)_4(\eta^2\text{-}C_2H_4)$ (**8a**) and $Fe(CO)_4(\eta^2\text{-}C_2H_2)$ (**9a**) are substantially less stable than their equatorial counterparts by 8.6 and 10.7 kcal mol^{-1}, respectively. In fact, the axial isomers are even found to represent transition states rather than local minima. Corresponding NBO data do not solve this discrepancy either, because the charge contributions obtained from this approach are not meaningful due to

indistinguishable σ-donating/π-accepting orbitals. Therefore, no definite classification of the ligand site preference in terms of a σ-donation/π back donation scheme is possible within the present approach.

Note that although the absolute values of σ-donation and π-back donation are somewhat larger for the acetylene complex than for the ethylene complex, this does not imply that the bond dissociation energy for Fe-$C_{acetylene}$ is higher than the bond dissociation energy of Fe–$C_{ethylene}$.[38]

3.3.8 $Fe(CO)_4CCH_2$ (10)

The calculated Fe-$C_{vinylidene}$ bond length of **10b** is 1.780 Å, which is consistent with experimental values ranging from 1.74 Å to 1.80 Å found for related complexes.[87] Similarly, the calculated C–C distance of 1.310 Å is also in reasonable agreement with experimental values in the range of 1.26 Å to 1.33 Å .[87]

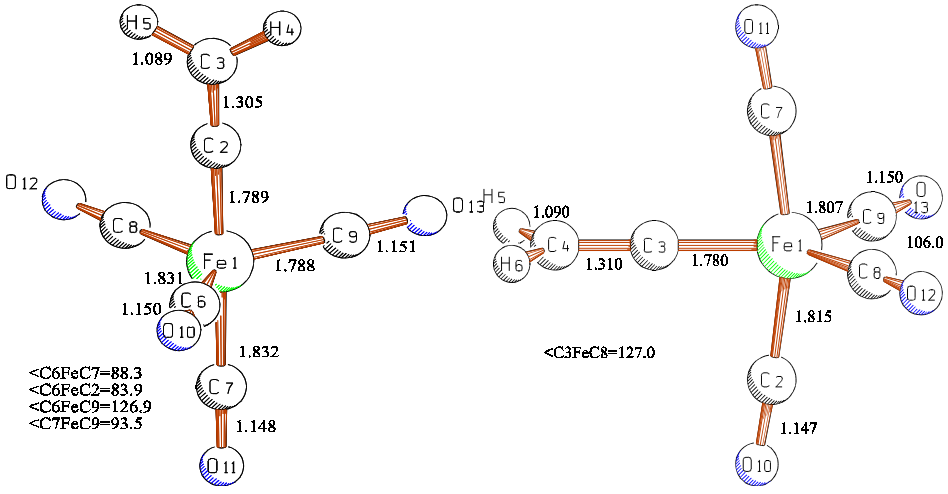

Figure 3.2.8 Optimized geometries (B3LYP/II) of $(CO)_4Fe(CCH_2)$, axial (**10a**) and equatorial (**10b**) isomers. Bond lengths are given in Å , bond angles in degree.

The bond dissociation energy of the Fe–CCH_2 bond is calculated to be 83.8 kcal mol^{-1} and is thus comparable in strength to the corresponding Fe–CN^- bond. The CDA results imply that the vinylidene ligand is a significantly better σ-donor than π-

acceptor. This, however, does not result in a distinct preference of the axial isomer. In fact, axial $Fe(CO)_4CCH_2$ (**10a**) is found to be a transition state structure and less stable than its corresponding equatorial isomer (**10b**) by 8.7 kcal mol^{-1}. The data from the corresponding NBO analysis, on the other hand suggest an opposite σ-donor/π-acceptor behaviour, that is, vinylidene acting as a somewhat stronger π-acceptor than σ-donor. With respect to the relative stabilities of the two isomers this is in agreement with the general classification of a stronger π-accepting ligand preferring an equatorial coordination site.[45,46]

3.3.9 $Fe(CO)_4CH_2$ (11) and $Fe(CO)_4CF_2$(12)

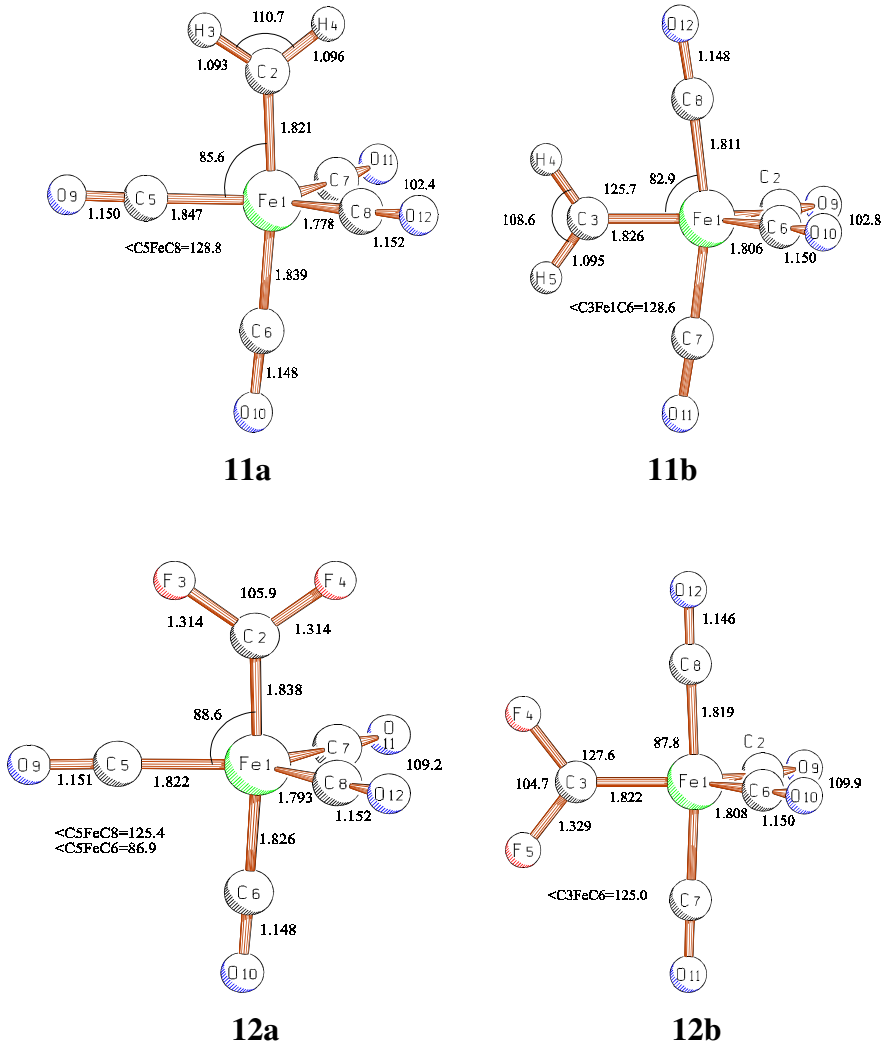

11a **11b**

12a **12b**

Figure 3.2.9 Optimized geometries (B3LYP/II) of $(CO)_4Fe(CH_2)$ and $(CO)_4Fe(CF_2)$, axial (**11a**, **12a**) and equatorial (**11b**, **12b**) isomers. Bond lengths are given in Å , bond angles in degree.

The Fe–CH_2 bond length of equatorial carbene iron tetracarbonyl **11b** is calculated to be 1.826 Å and significantly shorter than the experimental values ranging from 2.001 – 2.010 Å reported for hetero substituted, electron-rich carbene iron tetracarbonyl complexes.[88] Note, however, that the calculated iron-carbene bond length is still substantially larger than the experimental iron-carbyne bond of 1.734 Å reported for $[(CO)_3PPh_3FeC(N\textit{i}\text{-}Pr_2)]^+$.[89]

The iron-carbene bond length of difluorocarbene iron tetracarbonyl **12b** is shorter by 0.004 Å than its corresponding Fe–CH_2 bond analogue. The calculated bond dissociation energies D_o of 87.4 kcal mol^{-1} (**11b**) and 64.3 kcal mol^{-1} (**12b**) reveal an interesting feature of the complexes: the shorter bond found for **12b** does not necessarily imply a stronger bond. The same trend is also revealed when comparing the comparatively short Fe–CO bond lengths of **1** (1.805 Å) with the longer Fe–CH_2 and Fe-CF_2 bonds of **11b** and **12b**. Such an inversed correlation has been found before and was explained by the hybridization of the donor lone-pair orbital.[90] A higher s-character results in a more compact and more tightly bound donor lone-pair orbital. Whereas the former effect tends to shorten the donor-acceptor bond, the latter leads to a less pronounced donor-acceptor interaction yielding a weaker bond. With respect to our calculated bond dissociation energies this implies that the donor lone-pair orbital of the CF_2 ligand has a higher s-character than CH_2, and that the donor lone-pair of CO has an even higher s-character than CF_2. This, however, is in perfect agreement with the NBO data.[91]

As it was shown for analogous $W(CO)_5CH_2$ and $W(CO)_5CF_2$ complexes,[38c] the CDA suggests that both carbene ligands are better σ-donors than π-acceptors. This, however, does not match with the relative stabilities of the axial and equatorial isomers in that the axial isomers $Fe(CO)_4CH_2$ (**11a**) and $Fe(CO)_4CF_2$ (**12a**) represent transition states, which are less stable than their corresponding equatorial counterparts (**11b** and **12b**) by 8.3 and 4.6 kcal mol^{-1}, respectively. Referring to the corresponding NBO data, however, suggests that CH_2 as well as CF_2 are slightly better π-acceptors than σ-donors. Although the numerical differences in these charge contributions are comparatively small they are still consistent with an energy wise more stable equatorial than axial isomer.

3.3.10 $Fe(CO)_4(\eta^2\text{-}H_2)$ (13)

A recent theoretical examination reports on equatorial η^2-dihydrogen iron tetracarbonyl and its relevance to the water gas shift reaction.[49] It was found that the energy difference between this complex and the classical dihydride complex is quite small, with the latter isomer being more stable by 8 – 12 kcal mol^{-1}.[49] In this paper I focus only on η^2-dihydrogen isomers in which molecular hydrogen is either bound in an axial (**13a**) or equatorial (**13b**) coordination site. In both isomers, the H–H bond length of coordinated H_2 is calculated to be in the range of 0.8 – 0.9 Å. This resembles the value of free H_2 quite closely indicating that these complexes indeed contain molecular hydrogen rather than two hydrides. From an energetic point of view, the difference between axial and equatorial coordination of H_2 is small and the Fe–H_2 bond dissociation energies differ by only 1.6 kcal mol^{-1}. The calculated bond dissociation energies of 16.5 (**13a**) and 18.5 kcal mol^{-1} (**13b**) are the smallest found in this study and comparable in size to analogous bond values calculated for complexes of the general type $M(CO)_5(\eta^2\text{-}H_2)$ (M= Cr, Mo, W).[92]

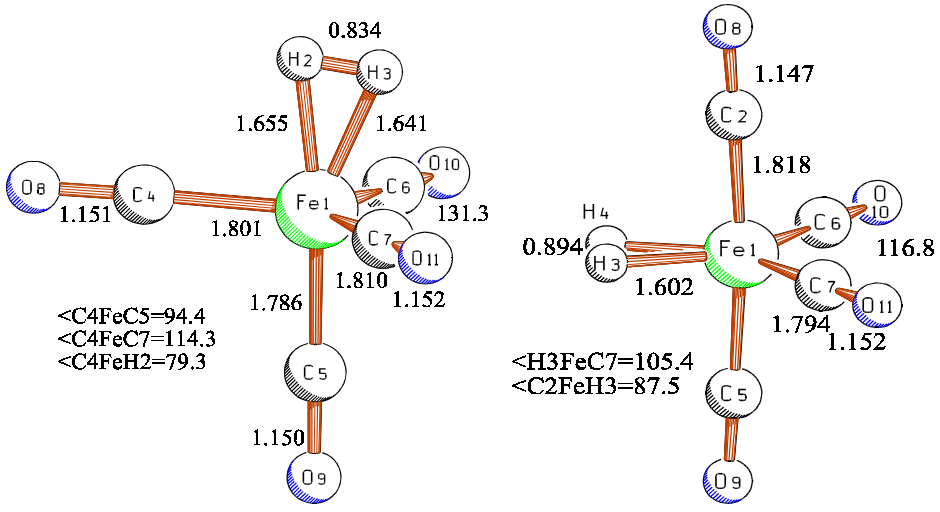

Figure 3.2.10 Optimized geometries (B3LYP/II) of $(CO)_4Fe(H_2)$, axial (**13a**) and equatorial (**13b**) isomers. Bond lengths are given in Å , bond angles in degree.

The CDA results show a non-negligible amount of π-back donation for both the axial as well as the equatorial isomers and a dominant charge contribution due to $H_2 \rightarrow Fe(CO)_4$ σ-donation. Consideration of an energetically favoured equatorial isomer **13b** leads to the same discrepancy found before for the corresponding acetylene and ethylene iron tetracarbonyl complexes. Suitable NBO data are not available for coordinated molecular hydrogen and thus an unequivocal characterization of the η^2-H_2 in terms of its relative σ-donor/π-acceptor strengths is not possible at this stage.

3.3.11 $Fe(CO)_4NH_3$ (14) and $Fe(CO)_4NF_3$ (15)

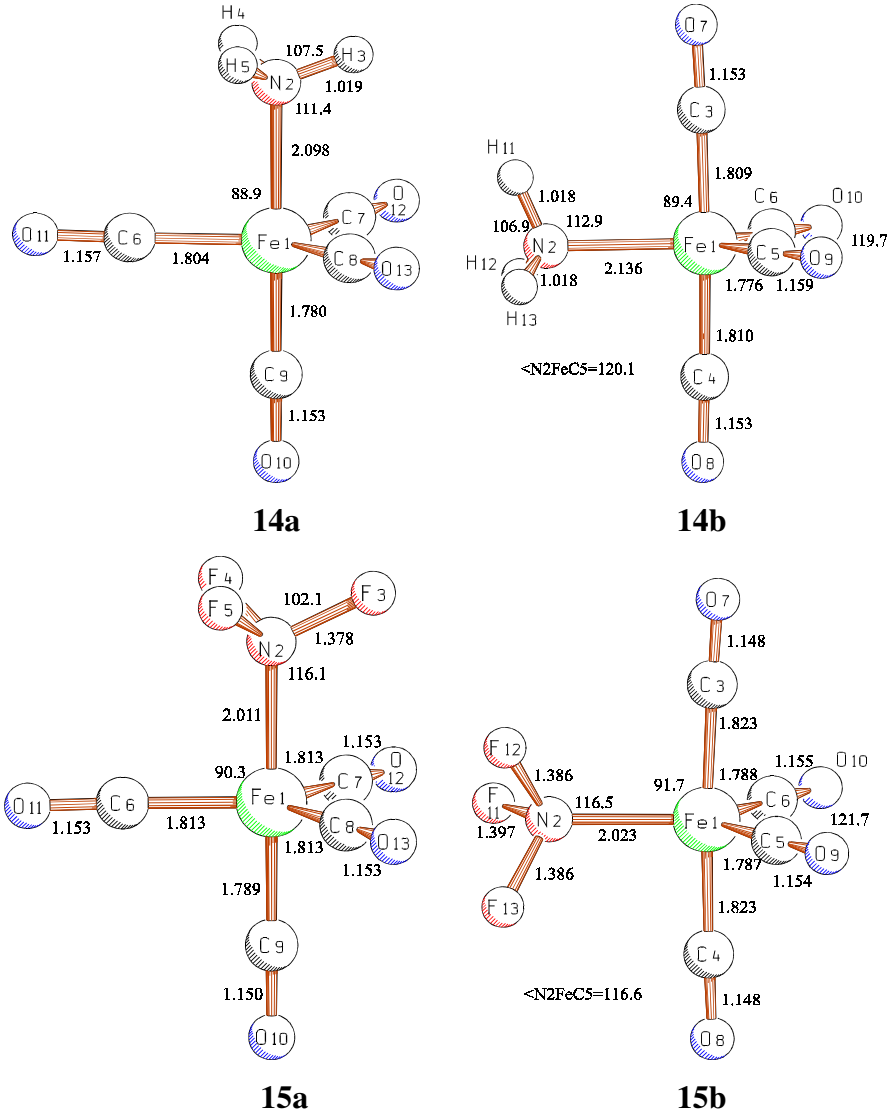

Figure 3.2.11 Optimized geometries (B3LYP/II) of $(CO)_4Fe(NH_3)$ and $(CO)_4Fe(NF_3)$, axial (**14a**, **15a**) and equatorial (**14b**, **15b**) isomers. Bond lengths are given in Å , bond angles in degree.

For both complexes the axial isomers (**14a** and **15a**) are more stable than their equatorial pendants (**14b** and **15b**). which agrees with crystallographic data[93] and IR spectra of related compounds.[93,94] The calculated differences in energy are 6.4 and 3.0 kcal mol^{-1}, respectively, implying a clear preference of these ligands towards axial coordination sites. The estimates for the Fe–NH_3 and Fe–NF_3 bond dissociation energies are 39.1 and 23.5 kcal mol^{-1}. These values are significantly smaller than those found for the Fe–CO bond in **1**, and are consistent with the experimentally observed low stability of such iron-amine complexes.[95] The comparatively long Fe–N bond lengths in the axial isomers of 2.098 Å (**14a**) and 2.011 (**15a**) with respect to that of Fe-C in **1**, respectively, are also consistent with low bond dissociation energies.

NH_3 and NF_3 are found to be stronger σ-donors than π-acceptors. For both ligands, the CDA yields π-back donations that are effectively zero. Based on the corresponding NBO data and previous studies,[96] it is thus justified to take NH_3 as an almost pure σ-donor. This bonding situation hardly changes when going to NF_3 and the only apparent difference is a slightly increased amount of π-back donation.

3.3.12 $Fe(CO)_4PH_3$ (16) and $Fe(CO)_4PF_3$ (17)

The energy difference between axial and equatorial $Fe(CO)_4PH_3$ (**16a** and **16b**) is 2.7 kcal mol^{-1} with isomer **16a** being more stable. Although the same trend is observed for the related $Fe(CO)_4PF_3$ isomers (**17a** and **17b**), the energy difference is reduced to 1.0 kcal mol^{-1}. The Fe–PH_3 and Fe–PF_3 bond dissociation energies for the axial isomers are calculated to be 38.9 and 45.2 kcal mol^{-1}, respectively. Interestingly, the Fe-PH_3 bond strength of **16a** is somewhat lower than that for Fe–NH_3 of **14a**, which is opposite to the trend reported previously for a series of related complexes $M(CO)_5XH_3$ (M = Cr, Mo, W and X = N, P).[96]

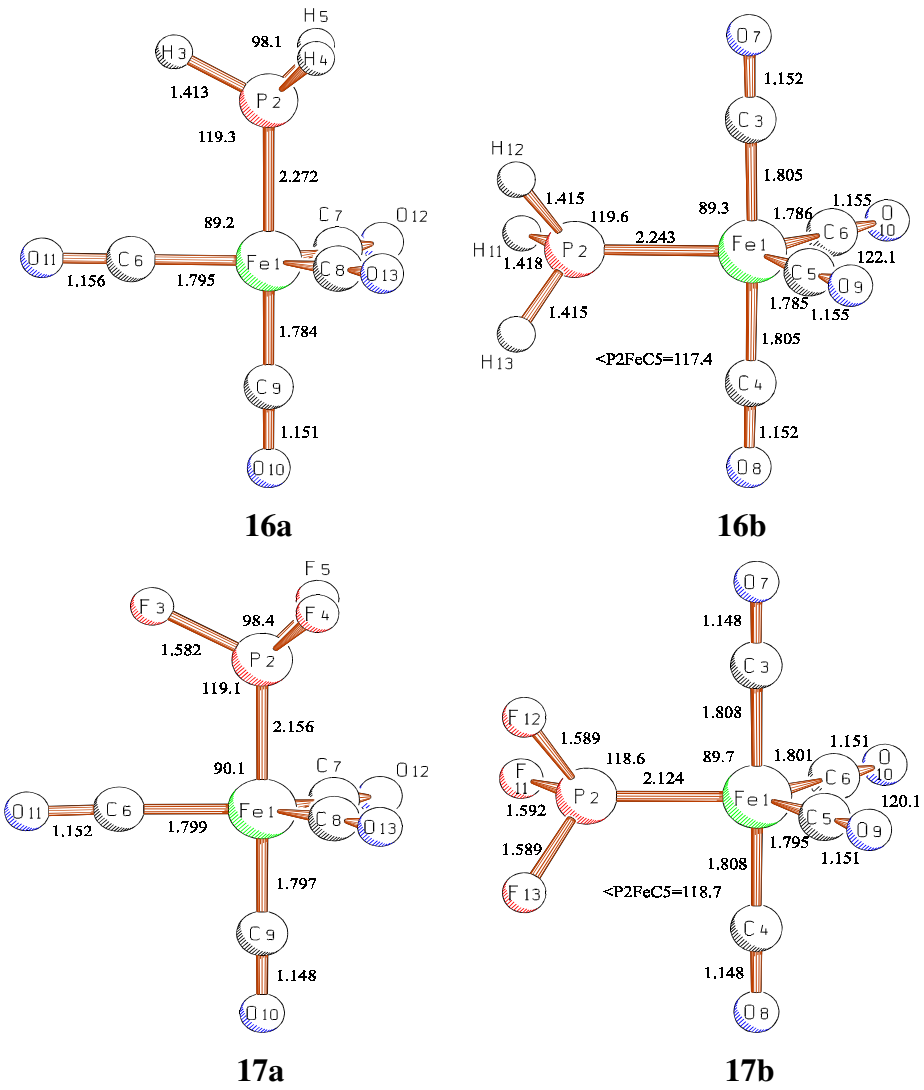

Figure 3.2.12 Optimized geometries (B3LYP/II) of $(CO)_4Fe(PH_3)$ and $(CO)_4Fe(PF_3)$, axial (**16a**, **17a**) and equatorial (**16b**, **17b**) isomers. Bond lengths are given in Å, bond angles in degree.

For isomers **16a** and **16b**, the Fe–PH_3 bond lengths are calculated to be 2.272 Å and 2.243 Å, respectively. Thus, these bond distances are substantially longer than the corresponding Fe–PF_3 bond lengths of 2.156 Å and 2.124 Å found for **17a** and **17b**. This is also reflected by the invariably higher bond dissociation energies of 45.2 and 44.1 kcal mol^{-1} calculated for the latter pair of isomers leading to a direct correlation of Fe–P bond lengths and its bond strengths. It should be pointed out that Branchadell *et al*. found that this correlation is in general absent for a series of different phosphane iron tetracarbonyls.[50,97]

The CDA and NBO results classify both PH_3 and PF_3 to be better σ-donors than π-acceptors. Compared to analogous NH_3 and NF_3 complexes, the amount of σ-donation is higher for the phosphanes, and the extend of π-back donation is non-negligible. With respect to the small energy differences of the axial and equatorial isomers of PH_3 and PF_3, respectively, the axial site-preference of these ligand is, however, less pronounced than for NH_3 and NF_3.

3.3.13 Ligand Site Preference in $Fe(CO)_4L$ Complexes

Figure 3.3 line up the ratios of σ-donation and π-back donation d/b (*viz.* d/b from CDA and q(σ)L/q(π)L from NBO analysis) for each ligand L according to its most stable isomer with the energy differences E_{rel}, calculated relative to the axial isomer of $Fe(CO)_4L$. Thus d/b ≥ 1 indicates stronger σ-donating ligands, whereas d/b ≤ 1 represents stronger π-acceptors. Furthermore, $E_{rel} < 0$ shows that the equatorial isomer is more stable than the axial one, while $E_{rel} > 0$ indicates the opposite trend. Due to their nature as transition states, the axial ethylene (**8a**), acetylene (**9a**), vinylidene (**10a**), carbene (**11a**) and difluorcarbene (**12a**) iron tetracarbonyl complexes are omitted in this Figure. Only structures that were verified as local minima are considered in this comparison.

The first point revealed by the data shown in Figure 3.3 is that the relative donor-acceptor strengths d/b predicted by the CDA and the NBO analysis are generally in good agreement with each other. Both partitioning schemes occasionally even give almost similar numerical values for the d/b ratios. The general trend predicted with respect to the extend of σ-donation/π–back donation supports the conventional classification of the ligand site preference in trigonal bipyramidal d^8-complexes.[45,46] Thus, a strong π-acceptor and poor σ- donor like NO^+ (d/b < 0.5) prefers an equatorial coordination site, which is clearly shown by a large negative value of E_{rel}. On the other hand, a strong σ-donor and poor π-acceptors like NC^- (d/b >> 1) only gives an energetically favourable structures if it is coordinated axially. This in turn leads to large positive value of E_{rel} (Figure 3.3a). This trend also holds for those ligands with smaller d/b ratios (d/b > 1) and ligands like CN^-, NH_3, NF_3 PH_3 and PF_3, which still exhibit a distinct affinity for the coordination in axial position.

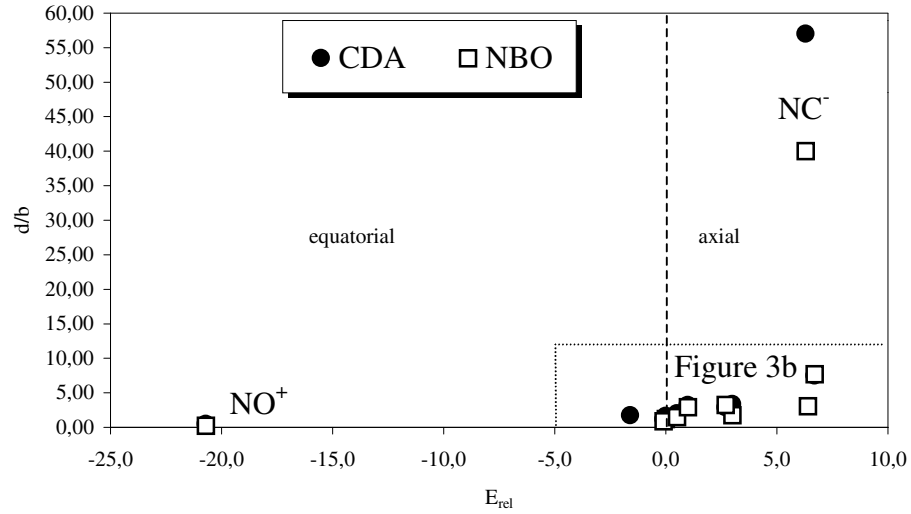

(a)

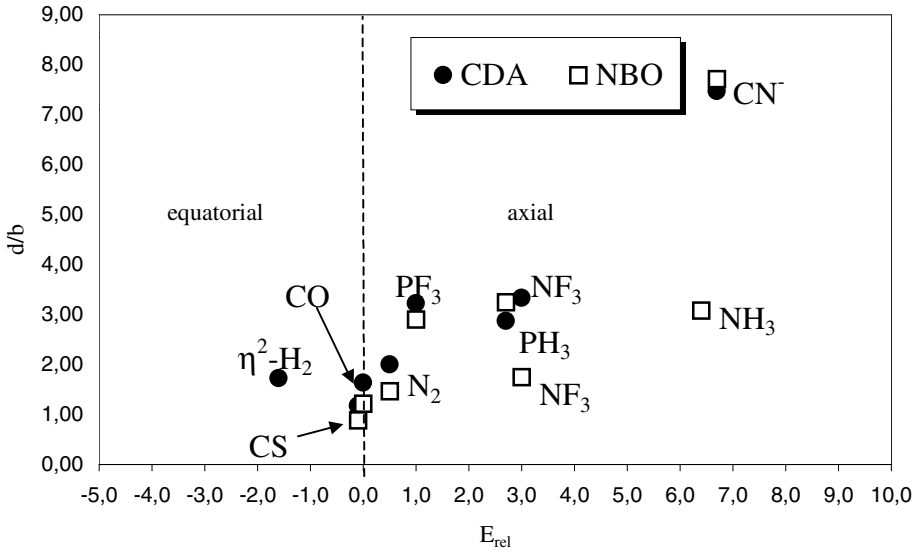

(b)

Figure 3.3 Plot of the calculated σ-donor/π-acceptor ratio d/b of the most stable isomers found for $Fe(CO)_4L$ and the energy difference $E_{rel} = E_{equatorial} - E_{axial}$. Energies are in kcal mol^{-1}. (a) plot with respect to all ligands L covered in the text. (b) enlarged subsection showing those ligands with smaller d/b ratios explicitly.

This is clearly shown by energy differences between their respective axial and equatorial isomers that are greater or equal than 1 kcal mol^{-1} (Figure 3.3b). Ligands with d/b ratios close to unity, however, result in *absolute* values for E_{rel} of less than 1 kcal mol^{-1}, indicating a somewhat indifferent ligand site preference. For the

complexes $Fe(CO)_4CS$ and $Fe(CO)_4N_2$ there is hardly any energy difference between their respective axial and equatorial isomers ($E_{rel} \approx 0$), which is consistent with the almost identical amounts of σ-donation and π-back donation predicted by the CDA method and the NBO analyses.

Note that amongst the various ligands considered in this study, only one noteworthy exception of the correlation between the d/b ratios and the energy difference between axial and equatorial isomers is found. Only the complex involving molecular hydrogen reveals an inverse trend with regard to the ligand site preference. Thus, although the equatorial isomer of $Fe(CO)_4(\eta^2\text{-}H_2)$ is more stable than its axial counterpart, its d/b ratio indicates a more pronounced σ-donating character for H_2. This however, might be due to an insufficiently large basis set used in the description of iron-coordinated molecular hydrogen. This point is under study with larger basis sets and different methods.

3.4 Summary

The theoretically predicted structural parameters of $Fe(CO)_4L$ complexes obtained at the B3LYP/II level of theory are in very good agreement with available experimental results and previous theoretical estimates, as are the refined bond dissociation energies using the CCSD(T)/II//B3LYP/II combination of theoretical methods. The strongest Fe–L bonds are found for the ligands NO^+, CN^-, CH_2 and CCH_2 with bond dissociation energies of 105.1, 96.5, 87.4 and 83.8 kcal mol^{-1}, respectively. For the corresponding complexes of NC^-, CF_2 and CS, these values decrease significantly to 78.6, 64.3 and 64.2 kcal mol^{-1}, respectively. Even weaker bonds in the range of 45.2 to 37.3 kcal mol^{-1} are found for CO, $\eta^2\text{-}C_2H_4$, $\eta^2\text{-}C_2H_2$, NH_3, PH_3 and PF_3, while the bond dissociation energies of complexes involving NF_3, N_2 and $\eta^2\text{-}H_2$ drop to less than 23.5 kcal mol^{-1}.

Both charge partitioning schemes lead to almost identical results suggesting that strong π-accepting ligands like NO^+ prefer equatorial coordination sites of $Fe(CO)_4L$ complexes, while strong σ-donor like CN^- and NC^- favor axial positions. This ligand site preference is found to be less pronounced as the ratio between the extend of σ-donation and π-back donation (d/b) approaches unity. However, ligands

with moderately large d/b values like NH_3, NF_3, PH_3, and PF_3 still show a pronounced axial preference. Ligands like CS and N_2, on the other hand, have almost equal charge contributions for σ-donation and π-back donation and consequently are thus characterized by an indifferent attitude with respect to the site preference in trigonal bipyramidal iron (d^8) complexes.

Chapter 4. Carbene-, Carbyne-, and Carbon Complexes of Iron — Possibility to Synthesize a Low-Valent Transition Metal Complex with a Neutral Carbon Atom as Terminal Ligand $(CO)_4FeC$

4.1 Introduction

Transition metal (TM) alkyl compounds which have a TM-CR_3 single bond are already known since 1848, when Frankland accidentally synthesized diethylzinc while he attempted to prepare a free ethyl radical. [2] Molecules with a TM=CR_2 double bond [98,99] and TM≡CR triple bond [100,101] became much later isolated. TM carbene and carbyne complexes have been the focus of intensive experimental investigations since that time, because it was soon recognized that they are versatile compounds for organometallic synthesis.[102] The bonding situation in molecules with transition metal-carbon multiple bonds attracted also the interest of theoreticians, who were intrigued by the finding that there are two classes of carbene and carbyne complexes which exhibit different chemical behavior. The different reactivity was explained with a bonding model which suggests different metal-carbene[103] and metal-carbyne[104] interactions in the two classes of compounds. It was proposed that one class of compounds have donor-acceptor metal-carbon bonds, while the other class has normal (shared-electron) covalent bonds where the metal and the carbon atom each contribute one electron to a two-electron bond. This is schematically shown in Scheme 4.1. Very recent *ab initio* calculations proved that the bonding situations depicted in Scheme 4.1 are useful models for Fischer-type and Schrock-type carbene and carbyne complexes having donor-acceptor bonds or shared-electron interactions, respectively.[38c] Because the metal-carbon bonds in Schrock-type compounds are not donor-acceptor bonds, they are better called alkylidenes and alkylidynes rather than carbene and carbyne complexes.

The next member in the series of metal-carbon bonds TM-CR_3, TM-CR_2, TM-CR is a bond with a terminal carbon atom TM-C. Transition metal carbide complexes are experimentally known, but all except one feature carbon atoms with at least two nearest neighbors. [105] The only example of a TM complex with a terminal carbon atom is the anion $(NRAr)_3MoC^-$ which is isoelectronic to the nitride complex $(NRAr)_3MoN$ (R = $C(CD_3)_2CH_3$, Ar = $C_6H_3Me_2$-3,5), [106] Scheme 4.1 shows also bonding models for a terminal TM-C

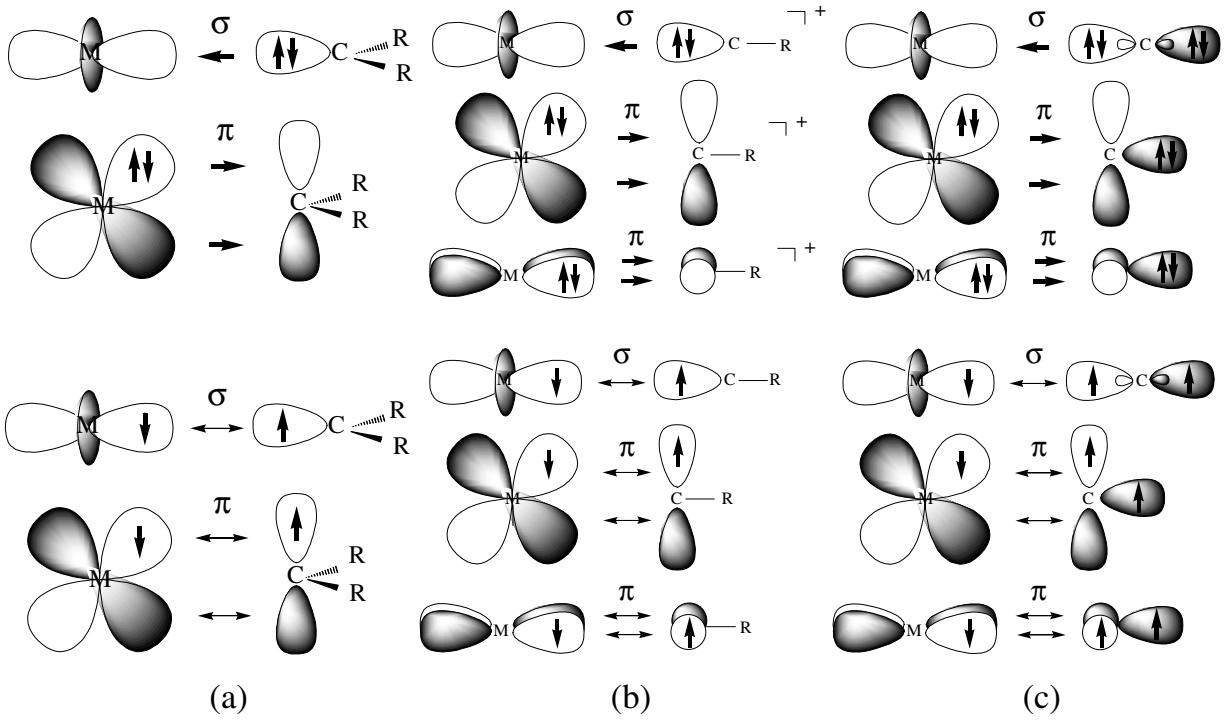

Scheme 4.1 Schematic representation of the orbital interaction between a transition metal and (a) carbene ligand; (b) carbyne ligand; (c) carbon ligand. Donor-acceptor interactions are shown on top, shared-electron bonding is shown on the bottom.

donor-acceptor bond and a TM-C shared-electron bond which are similar to the orbital models of the carbene and carbyne complexes. A carbon atom in the excited ^{1}D state (Scheme 4.2) has the same type of orbital interactions with a transition metal as a carbyne ligand (Scheme 4.1). An important difference is that the shared-electron TM-C bond leaves an unpaired electron at carbon which explains why most TM carbides have an unpaired electron at carbon atoms with more than one nearest neighbor. In contrast to the shared-electron bond has the TM-C donor-acceptor bond an electron lone-pair at the terminal carbon atom. The bonding situation in negatively charged $(NRAr)_3MoC^-$ is analogous to $(NRAr)_3MoN$, which has a shared-electron Mo≡N triple bond and an electron lone pair. Thus, a complex with a transition metal-carbon donor-acceptor bond has not been synthesized so far. The carbon complex $(CO)_4FeC$ has been suggested as a possible intermediate in the reaction of $(CO)_4FeCS$ with $P(NMe_2)_3$. [75i] It may be suggested that only compounds with a shared-electron TM-C bond should be called TM carbides, while those with a donor-acceptor bond are better called TM carbon complexes. [107]

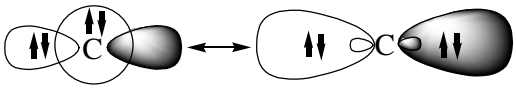

Scheme 4.2 Schematic representation of the electronic configuration of carbon in the ^{1}D state with(right) and without(left) hybridization.

In this chapter, quantum chemical calculations of the model compound $(CO)_4FeC$ (**1**) which has a Fe-C donor-acceptor bond are reported. The equilibrium geometry, Fe-C bond dissociation energy (BDE) and the vibrational frequencies of **1** are calculated. The nature of the chemical bond was analyzed with the help of the NBO [29] partitioning scheme and with the topological analysis of the electron density distribution.[28] For comparison, the report about the bonding situation of $(CO)_4Fe(CH_2)$ (**2**) , $I(CO)_3Fe(CH)$ (**3**) and $Fe(CO)_5$ (**4**) is also given. One has to be aware of the fact that **2** is not a good example for a stable Fischer-type carbene complex, because they can only become isolated when the carbene ligand has a π–donor substitute. [102a-d,i] The model compound **3** is a good reference species, however, for the discussion of the bonding situation and stability of **1**. The results of the calculations are used to predict the chemical properties of **1** and to discuss the possibilities to observe it experimentally. To this end $(CO)_4FeC\text{-}BCl_3$ (**5**) was also calculated, which is a complex of the Lewis base **1** with the Lewis acid BCl_3.

4.2 Computational Methodology

The geometries have been optimized at the NL-DFT level using the three-parameter fit of the exchange-correlation potential suggested by Becke [19] in conjunction with the LYP [18] correlation potential (B3LYP).[108] A small-core effective core potential (ECP) with a (441/2111/41) valence basis set for Fe [27c] , an ECP with a (31/31/1) valence basis set for I [26b] and 6-31G(d) basis sets [53] for C, O, H have been employed in the geometry optimizations. This is the standard basis set II. [55] The nature of the stationary points was examined by calculating the Hessian matrix. Improved energy calculations at the B3LYP/II optimized geometries have been carried out using coupled-cluster theory [21] at the CCSD(T) level. [109] The calculations have been performed with the program packages Gaussian94/98[56], ACES II[57] and MOLPRO96/2000[58].

4.3 Geometries, Bond Energies and Vibrational Frequencies

Figure 4.1 shows the optimized geometries of **1** - **5** at B3LYP/II. The structures of $(CO)_4FeCH_2$ (**2**) and $Fe(CO)_5$ (**4**) are shown previously in Fig 3.2.9 and 3.2.1 (Chapter 3), respectively. But for completeness, these structures are also included in Fig 4.1. This is also the case for $Fe(CO)_4$ (**6**). The calculated energies are given in Table 4.1.

$(CO)_4FeC$(**1a**) has a C_{3v} equilibrium geometry with an axial carbon ligand and a rather long Fe-CO_{trans} bond. The isomeric form **1b** which has the carbon ligand in the equatorial position is a transition state on the potential energy surface. **1b** is calculated to be 7.7 kcal/mol higher in energy than **1a** (Table 4.1). The $(CO)_4$Fe-C bond in **1a** is very short (1.614 Å). The Fe-CO_{trans} bond of **1a** (2.052 Å) is much longer than the axial Fe-CO bonds in $Fe(CO)_5$ (**4**) (1.819 Å). The short $(CO)_4$Fe-C bond and the lengthening of the Fe-CO_{trans} bond with respect to **4** indicate that the Fe $\rightarrow C_{carbon}$ π-backdonation is quite strong which concomitantly weakens the Fe $\rightarrow CO_{trans}$ backdonation.

The bonding model for the donor-acceptor bonds shown in Scheme 4.1 suggests that there are two Fe $\rightarrow$ C π bonds in carbon complexes, while there is only one Fe-CR_2 π bond in carbene complexes. Figure 4.1 shows that the Fe-CH_2 bond in **2** is significantly longer than the Fe-C bond in **1a**. This holds for the isomer with the axial carbene ligand **2a** and for the equatorial isomer **2b**. In contrast to the carbon complex **1** it is found that the equatorial form of the carbene complex **2b** is a minimum on the potential energy surface, while the axial form **2a** is a transition state which is 8.3 kcal/mol higher in energy than **2b** (Table 4.1). A previous qualitative analysis of the orbital interactions between $Fe(CO)_4$ and π bearing ligands L led to the suggestion that π-acceptor ligands should prefer the equatorial position in $(CO)_4FeL$. [46] This is in agreement with the calculated equilibrium structure of **2b** and the experimental geometry of $(CO)_4Fe(C_2H_4)$.[85] The calculated energy minimum structure of $(CO)_4FeC$ (**1a**), however, defies the predicted preference of a π–acceptor ligand for an equatorial position. [46] A possible explanation for this is given in the section about the bonding situation.

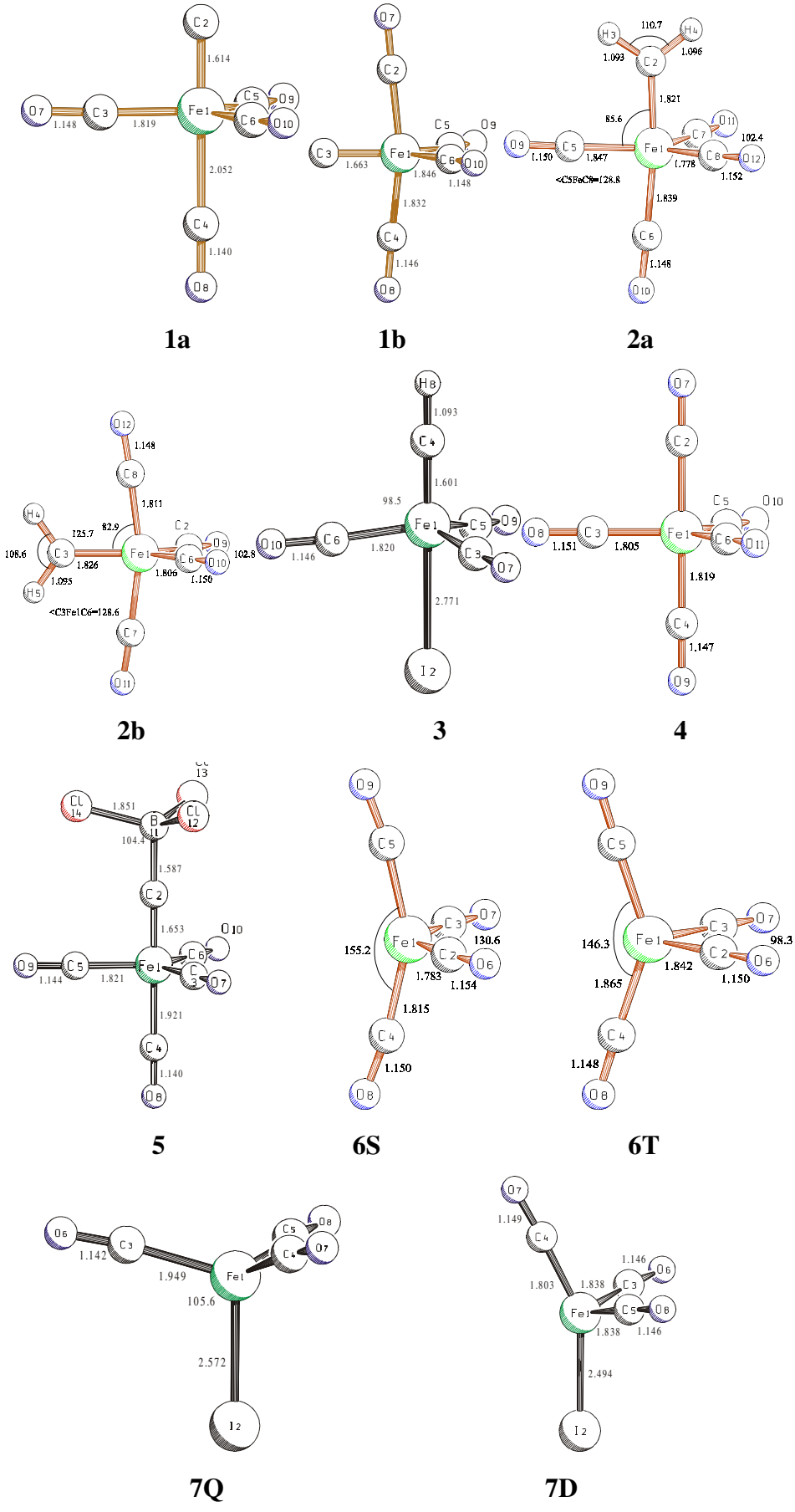

Figure 4.1 Optimized geometries (B3LYP/II) of **1** - **7**. Distances in Å , angles in degree.

Figure 4.1 shows also the calculated geometry of the carbyne complex $I(CO)_3Fe(CH)$ (**3**). The bonding model for the donor-acceptor bond of carbyne complexes L_nTM-CR requires a somewhat arbitrary choice of charged fragments L_nTM^q and CR^q, because the neutral fragments are open-shell species. Scheme 4.1 exhibits the most common choice of a positively charged carbyne ligand and a negatively charged metal fragment. A recent theoretical analysis of the bonding situation in carbyne complexes has shown that this model is a reasonable qualitative representation of the TM-CR bond. [38c] Thus, the bonding situation in TM carbon and carbyne complexes should be quite similar. There are two metal-ligand π bonds, but according to the model the π backdonation in carbyne complexes should be stronger than in carbon complexes because the carbyne ligand CR has formally a positive charge. Figure 4.1 shows that $I(CO)_3Fe$-CH bond of **3** is indeed slightly shorter (1.601 Å) than the $(CO)_4Fe$-C bond of **1a**. This lends some support to the bonding model for carbyne complexes (Scheme 4.1). It will be shown below, however, that the shorter Fe-CH bond is better explained with the hybridization of the donor orbital of the CH ligand. It should be pointed out that the calculated bond lengths of $Fe(CO)_5$ (**4**) are in excellent agreement with the most recent experimental value (Fe-CO(ax)=1.811(2) Å; Fe-CO(eq) = 1.803(2) Å). [63]

The analysis of the bonding situation which is given below suggests that the carbon ligand of **1** should exhibit nucleophilic rather that electrophilic behavior, and that **1** can be classified as a Lewis base. The adduct of **1** with BCl_3 is thus calculated. Figure 4.1 shows the equilibrium geometry of **5** which is a minimum on the potential energy surface. The B-C donor-acceptor bond of **5** is very short (1.587 Å). It is significantly shorter than the theoretically predicted donor-acceptor bond of the diaminocarbene complex with boron trichloride $(NH_2)_2C$-BCl_3 (1.637 Å). [110] The iron-carbon bond of **5** is clearly longer (1.654 Å) than in the parent compound **1a**, and the Fe-CO_{trans} bond of **5** becomes much shorter (1.918 Å) which indicate that the trans influence of the carbon ligand becomes weaker when it is bonded to a Lewis acid.

Figure 4.1 gives the geometries of $Fe(CO)_4$ in the ($^1A_1$) singlet (**6S**) and ($^3B_2$) triplet (**6T**) states. The triplet form **6T** is predicted at the B3LYP/II level to be 8.3 kcal/mol lower in energy than **6S**. This is in agreement with previous calculations. Li *et al.* [71] calculated at the NL-DFT level a value of 1.7 kcal/mol in favor of the triplet state. Barnes *et al.* [73] carried out MCPF calculations of **6S** and **6T**. They estimated that the triplet state of $Fe(CO)_4$ should be

15 ± 5 kcal/mol below the singlet state. Thus, the calculated value of 8.3 kcal/mol seems to be reasonable. Unfortunately, the CCSD(T) calculation of **6T** did not converge. A triplet ground state of $Fe(CO)_4$ has also been deduced from experimental studies by analysis of MCD measurements. [60d] The open-shell ($^4\Sigma$) state **7Q** of $I(CO)_3Fe$ is predicted at B3LYP/II to be 3.8 kcal/mol low in energy than the ($^2\Pi$) state **7D**.

Table 4.1 Calculated Total Energies E_{tot} (au), Relative Energies E_{rel} (kcal/mol), Zero-Point Vibrational Energies ZPE (kcal/mol), and Number of Imaginary Frequencies *i*

			B3LYP/II//B3LYP/II				CCSD(T)/II/B3LYP/II	
molecule	No.	*sym.*	E_{tot}	E_{rel}	ZPE	*i*	E_{tot}	E_{rel}
$(CO)_4FeC(ax)$	**1a**	C_{3v}	-614.77478	0.0	22.3	*0*	-612.94108	0.0
$(CO)_4FeC(eq)$	**1b**	C_{2v}	-614.76291	+7.5	22.7	*1*	-612.92881	+7.7
$(CO)_4FeCH_2(ax)$	**2a**	C_s	-616.05043	0.0	36.8	*1*	-614.18216	0.0
$(CO)_4FeCH_2(eq)$	**2b**	C_{2v}	-616.06076	-6.5	37.3	*0*	-614.19544	-8.3
$I(CO)_3FeCH$	**3**	C_{3v}	-513.51971		24.9	*0*	-511.82174	
$Fe(CO)_5$	**4**	D_{3h}	-690.15655		26.7	*0*	-688.13539	
$(CO)_4FeCBCl_3$	**5**	C_{3v}	-2020.36785		28.8	*0*	-2016.74903	
$Fe(CO)_4$ ($^1A_1$)	**6S**	C_{2v}	-576.78295	0.0	20.7	*0*	-575.02548	
$Fe(CO)_4$ ($^3B_2$)	**6T**	C_{2v}	-576.79610	-8.3	20.0	*0*	n.c. [a]	
$I(CO)_3Fe$ ($^4\Sigma$)	**7Q**	C_{3v}	-474.91911	0.0	14.4	*0*	n.c. [a]	
$I(CO)_3Fe$ ($^2\Pi$)	**7D**	C_1	-474.91299	3.8	15.7	*0*	n.c. [a]	
CO		$C_{\infty v}$	-113.30691		3.2	*0*	-113.03352	
CH_2 ($^3B_1$)		C_{2v}	-39.14912	0.0	10.9	*0*	-39.02160	0.0
CH_2 ($^1A_1$)		C_{2v}	-39.12705	+13.8	10.9	*0*	-38.99670	+15.6
CH ($^2\Pi$)		$C_{\infty v}$	-38.47770	0.0	4.0	*0*	-38.36240	0.0
CH ($^4\Sigma^-$)		$C_{\infty v}$	-38.44530	+20.2	4.4	*0*	-38.34544	+10.6
C (^3P)			-37.84469				-37.75180	
BCl_3		D_{3h}	-1405.55234		4.8	*0*	-1403.76470	

[a] not converged

Table 4.2 gives the theoretically predicted bond dissociation energies D_e and donor-acceptor interaction energies E_{int} of **1** - **5**. The D_e values and the ZPE corrected D_o data of the iron-ligand bonds have been calculated for the dissociation of the Fe-L complexes yielding $Fe(CO)_4$ or $I(CO)_3Fe$ and L in the electronic ground states. The interaction energies E_{int} have been calculated with respect to the lowest lying singlet states of the metal fragment and L which are relevant for the bonding models shown in Scheme 4.1. E_{int} value for the $I(CO)_3Fe$-CH bond of **3** is not given, because the dissociation of **3** into closed-shell fragments yields charged species. The associated dissociation energy thus involves a charge separation

reaction which should not be compared with the E_{int} values of **1a**, **2b** and **4**. The D_e and E_{int} values of **5** are the same because the fragments of the bond dissociation reaction have singlet ground state.

Table 4.2 Calculated Bond Dissociation Energies D_e[a] and Metal-Ligand Interaction Energies E_{int}[b] (kcal/mol). ZPE Corrected Energies are Given in Parentheses.

		B3LYP/II		CCSD(T)/II[c,e]	
Molecule	**No.**	D_e (D_o)	E_{int}	D_e (D_o)	E_{int}
$(CO)_4Fe$-C(ax)	**1a**	84.1(81.8)	121.4(119.8)[d]	94.5(92.9)	131.9(130.3)[d]
$(CO)_4Fe$-CH_2(eq)	**2b**	72.5(66.1)	94.6(88.4)	84.8(79.1)	108.7(103.0)
$I(CO)_3Fe$-CH	**3**	76.4(70.2)	-	-	-
$(CO)_4Fe$-CO	**4**	33.6(30.1)	41.8(39.0)	39.6(36.8)	47.9(45.1)
$(CO)_4FeC$-BCl_3	**5**	25.6(23.9)	25.6(23.9)	27.1(25.4)	27.1(25.4)

[a] calculated with respect to the fragments in the electronic ground state
[b] calculated with respect to the fragments in the lowest singlet state
[c] using the B3LYP/II value of the singlet-triplet energy difference for $Fe(CO)_4$ (8.3kcal/mol)
[d] calculated using the experimental value for the $^3P \rightarrow {}^1D$ excitation energy for carbon (29.1 kcal/mol)
[e] using the B3LYP/II optimized geometries

The theoretically predicted $(CO)_4Fe$-C bond dissociation energy of **1a** is very high. The calculated value at B3LYP/II is D_e = 84.1 kcal/mol. The CCSD(T)/II value 94.5 kcal/mol is even higher. The CCSD(T)/II value for the bond energies of **1** - **5** are always higher than the B3LYP/II results but not very much. The carbon complex **1a** has clearly the strongest metal-ligand bond of the investigated compounds. The carbyne complex **3** (D_e = 76.4 kcal/mol at B3LYP/II) and the carbene complex **2b** (D_e = 72.5 kcal/mol at B3LYP/II; D_e = 84.8 kcal/mol at CCSD(T)) also have strong Fe-L bonds, while $Fe(CO)_5$ (**4**) (D_e = 33.6 kcal/mol at B3LYP/II; D_e = 39.6 kcal/mol at CCSD(T)/II) is clearly weaker bonded. The latter values may be compared with the experimental value for the first bond dissociation energy of $Fe(CO)_5$ at 0 K D_o = 39 ± 2 kcal/mol). [74] However, this value refers to the dissociation of $Fe(CO)_5$ yield the singlet state **6S** of $Fe(CO)_4$ and CO and thus, must be compared with the ZPE corrected E_{int} data given in Table 4.2. The theoretical values (39.0 kcal/mol at B3LYP/II; 45.1 kcal/mol at CCSD(T)/II) are in very good agreement with experiment.

The calculations predict that the order of the Fe-L bond dissociation energies D_e has the trend C > CH > CH_2 >> CO. A comparison with the optimized geometries shows that the

Fe-L bond energies clearly do not correlate with the bond lengths. The $(CO)_4Fe$-CO bond of **4** is shorter but significantly weaker than the $(CO)_4Fe$-CH_2 bond of **2b**, and the $(CO)_4Fe$-C of **1a** is longer, but has a higher BDE than the $I(CO)_3Fe$-CH bond of **3**. An explanation for the trend of the bond energies and for the bond length/bond energy correlation is given below in the section about bonding analysis (section 4.4).

The thermodynamic stabilization of the carbon ligand of **1a** by the $Fe(CO)_4$ fragment was investigated. The latter moiety is isolobal to CH_2[111]. Thus, $(CO)_4FeC$ may be compared with vinylidene H_2CC. The reaction energies of the hydrogenation of **1a** and vinylidene were calculated as follows (reactions 4.1 and 4.2):

$$(CO)_4FeC\ (\mathbf{1a}) + H_2 \rightarrow (CO)_4FeCH_2\ (\mathbf{2b}) \qquad (4.1)$$

$$H_2CC + H_2 \rightarrow H_2CCH_2 \qquad (4.2)$$

The reaction energy for reaction 4.1 is predicted at B3LYP/II to be –69.3 kcal/mol (-80.1 kcal/mol at CCSD(T)/II). The theoretically predicted energy for reaction 4.2 is –95.6 kcal/mol (-107.5 kcal/mol at CCSD(T)/II). Thus, the $Fe(CO)_4$ fragment stabilizes a carbon atom 26.3 kcal/mol (B3LYP/II; 27.0 kcal/mol at CCSD(T)/II) more than methylene.

The interaction energies E_{int} involve the excitation energy of $Fe(CO)_4$ from the triplet ground state to the singlet excited state and the triplet → singlet excitation energies of C (in case of **1**) and CH_2 (in case of **2**). The first excited singlet state of carbon which is relevant to the bonding model shown in Scheme 4.1 is the ^1D state, which can not accurately be calculated at the single-determinant level.[112] The calculated energy of the ^3P ground state and the experimental value (29.1 kcal/mol)[113] for the $^3P \rightarrow {}^1D$ excitation energy are used in order to estimate E_{int} for **1a**. Table 4.2 shows that the E_{int} values discriminate the ligands C, CH_2 and CO even more than the D_e data. $(CO)_4Fe$-C (**1a**) has a particularly large interaction energy which correlates well with the short bond.

The calculated BDE of the $(CO)_4FeC$-BCl_3 bond (D_e= 25.6 kcal/mol at B3LYP/II; 27.1 kcal/mol at CCSD(T)/II) is large enough to make **5** a possible target for synthetic work.[118] It is interesting to compare the BDE of **5** with the calculated bond energy of the carbene complex $(NH_2)_2C$-BCl_3 which is D_e = 59.7 kcal/mol.[110] Thus, the latter carbene complex has a much stronger yet C-BCl_3 bond than **5**. It will be shown below that this can

be explained with the hybridization at the carbon donor atom. The BDE of the C-BCl_3 bond of **5** is much higher, however, than the bond energy of OC-BCl_3 (D_e = 2.3 kcal/mol). [110] The rotation of the BCl_3 ligand of **5** around the Fe-C-B axis is nearly unhindered. The rotational barrier is only 0.2 kcal/mol (B3LYP/II).

Table 4.3.1 Calculated Vibrational Frequencies (cm^{-1}) and IR Intensities (km mol^{-1}) at B3LYP/II of $(CO)_4FeC(ax)$ and $(CO)_4FeCBCl_3$

$(CO)_4FeC(ax)$ (**1a**)				$(CO)_4FeCBCl_3$ (**5**)			
Sym.	Mode	freq.	(int.)	Sym.	Mode	freq.	(int.)
A_1	[CO]	2185	(226)	A_1	[CO]	2203	(484)
	[CO]	2151	(207)		[CO]	2172	(228)
	$[FeC]_{carbon}$	969	(1)		[BC]	1128	(122)
	[δFeCO]	535	(36)		$[BC]+[FeC]_B$	705	(282)
	$[FeC]_{eq}$	419	(0)		[δFeCO]	550	(46)
	$[FeC]_{ax}$	227	(8)		$[FeC]_{eq}$	419	(1)
	[δFeCO]	112	(0)		$[BCl]+[FeC]_{ax}$	391	(0)
A_2	[δFeCO]	368	(0)		$[FeC]_{ax}$	359	(12)
E	[CO]	2116	(1043)		[δCBCl]	186	(20)
	[δFeCO]	573	(86)		[δCFeC]	107	(1)
	[δFeCO]	475	(2)	A_2	[δFeCO]	369	(0)
	[δFeCO]	468	(0)		$[\delta(BCl_3C)Fe(CO)]$	3	(0)
	[δFeCO]	343	(0)	E	[CO]	2150	(836)
	[δCFeC]	185	(4)		[δFeCB]	720	(76)
	[δFeCO]	86	(0)		[δCFeC]	642	(157)
	[δCFeC]	54	(0)		[δFeCO]	521	(1)
					[δFeCO]	467	(3)
					[δFeCO]	406	(4)
					[δFeCO]	346	(0)
					[δClBCl]	223	(0)
					[δCFeC]	103	(0)
					[δCFeC]	93	(0)
					[δCFeC]	64	(0)
					[δCFeC]	31	(0)

Table 4.3.1 shows the theoretically predicted vibrational spectra of $(CO)_4FeC$ (**1a**) and $(CO)_4FeC\text{-}BCl_3$ (**5**), which might help to identify the compound. The calculated wavenumbers and IR intensities of **2** – **4** are given in Table 4.3.2- 4.3.4. The Fe-C stretching mode of **1a** is predicted at ν = 969 cm^{-1}, but the IR intensity is very low. It could only be observed in the Raman spectrum. The Fe-C stretching mode in **5**, which is coupled to the B-C fundamental is shifted to lower wavenumbers at ν = 700 cm^{-1}. It now has a high IR intensity and should help to identify the molecule. Also the B-C stretching mode at ν = 1128 cm^{-1} might be useful for this purpose.

Table 4.3.2 Calculated Vibrational Frequencies (cm^{-1}) and IR Intensities (km mol^{-1}) at B3LYP/II of $(CO)_4FeCH_2$(eq, **2b**)

Sym	Mode	freq. (int.)	Sym	Mode	freq. (int.)
A_1	[CH]	3080 (31)	B_1	[CO]	2103 (964)
	[CO]	2174 (139)		[δHCH]	945 (0)
	[CO]	2119 (399)		[δFeCO]+ [δHCH]	629 (137)
	[δHCH]	1524 (1)		[δFeCO]	487 (2)
	[FeC]	734 (22)		[δFeCO]	392 (4)
	[δFeCO]	646 (85)		[δFeCO]	117 (0)
	[δFeCO]	523 (15)		[δCFeC]+ [δHCH]	20 (0)
	[FeC]	455 (0)	B_2	[δHCH]	3144 (17)
	[FeC]	421 (1)		[CO]	2116 (1242)
	[δFeCO]	120 (0)		[δHCH]	857 (0)
	[δCFeC]	76 (0)		[δFeCO]+[δHCH]	598 (125)
A_2	[δFeCO]+ [δHCH]	570 (0)		[δFeCO]	550 (9)
	[δHCH]	502 (0)		[δFeCO]	445 (6)
	[δFeCO]+ [δHCH]	359 (0)		[δHCH]	212 (2)
	[δCFeC]	92 (0)		[δCFeC]	106 (0)

Table 4.3.3 Calculated Vibrational Frequencies (cm^{-1}) and IR Intensities (km mol^{-1}) at B3LYP/II of $I(CO)_3FeCH$ (**3**)

Sym	Mode	freq. (int.)	Sym	Mode	freq. (int.)
A_1	[CH]	3190 (2)	E	[CO]	2135 (925)
	[CO]	2169 (9)		[δFeCH]	804 (1)
	$[FeC]_{carbyne}$	1031 (0)		[δFeCH]+[δFeCO]	519 (69)
	[δFeCO]	540 (134)		[δFeCO]+[δFeCH]	464 (23)
	[δFeCO]+ $[FeC]_{eq}$	407 (14)		[δFeCO]	404 (3)
	[FeI]	195 (1)		[δCFeC]	136 (4)
	[δCFeC]	117 (3)		[δCFeC]	95 (0)
A_2	[δFeCO]	373 (0)		[δCFeC]	43 (0)

Table 4.3.4 Calculated Vibrational Frequencies (cm^{-1}) and IR Intensities (km mol^{-1}) at B3LYP/II of $Fe(CO)_5$

Sym	Mode	freq.	(int.)	Sym	Mode	freq.	(int.)
A_1'	[CO]	2189	(36)	E′	[CO]	2094	(1135)
	[CO]	2119	(0)		[δFeCO]	670	(149)
	[FeC]	439	(0)		[δFeCO]	494	(2)
	[FeC]	416	(0)		[FeC]	450	(12)
A_2'	[δFeCO]	372	(0)		[δCFeC]	108	(0)
A_2''	[CO]	2119	(1331)		[δCFeC]	52	(0)
	[δFeCO]	623	(135)	E″	[δFeCO]	573	(0)
	[FeC]	472	(9)		[δFeCO]	371	(0)
	[δCFeC]	110	(1)		[δCFeC]	98	(0)

4.4 Analysis of the Bonding Situation

The NBO results shown in Table 4.4 are first discussed, which give insight into the Fe-L σ and π bonds of **1a** – **5**. The NBO method suggests for **1a** a Lewis structure which has a $(CO)_4$Fe-C σ and a degenerate π bond. The σ and π bonds are strongly polarized towards the iron atom. This holds particularly for the degenerate π bond, which has a weight of 81.5% at the iron side. The polarization of the Fe-C σ bond of **1a** is noteworthy, because it is the only one of the complexes **1a** –**5** which has a larger amplitude on the iron side, while the other σ bonds are more polarized towards carbon. This indicates that the carbon ligand is a strong donor in **1a**.

Table 4.4 Result of the NBO Analysis and Wiberg Bond Indices *P* at B3LYP/II

No.	Formula	*P* (Fe-C)		occ.	%Fe	4s(Fe)	4p(Fe)	3d(Fe)	2s(C)	2p(C)
1a	$(CO)_4$ Fe-C(ax)	1.55	σ	1.98	65.77	2.65	0.13	97.22	14.42	85.16
			π	1.84	81.54	0.00	0.05	99.99	0.00	99.71
			π	1.84	81.54	0.00	0.05	99.99	0.00	99.71
2b	$(CO)_4$ Fe-CH_2(eq)	0.93	σ	1.75	31.58	47.04	0.16	52.80	37.69	62.28
			π	1.84	68.26	0.00	0.28	99.72	0.00	99.99
3 [a]	$I(CO)_3$ Fe-CH	1.73	σ	1.85	38.24	16.81	9.27	73.92	53.44	46.49
			π	1.39	53.28	0.11	40.39	59.49	0.00	99.93
			π	1.48	57.40	0.34	28.64	71.02	0.00	99.93
4	$(CO)_4$ Fe-CO(ax)	0.69	σ	1.90	29.92	42.03	0.16	57.81	63.73	36.27
5	$(CO)_4$ Fe-$CBCl_3$	1.32	σ	1.90	44.71	26.22	0.10	73.68	39.84	60.09
			π	1.80	80.04	4.42	0.08	95.50	0.00	99.90
			π	1.69	78.78	13.27	0.19	86.54	0.00	99.90
		P (C-B)		occ.	%C	2s(C)	2p(C)		2s(B)	2p(B)
		0.88	σ	1.98	68.45	60.07	39.88		23.51	76.32

[a] Keyword for 3-center bond was used

The carbon complex **1a** possesses the strongest polarized Fe-L bonds of the complexes **1a** – **5**. Another extreme value of **1a** is the hybridization of the σ bond at the carbon ligand. The NBO has mainly p character at carbon and only 14.4% s contribution. This is in strong contrast to the hybridization at the carbon atom of the CO ligand in $Fe(CO)_5$, which has 63.7% s character in the Fe-CO bond. The

hybridization at carbon is one reason why the $(CO)_4$Fe-CO bond of **4** is comparatively short and yet significantly weaker than the Fe-L bonds of **1a** - **5**. The high %s character of the CO donor orbital means that it is rather compact and that the σ orbital interactions take only place at shorter distances compared with donor orbitals which have more %p character. Orbitals with higher %s character are also energetically lower lying than those with more %p character and thus, lead to weaker donor-acceptor interactions. However, the strength of the metal-ligand interactions is mainly determined by the Fe→L π-backdonation. This will be discussed below.

Table 4.5 Calculated Charge Distribution Given by the NBO Analysis at B3LYP/II [a]

			q			*p*(π)		
No.	[TM]	L	[TM]	Fe	C(L)	C(L)	[TM]→L(π)	[TM] ←L(σ)
1a	$(CO)_4$ Fe	C	-0.16	-0.49	0.16	0.47 [b]	0.94	1.10
2b	$(CO)_4$ Fe	CH_2	0.13	-0.42	-0.54	0.78	0.78	0.65
3	$I(CO)_3$ Fe	CH	-0.16	-0.23	-0.05	0.74 [b]	0.48	0.64
4	$(CO)_4$ Fe	CO(ax)	-0.17	-0.54	0.59	2.16 [b,c]	0.32	0.49
5	$(CO)_4$ Fe	$CBCl_3$	0.24	-0.44	0.12	0.60 [b]		

[a] Partial charge *q*, and population of the p(π) AO of ligands.
[b] Doubly degenerated orbital. The data give the occupation of a single orbital.
[c] Occupation of the π orbital of CO.

Table 4.5 gives the charge distribution at the atoms and the orbital populations. The atomic partial charges indicate that the iron atom always carries a negative charge. The charge at Fe in **3** is smaller than in the other complexes. The ligand C, CH and CO in **1a**, **3** and **4** are positively charged and thus, are net charged donor ligands, while CH_2 and $CBCl_3$ in **2b** and **5** are negatively charged (net acceptor ligands). It is noteworthy that the attachment of BCl_3 in **5** reverses the net charge flow from the $Fe(CO)_4$ metal fragment to the ligand. However, it should be pointed out that the total atomic charges are not a very useful probe for the interactions between the metal and the ligand, because they do not say anything about the topography of the charge distribution. A better probe for the charge distribution are the bond polarities shown in Table 4.4 and the orbital populations given in Table 4.5. The population of the p(π) orbitals of the ligand atoms in the complex and in the free

ligand and the partial charges make it possible to estimate the amount of Fe←L σ donation and Fe→ L π-backdonation.

The results in Table 4.5 show that the carbon ligand is the strongest σ donor and the strongest π acceptor of the four ligands. This explains the very short and strong Fe-C bond of **1a**. A surprising feature of **1a** is that it is energetically lower lying than **1b**. A qualitative discussion of the orbital interactions between a X_4TM fragment and a ligand L in a trigonal bipyramidal complex X_4TML led to the suggestion that strong π acceptor ligand tend to occupy the equatorial site.[46] Yet, the strong π accepting carbon ligand clearly prefers the axial position in $(CO)_4FeC$. Thus, the preference for the axial position comes from the $(CO)_4Fe$-C σ interaction. Table 4.5 shows that the Fe←C donation is even larger than the Fe→C backdonation. The discussion about the orbital interactions in X_4TM-L considered only the π orbitals of the L, but not the σ orbitals.[46] Strong σ donor ligands such as CN^- occupied the axial position in $(CO)_4 FeCN^-$, which has been explained with the weak π acceptor ability of the cyanide ligand.[46] Therefore, the preference for the axial or equatorial site is not only determined by the π orbital interactions, but also by the σ orbitals. The latter effect is then responsible for the finding that **1a** is energetically lower lying than **1b**. The relative σ donor/π acceptor strength explains also why the equatorial form of the carbene complex **2b** is lower in energy than the axial form **2a**. Table 4.5 shows that the CH_2 ligand is a stronger π acceptor than σ donor, while the carbon ligand is a stronger σ donor than π acceptor.

The carbyne complex **3** has a still shorter Fe-L bond than **1a**, and the Wiberg bond index [114] (Table 4.4) for the Fe-CH bond is higher (1.73) than for the Fe-C bond (1.55) . However, the CH ligand has already one p(π) electron in the reference state of the neutral ligand, while carbon (^{1}D) has none. The Fe-CH π bonds of **3** are less polarized towards the iron end than the π bonds of **1a** (Table 4.4), but one of the four π electrons of the former bonds comes from the ligand, while all four π electrons of the Fe-C bond of **1a** come from Fe. Thus the neutral CH ligand is actually a weaker π acceptor than C and CH_2 (Table 4.5). The bonding situation of the neutral carbyne ligand in **3** is not directly comparable to the ligands in the carbon complex **1a** and the carbene complex **2b** because of the unpaired p(π) electron of CH. The very

short Fe-C bond of **3** is caused by the large %s character of the carbon σ donor orbital (Table 4.4). The main conclusion from the NBO analysis is that the carbon ligand is a strong π acceptor and an even stronger σ donor.

The NBO results of **1** and **5** show that the p(π) population of the carbon ligand atom is enhanced by the complexation with BCl_3. The population of the p(π) AOs of carbon in **5** is 1.20 e (0.60 e in each orbital), which is a significantly higher value than in the parent complex **1a** (0.94 e). Since the BCl_3 moiety induces a charge flow from $Fe(CO)_4$ to the $CBCl_3$ ligand, it may be argued that there is a stronger Fe→C π-backdonation in **5** than in **1a**. However, a part of the carbon p(π) population of **5** may also be due to hyperconjugation from the BCl_3 ligand. The most important conclusion is, that the carbon ligand atom in **5** becomes electronically stabilized and sterically shielded by the BCl_3 moiety.

The hybridization at the carbon donor atom of **5** explains why the C-BCl_3 bond is shorter yet weaker than the C-BCl_3 bond of $(NH_2)_2$C-BCl_3. Table 4.4 shows that the bond orbital of the C-BCl_3 bond has 60.1 %s and 39.9%p character at the carbon side, while it has a much higher p character in the carbene complex (25.5 %s, 74.3 %p).[110] The more diffuse and energetically higher lying p orbital induces stronger bonding at a larger distance. The $(CO)_4$Fe-C σ bond of **5** is now more polarized towards the carbon end, while in **1a** it was more polarized towards Fe.

Topological analyses of the electron density distribution of **1a** – **5** were carried out in order to seek further information about the electronic structure of molecules. Figure 4.2a shows the contour line diagram of the Laplacian distribution $\nabla^2\rho(\mathbf{r})$ of **1a** in the plane which contains the carbon ligand atom. The most important finding is the continuous area of charge concentration ($\nabla^2\rho(\mathbf{r}) < 0$, solid lines) which is found around the carbon ligand. This is in strong contrast to the shape of the Laplacian distribution of the carbene carbon atom of **2b** which is displayed in Figure 4.2b and 4.2c. The contour line diagram shown in Figure 4.2c exhibits the Laplacian distribution in the molecular plane which is perpendicular to the plane of the CH_2 ligand. There is clearly a "hole" in the area of charge concentration, which is

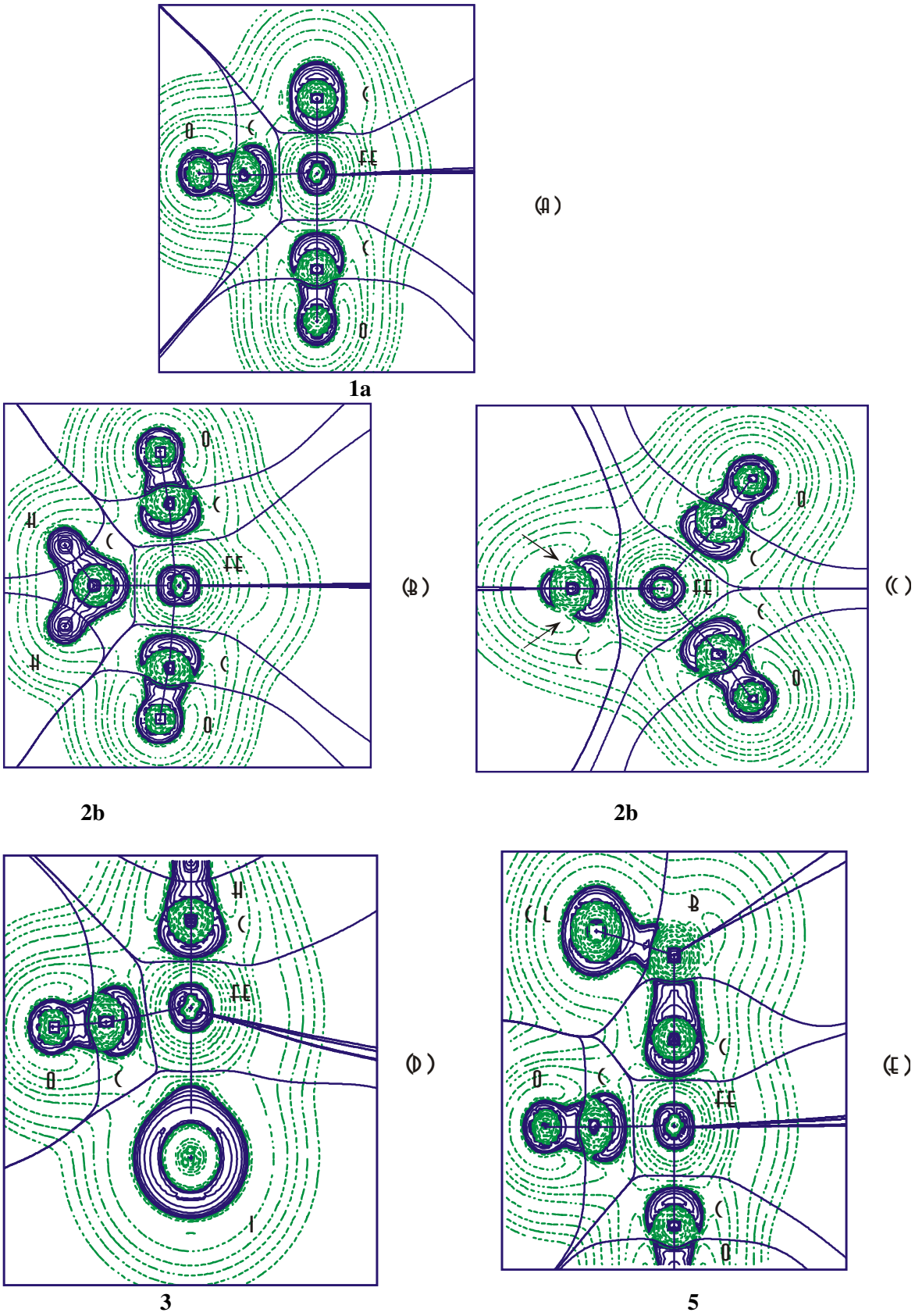

Figure 4.2 Contour line diagrams of the Laplacian distribution $\nabla^2\rho(r)$ at B3LYP/II. Dashed lines indicate charge depletion ($\nabla^2\rho(r) > 0$); solid lines indicate charge concentration ($\nabla^2\rho(r) < 0$). The solid lines connecting the atomic nuclei are the bond paths; solid lines separating the atomic nuclei indicate the zero-flux surfaces in the plane. The crossing points of the bond paths and zero-flux surfaces are the bond critical points r_b. The arrows in (c) show the hole in the valence sphere of the carbene ligand that is prone to attack by a nucleophilic agent.

Table 4.6 Results of the Topological Analysis of the Electron Density Distribution of $(CO)_4FeC$(**1a**), $(CO)_4FeCH_2$(**2b**), $I(CO)_3FeCH$(**3**), $Fe(CO)_5$(**4**), $(CO)_4FeCBCl_3$(**5**). [a]

Molecule	No.	Bond X-Y	$\rho(r_b)$ [1/Å^3]	H_b [au/Å^3]	$R(X-r_b)$ [Å]	$R(r_b-Y)$ [Å]	$\nabla^2\rho(r_b)$ [1/Å^5]
$(CO)_4FeC$	**1a**	Fe-C	1.778	-1.726	0.881	0.733	-1.358
		Fe-C(ax)	0.525	-0.116	1.010	1.042	8.513
		Fe-C(eq)	0.963	-0.506	0.940	0.879	10.064
		C-O(ax)	3.153	-5.159	0.377	0.763	32.337
		C-O(eq)	3.092	-5.064	0.380	0.768	29.270
$(CO)_4FeCH_2$	**2b**	Fe-C	1.032	-0.587	0.955	0.871	5.610
		C-H	1.850	-1.829	0.703	0.392	-22.743
		Fe-C(ax)	0.946	-0.493	0.909	0.902	11.031
		Fe-C(eq)	0.967	-0.515	0.921	0.885	10.593
		C-O(ax)	3.096	-5.081	0.380	0.768	28.663
		C-O(eq)	3.080	-5.044	0.381	0.769	28.539
$I(CO)_3FeCH$	**3**	Fe-C	1.628	-1.404	0.852	0.749	8.947
		C-H	1.854	-1.894	0.725	0.368	-24.912
		Fe-C(eq)	0.969	-0.512	0.935	0.885	9.472
		C-O(eq)	3.106	-5.091	0.379	0.767	29.966
		Fe-I	0.276	-0.027	1.183	1.588	1.821
$Fe(CO)_5$	**4**	Fe-C(ax)	0.907	-0.448	0.900	0.919	11.508
		Fe-C(eq)	0.989	-0.517	0.933	0.872	10.332
		C-O(ax)	3.100	-5.089	0.380	0.767	29.031
		C-O(eq)	3.071	-5.026	0.381	0.770	28.349
$(CO)_4FeCBCl_3$	**5**	Fe-C(B)	1.506	-1.211	0.861	0.792	7.940
		C-B	1.085	-0.991	1.087	0.500	3.802
		Fe-C(ax)	0.716	-0.274	0.947	0.974	9.718
		Fe-C(eq)	0.965	-0.508	0.941	0.880	9.596
		C-O(ax)	3.155	-5.178	0.377	0.763	32.146
		C-O(eq)	3.125	-5.126	0.379	0.765	31.024
		B-Cl	0.855	-0.801	0.563	1.288	-2.629

[a] $\rho(r_b)$, H_b , $\nabla^2\rho(r_b)$ are the electron density, the energy density, Laplacian at the bond critical point r_b, respectively. $R(X-r_b)$ and $R(r_b-Y)$ give the distance between the bond critical point r_b and the X or Y atom.

indicated by the arrows. The charge depletion ($\square^2\rho(\mathbf{r}) > 0$, broken lines) at the carbene ligand of **2b** is directed towards the in-plane p(π) orbital of the carbon atom. It shows the local electron deficiency at the carbene atom and it indicates the preferred direction for a nucleophilic attack.

The shape of the Laplacian distribution around the carbon ligand in **1a** (Figure 4.2a) is similar to that of carbyne ligand in **3** (Figure 4.2d). The difference between the two ligands is that the carbon ligand of **1a** has an area of charge concentration pointing away from the metal, while the CH ligand of **3** has a bonded hydrogen atom. The large area of charge concentration at the carbon ligand pointing away from Fe suggests a possibly nucleophilic behaviour of **1a** in chemical reactions.[115] The nucleophilicity of **1a** comes to the fore by the strong attraction of BCl_3 moiety in **5**. The Laplacian distribution of **5** is shown in Figure 4.2e. The shapes of the Laplacian distribution around the carbon atom of the $CBCl_3$ ligand of **5** and the carbon atom of the CH ligand of **3** are very similar. Thus, the bond energy calculations, the topological analysis of the electron density distribution and the NBO calculations suggest that **5** might perhaps become isolated under appropriate conditions.

Table 4.6 gives the numerical results of the topological analysis of the electron density distribution. The data support the suggestion that the iron-carbon bonds of **1a** and **5** have a significant covalent character. It has been shown that typical covalent bonds have large charge densities at the bond critical point ρ_b [116], and that the energy densities at the bond critical point H_b is negative and large in magnitude. [117] Table 4.6 shows that the Fe-C bonds of **1a** and **5** have strongly negative H_b values and large positive ρ_b values.

4.5 Summary and Conclusion

The results of this chapter can be summarized as follows. The carbon complex $(CO)_4FeC$ (**1a**) is a minimum on the singlet potential energy surface. Structure **1a** possesses an axial Fe-C bond which has a theoretically predicted large dissociation energy D_e = 84.1 kcal/mol at B3LYP/II and D_e = 94.5 kcal/mol at CCSD(T)/II. The carbon ligand is a strong π–acceptor and an even stronger σ donor. The analysis of

the electronic structure of **1a** suggests that the carbon ligand atom should behave like a nucleophile. The donor-acceptor complex $(CO)_4FeC\text{-}BCl_3$ (**5**) has a calculated C-B bond energy of D_e = 25.6 kcal/mol at B3LYP/II (D_e = 27.1 kcal/mol at CCSD(T)/II) and might become isolated under appropriate conditions.

Chapter 5. The Relevance of Mono- and Dinuclear Iron Carbonyl Complexes to the Fixation and Stepwise Hydrogenation of N_2

5.1 Introduction

The stepwise hydrogenation of dinitrogen to ammonia is one of the most important processes in biochemical research[119] and of utmost interest to chemical industry.[120] Beside the well understood heterogeneously catalyzed reduction following the Haber-Bosch process,[121] deeper insight into the reduction of dinitrogen is necessary, particularly when dealing with biologically relevant systems. An example for this is the enzymatic fixation of N_2 catalyzed by nitrogenases.[122] Although the molecular structure of the Fe-Mo cofactor of a nitrogenase enzyme is well characterized by X-ray structure analysis,[123] details of catalytically important features involved in the N_2-reduction are, however, still not unequivocally answered.[124] To this end, the binding site, the binding mode of N_2 and the intermediates involved in the catalytic processes are still the source of much speculation.[122, 124] It is, however, widely accepted that the initial binding of dinitrogen occurs at the iron rather than the molybdenum centers.[122] Theoretical studies based on different model systems of the Fe-Mo cofactor and various levels of theory are available.[125] However, due to the complexity of the overall reduction process and the structure of the Fe-Mo cofactor, a suitable model system for the Fe-Mo nitrogenases that reasonably mimics its catalytic activity may be too large for a quantum chemical treatment at a reasonable level of theory.[125] In addition to that, the nature of the actual intermediates of the enzymatic N_2-fixation process still is a wide area of speculation.[126] Although there are numerous results indicating that biological N_2-fixation includes species of diazene and hydrazine,[122] even the structure of the small four-atomic diazene in solution was discussed controversially for some time and only recently Sellmann and Hennige isolated *trans*-N_2H_2 by complexation out of solution.[127]

Due to the interest in the structure and reactivity of iron carbonyl complexes,[128] the present study focuses on the influence and relevance of mono- and dinuclear iron carbonyl complexes of the general type $[\{Fe(CO)_4\}_nL]$ (n = 1 for L =

NH_3 and n=1, 2 for L = N_2, N_2H_2, N_2H_4) to the fixation and stepwise hydrogenation of N_2. It should be emphasized that this approach is not intended to serve as a model study of the Fe-Mo cofactor, but to gain a deeper insight to the reduction steps of N_2 that are most affected by coordination to iron carbonyl fragments.[124] Particular interest is thus drawn to thermodynamic changes between the "metalated" reaction in which the nitrogen-containing ligands are either coordinated by one or two iron tetracarbonyl fragments and the isolated, metal-free hydrogenation of N_2. Moreover, the bonding situation of the Fe─L (L = N_2, N_2H_2, N_2H_4 and NH_3) bond in terms of σ-donor/π-acceptor abilities and the preferred coordination site of the ligands are addressed

5.2 Computational Details

Geometry optimizations are performed with Becke's three-parameter hybrid functional in combination with the correlation functional according to Lee, Yang and Parr (B3LYP).[52] A small core pseudopotential and a (441/2111/41) split-valence basis set according to Hay and Wadt are used for iron,[27c] whereas an all-electron 6-31G(d) basis set is chosen for the main group elements.[109] It was shown previously that this combination of basis sets (further abbreviated as basis set II) in combination with the aforementioned functional predicts equilibrium geometries of transition metal complexes reasonably well.[55] All structures discussed in this paper are verified to represent local minima on their potential energy surfaces by harmonic frequency calculations at the same level of theory. Refined estimates of relative energies are obtained by single-point calculations of the B3LYP/II geometries using both the B3LYP functional and coupled-cluster theory with singles, doubles and pertubative estimates of triple substitution (CCSD(T)).[21] CCSD(T) and basis set II are used for estimating relative energies between isomeric forms of diazene, hydrazine and all iron carbonyl complexes. Refined reaction enthalpies ΔH_R^0 (T = 0K) for the individual hydrogenation reactions, however, are predicted using basis sets that consists out of the aforementioned basis set for the metal and the elements C and O, but are extended by either the 6-31G(d,p) and the 6─311+G(d,p) basis sets for N and H. These combinations of basis sets are further abbreviated as {II & 6-31G(d,p)} and {II & 6-311+G(d,p)}, respectively.

The ΔH_R^0 values obtained for the hydrogenation steps of the metal-free reactions are compared with their analogous steps involving mononuclear iron carbonyl fragments. The resulting $\Delta\Delta H_R^0$ values indicate whether ΔH_R^0 of an individual reduction step decreases ($\Delta\Delta H_R^0 < 0$) or increases ($\Delta\Delta H_R^0 > 0$) on going from the reactions of the isolated to the coordinated species. The corresponding $\Delta\Delta H_R^0$ values obtained for the individual reduction steps involving mono- and dinuclear iron carbonyl fragments are used likewise. Unless otherwise noted, relative enthalpies obtained at the CCSD(T)/{II & 6-311+G(d,p)}//B3LYP/II level of theory are the basis for the comparison between the metal-free hydrogenation steps of N_2 and the reactions following the reduction of $(CO)_4Fe{-}N_2$. With respect to the large resources needed for a proper description of the reactions involving dinuclear species, the comparisons between the hydrogenation steps involving mono and dinuclear iron carbonyl complexes are based on the B3LYP/{II & 6-311+G(d,p)}//B3LYP/II energies only. For the evaluation of the reaction enthalpies only the most stable isomers within a reaction sequence are considered.

Reaction enthalpies and relative energies are corrected by zero-point vibrational energy (ZPE) contributions obtained at the B3LYP/II level of theory. The nature of the Fe–N and N–N bonds is examined using the natural bond orbital (NBO)[29] partitioning scheme and the charge decomposition analysis (CDA).[33] All calculations use the program packages Gaussian94/98,[56] MOLPRO96/2000,[58] and CDA2.1.[59]

5.3 Results and Discussion

5.3.1 Stepwise Hydrogenation of Isolated Dinitrogen

Calculated geometries and structural parameters of dinitrogen **1**, diazene **2a** and **2b**, hydrazine **3a** – **3c** and ammonia **4** are shown in Figure 5.1. Reaction enthalpies obtained using a variety of energy evaluations based on the B3LYP/II geometries are summarized in Table 5.2. Details of the levels of theory necessary for a reasonable treatment of the stepwise hydrogenation of isolated dinitrogen to

ammonia have been reported in a previous paper and the reaction enthalpies provided by this study serve as reference values for the present work.[129] Thus, for the individual hydrogenation steps shown in Equations (1) - (3) the benchmarks for the reaction enthalpies ΔH_R^0 are 49.2 kcal mol^{-1} (1), -23.1 kcal mol^{-1} (2) and -44.7 kcal mol^{-1} (3).[129]

$$N_2 + H_2 \rightarrow N_2H_2 \quad (1)$$
$$N_2H_2 + H_2 \rightarrow N_2H_4 \quad (2)$$
$$N_2H_4 + H_2 \rightarrow 2\,NH_3 \quad (3)$$

The data summarized in Table 5.1 clearly show that for all three hydrogenation steps convergence of the results is achieved when basis sets of at least 6-311+G(d,p) quality are used. At our highest level of theory, the enthalpies of reaction are 51.4 kcal mol^{-1} for (1), −19.3 kcal mol^{-1} for (2) and –43.3 kcal mol^{-1} for (3), respectively, which is in good agreement with the aforementioned reference data.[129] We note, however, that the predicted ΔH_R^0 for the second reduction step (2) is 3.8 kcal mol^{-1} too high, while the reaction enthalpies of reactions (1) and (3) are off by 2.2 and 1.4 kcal mol^{-1}, respectively. A more economic, yet reasonably accurate alternative is given by CCSD(T) energy evaluations in combination with the 6−311+G(d,p) basis set. The deviations from the reference values are then between 4.8 and 1.2 kcal mol^{-1}, *i.e.* the ΔH_R^0 values are 51.9 kcal mol^{-1} for (1), -18.3 kcal mol^{-1} for (2) and −43.5 kcal mol^{-1} for (3). For larger molecules, for which CCSD(T) is no longer affordable, B3LYP/{II & 6-311+G(d,p)} single-point energies are recommended. This approach leads to deviations from the reference that are particular small for reaction (2) and (3). The calculated ΔH_R^0 values of 45.3 kcal mol^{-1} for (1), -22.4 kcal mol^{-1} for (2) and –44.1 kcal mol^{-1} for (3) thus show that this approach offers a very economic way to reliable hydrogenation enthalpies.

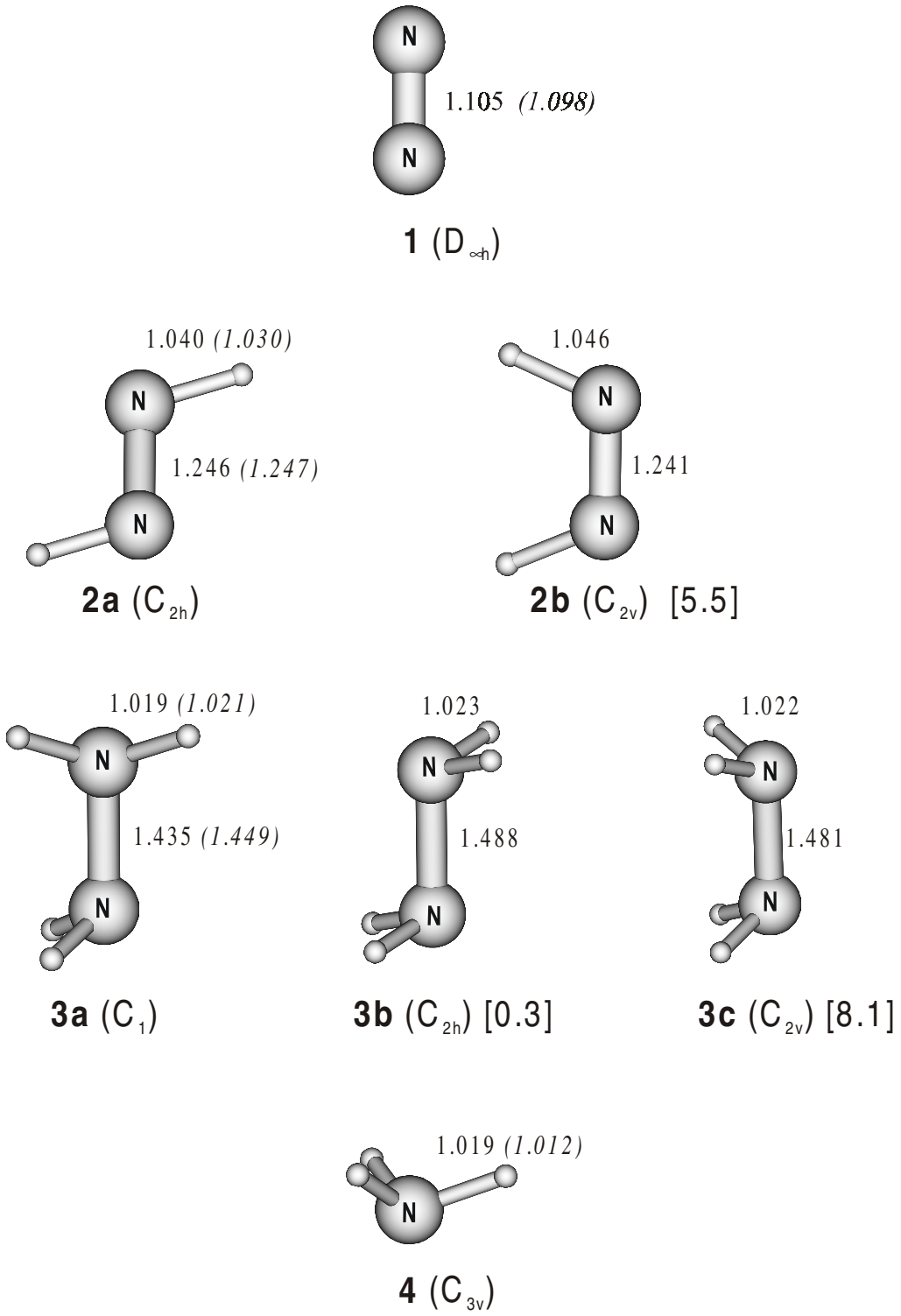

Figure 5.1 Optimized geometries of N_2 (**1**), N_2H_2 (**2**), N_2H_4 (**3**) and NH_3 (**4**). Experimental values are given in *italics*. All bond lengths are in Å. The symmetry used for the geometry optimization is given in parentheses, while relative energies (kcal mol^{-1}) with respect to the most stable isomers are given in square brackets. Angles are omitted for clarity.

Table 5.1 Hydrogenation enthalpies ΔH_R^0 (in kcal mol $^{-1}$) for the stepwise reduction of isolated dinitrogen.

	(1) $N_2 + H_2 \rightarrow N_2H_2$	**(2)** $N_2H_2 + H_2 \rightarrow N_2H_4$	**(3)** $N_2H_4 + H_2 \rightarrow 2\ NH_3$
B3LYP/			
6-31G(d)	46.9	-18.0	-37.2
6-31G(d,p)	43.2	-19.6	-40.0
6-31+G(d,p)	43.3	-22.0	-43.3
6-31+G(2df,p)	44.1	-22.6	-43.4
6-31++G(2df,p)	44.1	-22.2	-43.1
6-311G(d,p)	47.1	-20.9	-41.6
6-311+G(d,p)	45.3	-22.4	-44.1
6-311+G(2df,p)	46.5	-22.0	-43.7
6-311++G(2df,p)	46.4	-22.0	-43.7
CCSD(T)/			
6-31G(d)	55.8	-11.7	-37.3
6-31G(d,p)	49.1	-15.6	-41.6
6-311G(d,p)	44.1	-16.7	-41.7
6-311+G(d,p)	51.9	-18.3	-43.5
6-311+G(2df,p)	51.5	-19.3	-43.2
6-311++G(2df,p)	51.4	-19.3	-43.3
exp. [a]	49.2	-23.1	-44.7

[a] Ref 129.

The calculated N─N bond lengths of **1** is 1.105 Å, whereas the analogue bond length of **2a** and **2b** are calculated to be 1.246 and 1.241 Å, respectively. Compared to corresponding experimental data, the differences are quite small and in the range of 0.001 to 0.007 Å.[130,131] The same also holds for the N─H bond length of NH_3 (**4**), that is, a small deviation from the experimental data by 0.007Å is found.[132] Relatively large deviations from the experiment are, however, found for the structural parameters of **3a** – **3c**. The experimental N─N bond length of 1.449 Å is larger than the one in the most stable hydrazine isomer **3a** by 0.014 Å.[132] The calculated value is, however, in perfect agreement with other high-level *ab initio* estimates,[129] implying that a re-examination of the experimental N─N bond length might be worthwhile. The calculated bond angles of **2**, **3** and **4** are generally in good agreement with the available literature data and no significant deviations are found.

At the standard level of theory, *viz.* CCSD(T)/II//B3LYP/II the *trans*-isomer of diazene **2a** is predicted to be more stable than the *cis*-isomer **2b** by 5.5 kcal mol^{-1}, which is in line with previous results.[129,133] Furthermore, the calculations predict the *gauche* isomer **3a** to be the most stable form of hydrazine, which is consistent with other data.[133] The energy difference to the corresponding *trans*-isomer **3b** is, however, very small and only 0.3 kcal mol^{-1}, whereas the analog *cis*-hydrazine **3c** is significantly less stable than **3a** by 8.1 kcal mol^{-1}.

5.3.2 Stepwise Hydrogenation in the Presence of Mononuclear Iron Carbonyl Complexes

The influence of mononuclear iron carbonyl complexes to the stepwise hydrogenation of coordinated N_2 is evaluated by comparing the individual reduction steps shown in Equations (4) – (6) with their metal-free analogues (1) – (3).

$$(CO)_4Fe{-}N_2 + H_2 \rightarrow (CO)_4Fe{-}N_2H_2 \quad (4)$$

$$(CO)_4Fe{-}N_2H_2 + H_2 \rightarrow (CO)_4Fe{-}N_2H_4 \quad (5)$$

$$(CO)_4Fe{-}N_2H_4 + H_2 \rightarrow (CO)_4Fe{-}NH_3 + NH_3 \quad (6)$$

Optimized geometries of the iron carbonyl complexes and the relative energies between the respective axial and equatorial isomers are shown in Figure 5.2. Table 5.2 summarizes the hydrogenation enthalpies ΔH_R^0 for reactions (4) – (6) obtained at various levels of theory. Table 5.3 lists the calculated bond dissociation energies D_0 between the $Fe(CO)_4$ fragment and the nitrogen-containing ligands together with the NBO and CDA data.

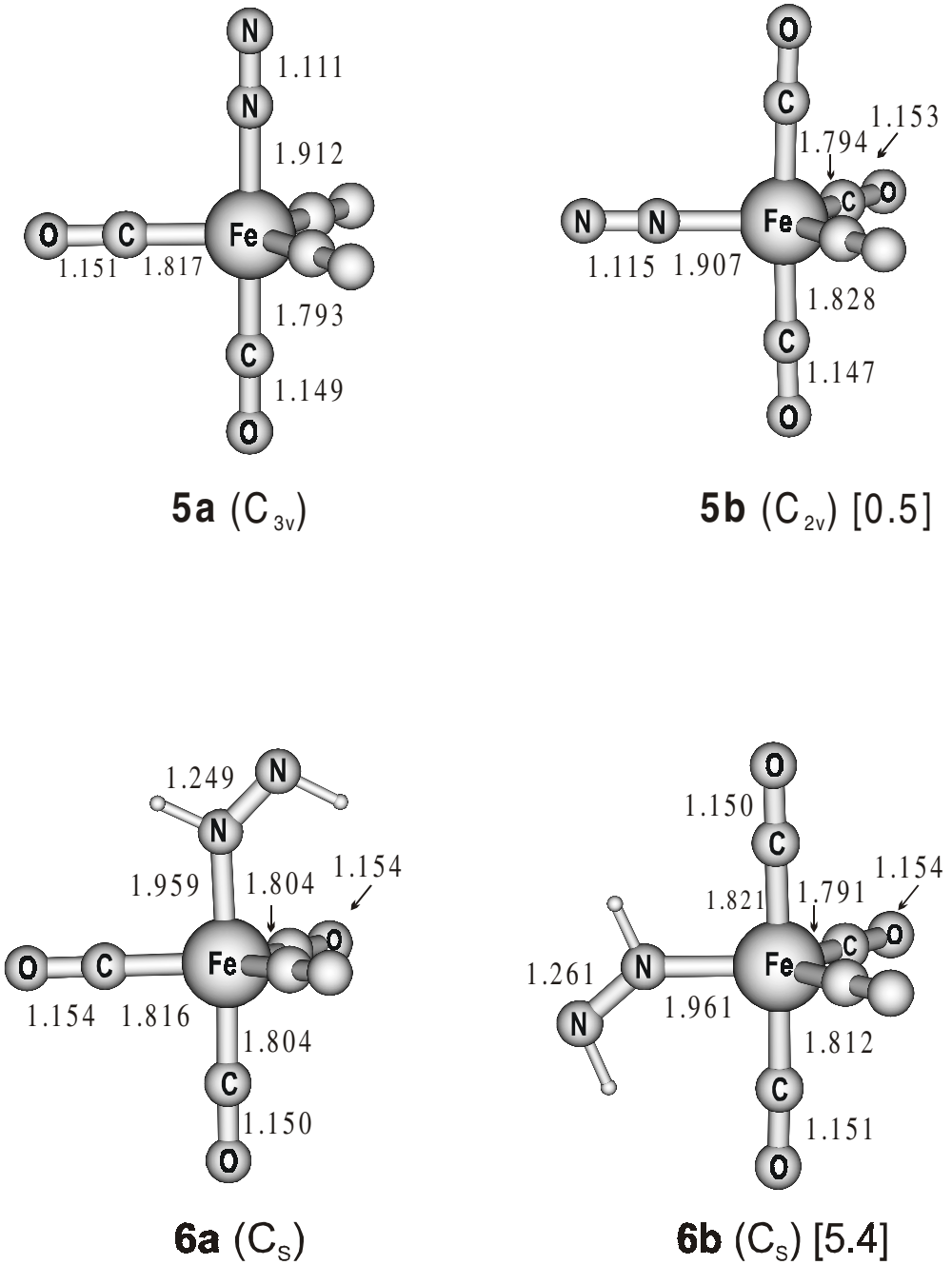

Figure 5.2 Optimized geometries of the complexes $(CO)_4Fe{-}N_2$ (**5**), $(CO)_4Fe{-}N_2H_2$ (**6**), $(CO)_4Fe{-}N_2H_4$ (**7**), and $(CO)_4Fe{-}NH_3$ (**8**). All bond lengths are in Å and the symmetry used for the geometry optimisation is given in parentheses. Relative energies (kcal mol^{-1}) with respect to the most stable isomers are given in square brackets. Angles and N–H bond lengths are omitted for clarity.

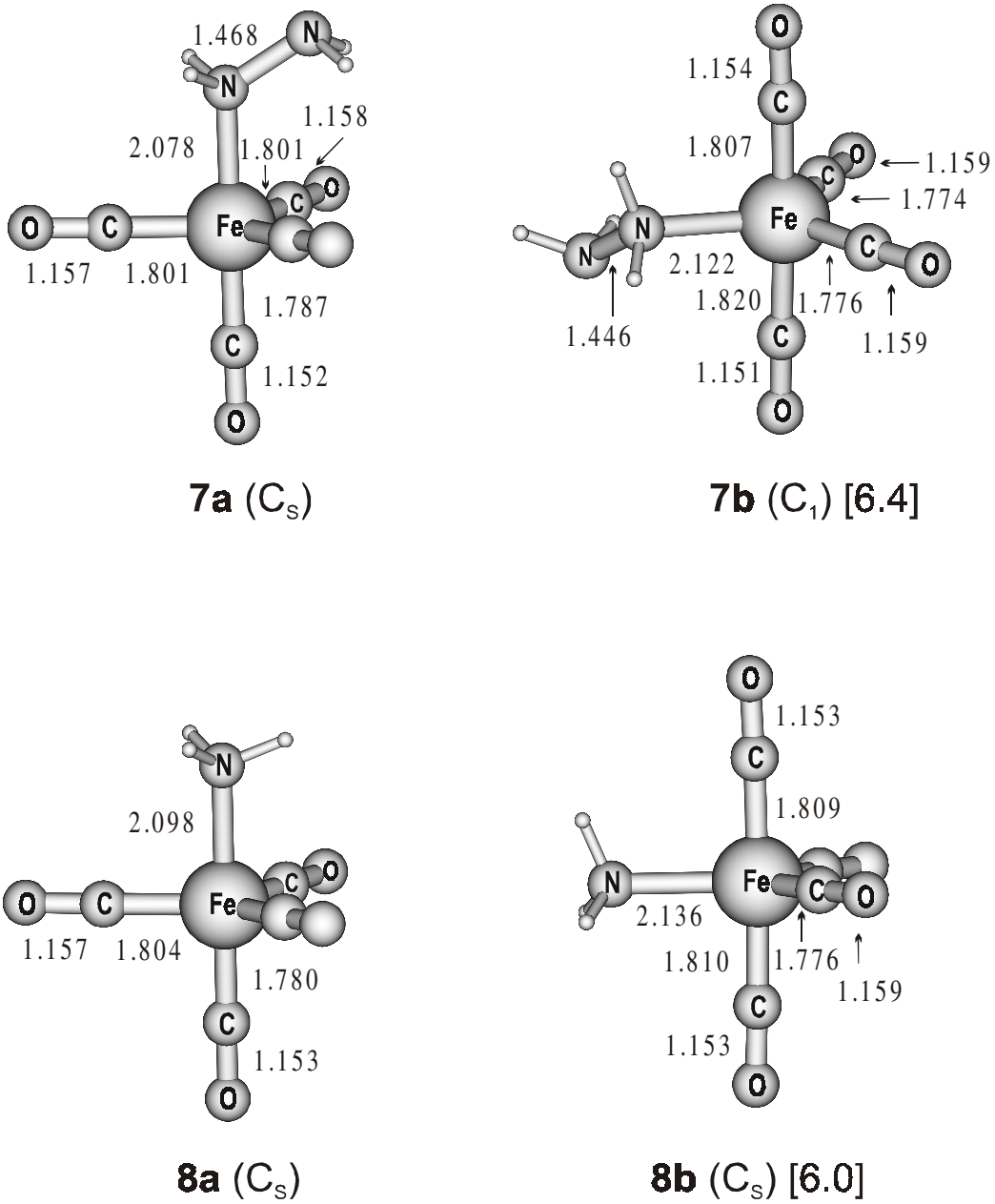

Figure 5.2 (Continued)

The most intriguing effect of the $Fe(CO)_4$ fragment on the stepwise hydrogenation of coordinated N_2 is that the enthalpy of hydrogenation of 35.8 kcal mol^{-1} for the first reduction step (4) is significantly lower by $\Delta\Delta H_R^0$ = -16.1 kcal mol^{-1} compared to the analogue step of isolated N_2 (1). One can not observe similarly drastic effect for the second and third reduction steps. To this end, the reduction of $(CO)_4Fe{-}N_2H_2$ (5) is almost as exothermic as the corresponding hydrogenation (2) of

isolated N_2H_2 ($\Delta\Delta H_R^0$ = -0.2 kcal mol^{-1}). For the hydrogenation of $(CO)_4Fe{-}N_2H_4$ (6), an even less exothermic behavior than for the metal-free analogue (3) is found and $\Delta\Delta H_R^0$ is calculated to be 4.00 kcal mol^{-1}.

Table 5.2 Hydrogenation enthalpies ΔH_R^0 (in kcal mol^{-1}) for the stepwise reduction of $(CO)_4Fe{-}N_2$. [a]

	(4) $(CO)_4FeN_2 + H_2 \rightarrow (CO)_4FeN_2H_2$	**(5)** $(CO)_4FeN_2H_2 + H_2 \rightarrow (CO)_4FeN_2H_4$	**(6)** $(CO)_4FeN_2H_4 + H_2 \rightarrow (CO)_4FeNH_3 + NH_3$
B3LYP			
6-31G(d)	32.4	-18.6	-35.4
6-31G(d,p)	30.7	-20.2	-38.8
6-311+G(d,p)	31.3	-20.4	-41.6
CCSD(T)			
6-31G(d)	39.2	-15.3	-33.4
6-31G(d,p)	35.9	-18.8	-39.0
6-311+G(d,p)	35.8	-18.5	-39.5

[a] The basis sets given in the table refer to N and H, only. For all other main group elements the 6-31G(d) basis set is used.

Table 5.3 Bond dissociation energies D_o (kcal/mol) and NBO/CDA data for mononuclear iron tetracarbonyl complexes $(CO)_4Fe{-}L$ obtained at the CCSD(T)/II//B3LYP/II level of theory.

			NBO [a]			*CDA* [a]	
complex	D_o	L	q[$Fe(CO)_4$] [b]	q(π)→L	q(σ)→[TM]	*b*	*d*
5a	22.9	N_2	-0.08	0.18	0.26	0.14	0.28
6a	39.3	N_2H_2	-0.18	0.15	0.33	0.10	0.30
7a	42.8	N_2H_4	-0.29	0.10	0.39	0.03	0.36
8a	38.9	NH_3	-0.27	0.13	0.40	-0.01	0.33

[a] [TM] = [$(CO)_4Fe$]; q(σ)→[TM] σ-donation (*d*) and q(π)→L π-back donation (*b*) according to the NBO (*CDA*) analysis.
[b] Total charge of the $Fe(CO)_4$ complex fragment.

1 is both a weak σ-donor and π-acceptor ligand. The small energy difference between the two possible isomers **5a** and **5b** of the complex $(CO)_4Fe{-}N_2$, in which N_2 is either coordinated axially or equatorially, implies no pronounced coordination site preference.[134] The structures of **5a** and **5b** show Fe–N_2 bond lengths of 1.912 Å and 1.907 Å, respectively. This is in contrasts to the results of Radius *et al.*,[47] who

predicted the Fe–N_2 bond length of axial N_2 to be shorter than that of equatorial N_2. The energy difference of 0.5 kcal mol^{-1} between **5a** and **5b** is in favour of the axial isomer, which again contrast the results of the aforementioned group.[47] Note, however that the chosen level of theory is surely beyond chemical accuracy ($\leq$ 1.0 kcal mol^{-1}) and therefore the small energy difference is not conclusive. Interestingly, however, the discrepancy of the calculated relative energy between **5a** and **5b** also has it's pendant in experimental chemistry. On the one hand, the reaction of $Fe(CO)_5$ with N_2 in polyethylene film implies that N_2 *may* occupy an equatorial rather an axial coordination site,[79] whereas photolysis experiments of $Fe(CO)_5$ in nitrogen-containing matrices[60a] show an opposite behaviour, that is a more stable axial than equatorial isomer. The N─N distances of isomers **5a** and **5b** are both slightly longer than in isolated dinitrogen **1**. The elongation on coordination is in the range of 0.006 to 0.010 Å indicating that the N─N triple bond only experiences a weak "activation". In addition, the calculated Fe─N bond energy of 22.9 kcal mol^{-1} also implies a relatively weak interaction between N_2 and the $Fe(CO)_4$ fragment.

The diazene complex formed by the first hydrogenation step (4) shows a somewhat different behavior compared to the analogue dinitrogen complex. First, the energy difference of 5.4 kcal/mol^{-1} between the axial **6a** and equatorial **6b** isomers is indeed significant and in favour of the axial isomer. Second, this preference towards axial coordination is also mirrored by the σ-donor/π-acceptor abilities of diazene.[134] NBO as well as CDA data both imply that N_2H_2 is at least as worse as π-acceptor as N_2, but at the same time a slightly better σ-donor (Table 5.3). Finally, the Fe─N bond dissociation energy of **6a** is calculated to be 39.3 kcal mol^{-1}, which is considerably higher than the corresponding value calculated for **5a**. The much stronger bond in $(CO)_4Fe{-}N_2H_2$ than that in $(CO)_4Fe{-}N_2$ is the reason why the first hydrogenation step of N_2 becomes energetically more favored by the $Fe(CO)_4$ complexation. Structural changes of diazene on complexation are again very small and the N─N bond is lengthened by only 0.003 Å.

Further hydrogenation of coordinated N_2H_2 leads to the corresponding hydrazine complex (5). NBO and CDA suggest that hydrazine is a significantly stronger σ-donor than diazene or dinitrogen (Table 5.3). Axial coordination of N_2H_4 should therefore be predominant, which is supported by the large energy difference of

6.4 kcal mol[1] that favors the axial isomer **7a** over its equatorial pendant **7b**. Interestingly, the former more stable isomer has hydrazine coordinated as *trans*-N_2H_4, which is not the most stable conformation for the isolated case. At the same time, the less stable equatorial isomer has N_2H_4 coordinated in its most stable *gauche* conformation. Structural changes of N_2H_4 on coordination are significant as shown by the lengthening of the N─N bond in **7a** of 0.033 Å with respect to isolated N_2H_4. This relatively strong influence on the internal structure of N_2H_4 is also mirrored by the large Fe─N bond dissociation energy of 42.8 kcal mol^{-1}, which is in fact the highest D_0-value encountered in this study. Note, that at the same time the calculated Fe─N bond length of **7a** of 2.078 Å is significantly larger than the corresponding bond lengths found in complexes **5** and **6**, which exhibit weaker bonds between iron and the nitrogen containing ligands.

In the final step (6) of the overall reduction process, coordinated hydrazine is reduced to ammonia. The NH_3 ligand is found by CDA and NBO to be an equally strong σ-donor as N_2H_4, whereas its π-acceptor capability is close to zero (Table 5.3). Again a dominant preference of the axial $(CO)_4Fe{-}N_2$ isomer **8a** over the equatorial isomer by 6.0 kcal mol^{-1} is found, which is in line with crystallographic data and IR spectra.[93] The estimate for the Fe─N bond dissociation energy is 38.9 kcal mol^{-1} and the calculated Fe─N bond length is 2.098Å. Both values show slight deviations from those found for the analogous hydrazine complex **7a**. These differences are, however, small thus indicating a close resemblance of these two complexes.

5.3.3 Stepwise Hydrogenation in the Presence of Dinuclear Iron Carbonyl Complexes

Figure 5.3 shows the optimized geometries of the dinuclear complexes $(CO)_4Fe{-}N_2{-}Fe(CO)_4$ (**9**), $(CO)_4Fe{-}N_2H_2{-}Fe(CO)_4$ (**10**) and $(CO)_4Fe{-}N_2H_4{-}Fe(CO)_4$ (**11**), considered in the hydrogenation steps according to equations (7) – (9). Tables 5.3 and 5.4 summarize the hydrogenation enthalpies for the individual steps and the bond dissociation energies as well as the NBO/CDA data, respectively.

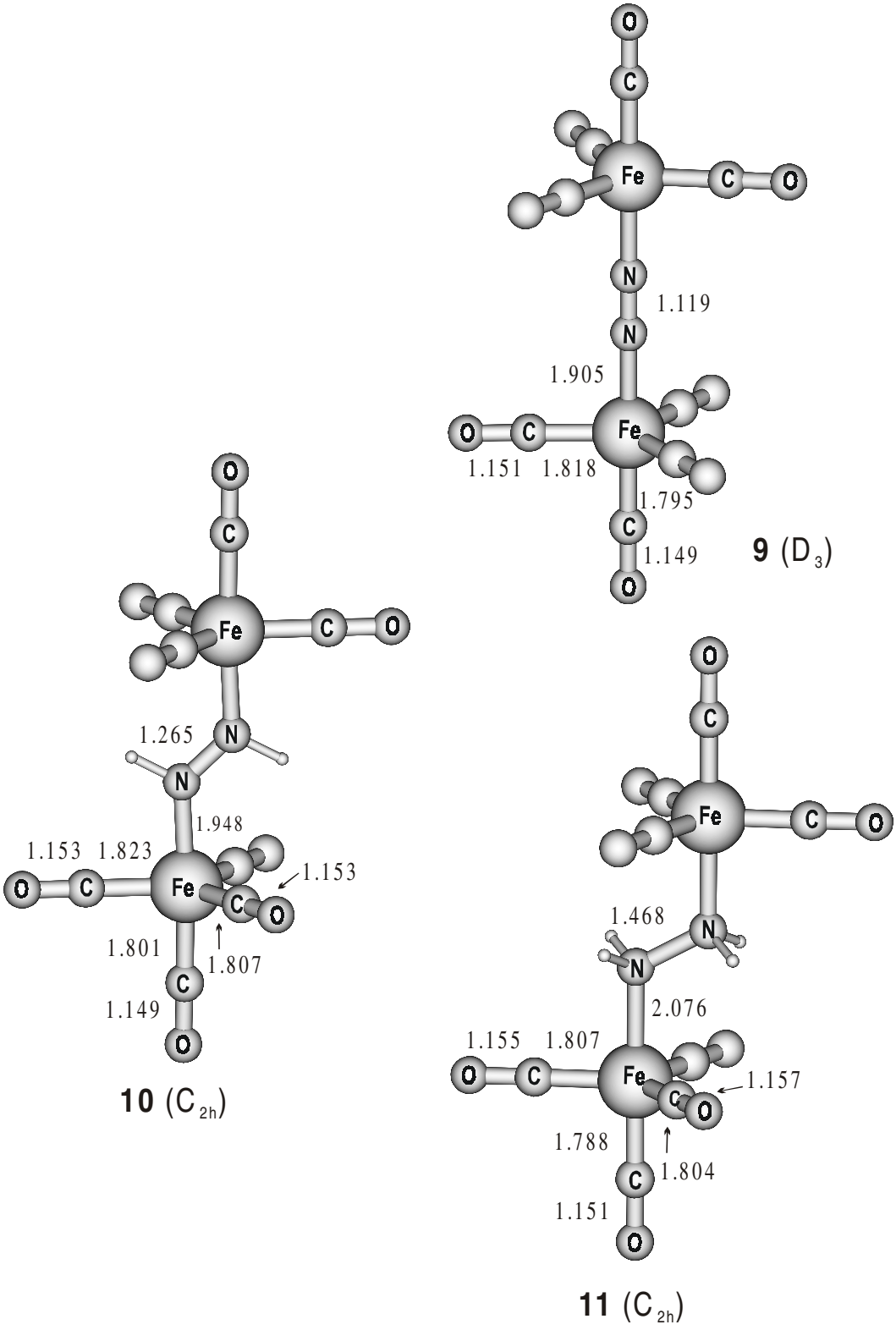

Figure 5.3 Optimized geometries of the dinuclear iron tetracarbonyl complexes $(CO)_4Fe{-}N_2{-}Fe(CO)_4$ (**9**), $(CO)_4Fe{-}N_2H_2{-}Fe(CO)_4$ (**10**), and $(CO)_4Fe{-}N_2H_4{-}Fe(CO)_4$ (**11**). All bond lengths are in Å. The symmetry used for the geometry optimization is given in parentheses.

Table 5.4 Hydrogenation enthalpies ΔH_R^0 (in kcal mol $^{-1}$) for the stepwise reduction of $(CO)_4Fe{-}N_2{-}Fe(CO)_4$. [a]

	(7) $[(CO)_4Fe]_2N_2 + H_2 \rightarrow [(CO)_4Fe]_2N_2H_2$	**(8)** $[(CO)_4Fe]_2N_2H_2 + H_2 \rightarrow [(CO)_4Fe]_2N_2H_4$	**(9)** $[(CO)_4Fe]_2N_2H_4 + H_2 \rightarrow 2(CO)_4FeNH_3$
B3LYP			
6-31G(d)	19.9	-16.2	-39.2
6-31G(d,p)	17.6	-17.0	-42.0
6-311+G(d,p)	18.2	-16.4	-40.5

[a] The basis set given in the table refers to N and H, only. All of the other elements use the 6-31G(d) basis set.

Table 5.5 Bond dissociation energies D_o (kcal/mol) and NBO/CDA data for dinuclear iron tetracarbonyl complexes $(CO)_4Fe{-}L{-}Fe(CO)_4$ obtained at the B3LYP/II//B3LYP/II level of theory.

			NBO[a]			CDA[a]	
complex	D_o[b]/D_o[c]	L	*q*[$Fe(CO)_4$] [d]	$q(\pi)\rightarrow L$	$q(\sigma)\rightarrow[TM]_2$	*b*	*d*
9	16.0/32.5	N_2	-0.05	0.40	0.50	0.28	0.50
10	28.6/59.6	N_2H_2	-0.11	0.38	0.60	0.24	0.57
11	26.1/57.7	N_2H_4	-0.24	0.18	0.66	0.11	0.63

[a] [TM] = [$(CO)_4Fe$]; $q(\sigma)\rightarrow[TM]$ σ-donation (*d*) and $q(\pi)\rightarrow L$ π-back donation (*b*) according to the NBO (*CDA*) analysis with respect to both $Fe(CO)_4$ fragments. Half of this value equals the charge transferred per $Fe(CO)_4$ unit.

[b] Fe─L bond dissociation energy per $Fe(CO)_4$ fragment according to: $[TM]_2L \rightarrow [TM]L + TM$.

[c] Total Fe─L bond dissociation energy according to: $[TM]_2L \rightarrow TM + TM + L$

[d] Total charge of the $Fe(CO)_4$ complex fragment

$$(CO)_4Fe{-}N_2{-}Fe(CO)_4 + H_2 \rightarrow (CO)_4Fe{-}N_2H_2{-}Fe(CO)_4 \quad (7)$$

$$(CO)_4Fe{-}N_2H_2{-}Fe(CO)_4 + H_2 \rightarrow (CO)_4Fe{-}N_2H_4{-}Fe(CO)_4 \quad (8)$$

$$(CO)_4Fe{-}N_2H_4{-}Fe(CO)_4 + H_2 \rightarrow 2\,(CO)_4Fe{-}NH_3 \quad (9)$$

The coordination of dinitrogen by two iron tetracarbonyl fragments results in a further significant decrease of the hydrogenation enthalpy of the first reduction step (7) by $\Delta\Delta H_R^0 = -13.1$ kcal mol^{-1} compared to the analogue step (4) involving only one $Fe(CO)_4$ fragment.[135] The overall decrease of the hydrogenation enthalpy with respect to the metal free reaction (1) thus becomes 27.1 kcal mol^{-1}. [135] This considerable change of the thermochemistry is so much more interesting as it affects the first reduction step only. To this end, the second (8) and third (9) hydrogenation

steps are even less exothermic than their mononuclear analogues (5) and (6). The $\Delta\Delta H_R^0$ values calculated on going from (5) to (8) and from (6) to (9) are 4.0 and 1.1 kcal mol^{-1}, respectively.

The $Fe(CO)_4$ fragments in **9** are twisted against each other by 8.7°. The rotation barrier is extremely low and one can find several different isomers that are energetically not distinguishable from each other. In comparison to the mononuclear analogue **5a** further significant alterations of structural parameters can not be observed. Note that the Fe─N bond length becomes shorter by 0.007Å, which is paralleled by the lengthening of the N─N bond by 0.008Å. The CDA and NBO data in Table 5.5 show that the σ-donor properties of N_2 embraced by two iron tetracarbonyl fragments is hardly changed compared to **5a** and only the π-acceptor characteristics are somewhat enhanced. The overall Fe─N_2─Fe bond dissociation energy is calculated to be 32.5 kcal mol^{-1}, which translates to a Fe─N bond dissociation energy per $Fe(CO)_4$ fragment of 16.0 kcal mol^{-1}. Comparison of these data with the bond dissociation energy obtained for **5a** implies a decreased bond strength between an *individual* $Fe(CO)_4$ subunit and N_2.

Further hydrogenation of **9** results in the formation of the corresponding diazene complex $(CO)_4Fe{-}N_2H_2{-}Fe(CO)_4$ (**10**). The Fe─N as well as the N─N bond lengths of **10** are calculated to be 1.948 Å and 1.265 Å, respectively. These values are in good agreement with the structural data of the related $[\mu\text{-}N_2H_2\{Fe(PPr_3)('S_4')\}_2]$ ($'S_4'^{2-}$ = 1,2-bis(2-mercaptophenylthio) ethane(2-)) complex reported by Sellmann and co-workers.[136] The small deviations of less than 0.052 Å are noteworthy as such Fe(II)($'S_4'$) complexes involving multidentate organosulfur ligands are often used as model compounds for the Fe-Mo-, Fe-V- and Fe-Fe-nitrogenases.[122,124,136] A non-negligible shortening of the Fe─N bond by 0.011 Å and a lengthening of the N─N bond by 0.016 Å on going from **6a** to its dinuclear pendant **10** should be noted. Interestingly, CDA and NBO data indicate that the ability of diazene to act as σ-donor is almost unaltered. Only a slight increase of the π-acceptor capabilities of N_2H_2 is observed. The Fe─N bond dissociation energy of **10** follows the same trend as shown above for the corresponding dinitrogen complex. That is, the bond strength per $Fe(CO)_4$ fragment is smaller when compared to the mononuclear case, whereas

the overall binding energy obtained by complexation with two $Fe(CO)_4$ fragments is significantly larger.

In the second step of the overall reduction process (8), the analogue hydrazine complex $(CO)_4Fe{-}N_2H_4{-}Fe(CO)_4$ (**11**) is formed by hydrogenation of coordinated diazene. The comparison with complex **7a** shows hardly any shortening of the Fe–L bond length or lengthening of the N–N bond. It should be pointed out that the NBO data imply that both the σ-donor as well as the π-acceptor abilities of N_2H_4 decrease slightly on going from the mononuclear complex to **11**. With respect to the σ-donor character this is also supported by the corresponding CDA values. Although the analogue π-acceptor value implies a stronger π-backdonation of N_2H_4 in the dinuclear complex **11**, the predicted magnitude is too small to account for a significant π-acceptor character of N_2H_4.

5.4 Conclusion

Density functional and *ab initio* calculations were used to evaluate the influence of iron tetracarbonyl complexes to the stepwise hydrogenation of dinitrogen. In comparison to the metal-free reduction process, it is found that complexation by one or two $Fe(CO)_4$ fragments results in a pronounced change of the thermochemistry of the first hydrogenation step, namely the reduction of coordinated N_2 to N_2H_2. The effects on the second and third hydrogenation steps, *viz* the hydrogenation of coordinated N_2H_2 and N_2H_4 are much weaker and even less exothermic reduction processes compared with the metal-free hydrogenation are predicted. The decrease of the hydrogenation enthalpy is larger for the reduction of the $(CO)_4Fe{-}N_2{-}Fe(CO)_4$ than it is for the reduction of $(CO)Fe{-}N_2$. Furthermore, NBO and CDA data imply a consistent trend of the σ-donor/π-acceptor behavior of the nitrogen-containing ligands that correlates with the relative energies between the respective isomers. Thus, ligands with comparatively high σ-donor capabilities like N_2H_4 and NH_3 give iron tetracarbonyl complexes in which the axial isomers are considerably more stable than their equatorial pendant. In addition to that, only ligands like N_2 and N_2H_2, which show noticeable π-acceptor quantities in their respective $Fe(CO)_4$ complexes, are affected by the formation of dinuclear complexes.

Thus, their Fe─N bond lengths are shorter and the N─N bonds are longer in the dinuclear complexes than in their mononuclear analogues. This behavior is also mirrored by a slight increase of the π-acceptor ability on going from $(CO)_4Fe─X$ to $(CO)_4Fe─X─Fe(CO)_4$ (X = N_2, N_2H_2) complexes. Such structural changes are absent for N_2H_4, and both its σ-donor as well as its π-acceptor behavior are less pronounced in $(CO)_4Fe─N_2H_4─Fe(CO)_4$ than in $(CO)_4Fe─N_2H_4$.

Chapter 6. ^{13}C and ^{19}F NMR Chemical Shifts of the Iron Carbene Complex $(CO)_4FeCF_2$ — A Theoretical Study at Non-Local DFT (BP86 and B3LYP) Level

6.1 Introduction

Metal carbene complexes have remarkable importance as intermediates of many organometallic reactions[98,137-138] such as olefin metathesis[139] catalytic reduction of CO by H_2[140], Ziegler-Natta polymerization reaction,[141] etc. What drew the attention of the theoreticians soon after the report of the first stable TM carbene complex 1964 [98] is the nature of the chemical bond between a transition metal (TM) and a carbene fragment CR_2. The most successful bonding model explains the difference between Fischer and Schrock carbene complexes by using the singlet and triplet states of the CR_2 fragments and the residual as building blocks for the respective complexes (Scheme 4.1 (a) in Chapter 4).

Fischer-type complexes[102] are characterized by electrophilic reactivity of the carbene ligand. The TM-carbene bond in this type of complexes is described in terms of donor-acceptor interactions between a ($^1A_1$) singlet carbene and a singlet metal fragment with $R_2C \rightarrow$ TM σ-donation and π-back donation $R_2C \leftarrow$ TM. The TM-C bond in Schrock complexes[142] is described as a covalent bond between a ($^3B_1$) triplet carbene and a triplet metal fragment. Generally, stable Fischer complexes have a π-donor group such as OR, NR_2 or halogens at the carbene ligand which is bound to a TM in a low oxidation state, while Schrock-type complexes have nucleophilic carbene ligands typically with hydrogen, alkyl or aryl groups but no π-donor substituents at the carbene carbon atom. Although many TM carbene complexes can easily be identified to belong to one of the two classes, some species are difficult to classify. For example, dihalocarbenes have singlet ground state and large singlet $\rightarrow$ triplet excitation energy[143] and thus donor-acceptor bonding should be exclusively formed in their respective TM complexes, i.e. they are typical Fischer complexes. However, they may in fact exhibit either nucleophilic or electrophilic behaviour at the carbene center indicating no strict separation between these two classes.[144]

In the past decades, a lot of experimental techniques have been applied to characterize carbene complexes. NMR spectroscopy is the most important analytical method for monitoring and controlling the success of the syntheses and providing the first indications to which class of compounds the molecule belongs. NMR data often give detailed information about the electronic structure of the products.

However, because of the high activity of carbene complexes, it is often difficult to isolate the monomer, determine the structure parameters and characterize the nature of the complex. Iron tetracarbonyl complex with fluorine substituted carbene ligand may be a good example for illustrating this case.[145] As all attempts to directly observe and designate NMR spectroscopy were unsuccessful, theoretical calculations maybe helpful to predict the electronic structure.

It is now possible to calculate heavy-atom molecules like TM compounds reliably by using either classical quantum chemical methods in conjunction with pseudopotentials[55] or density functional theory (DFT).[146] Though DFT methods for calculating NMR chemical shifts are still young, some standards have already been established. The excellent performance of DFT methods in predicting NMR parameters for TM compounds was reviewed recently.[147] Here, calculated NMR results of the model complex $(CO)_4FeCF_2$ at the non-local DFT (BP86 and B3LYP) level are reported. To my best knowledge, it is the first report of fully optimized geometry of the iron carbene complex at the DFT (BP86) level. The electronic structure of the complex was analyzed within the framework of natural bond orbital analysis (NBO).[29] The nature of donor-acceptor bonding was examined by charge decomposition analysis (CDA).[33] The gauge-invariant atomic orbitals (GIAO)[148] were used to calculate chemical shifts of relevant compounds for its varieties of advantages[149] over the individual gauge for localized orbitals (IGLO)[150], although there is no definite statement about the accuracy of these two methods.[147]

However, as the accurity of the theoretically predicted NMR chemical shift for this kind of carbene complexes is unknown, it is ambiguous to say the calculated NMR values are reliable. Any way, the ^{13}C chemical shifts of the parent compound $Fe(CO)_5$ have been experimentally obtained, and the theoretical NMR values of

$Fe(CO)_5$, such as chemical shifts, magnetic susceptibility, and spin-spin coupling constants are available.[151] A comparison between experimental and theoretical works could be done, at least for $Fe(CO)_5$, and the extension from $Fe(CO)_5$ to $Fe(CO)_4CF_2$ should be reliable for ^{13}C NMR calculations at the same theoretical level. As for ^{19}F NMR data, some previous theoretical works make it possible to compare them with the results reported here.

6.2 Methods

Geometries of $(CO)_4FeCF_2$ and related complexes $Fe(CO)_5$ and $Fe(CO)_4$ were optimized at the BP86[15,17] level of theory with the help of Gaussian 94/98[56] suite of *ab initio* programs. Vibrational analyses were done numerically at the same level. CCSD(T)[21] calculations were carried out with Molpro96/2000[58] using the BP86-optimized geometries. In CCSD(T) calculations, triple excitations were taken into consideration noniteratively and core orbitals were excluded from the active space.

Three kinds of basis set systems (denoted as BS-A, BS-B, and BS-C) were used in the work. The standard basis II[55] (here denoted as BS-A) was employed for geometry optimization and for following frequency calculations, which has small-core effective potential (ECP) with a (441/2111/41) valence for Fe[27c] and 6-31G(d)[53] basis for other atoms. In BS-B, the core electrons of Fe were replaced with a Stuttgart ECP[26a] with a more flexible (311111/2111/411) basis set. D95[152] basis sets were used for C, H, Cl, F. In BS-C, the same basis set and ECPs as those in BS-B were used for iron. For other atoms, the Bochum basis set II[153] was employed. No corrections were introduced concerning the use of ECPs in the NMR chemical shift calculation of this work.

^{13}C and ^{19}F NMR chemical shifts were calculated using GIAO[148] approach with the help of Gaussian 94/98[56]. CDA calculations have been performed using the program CDA 2.1.[59]

6.3 Results and Discussion

6.3.1 Geometries, Vibrational Frequencies and Bond Dissociation Energies

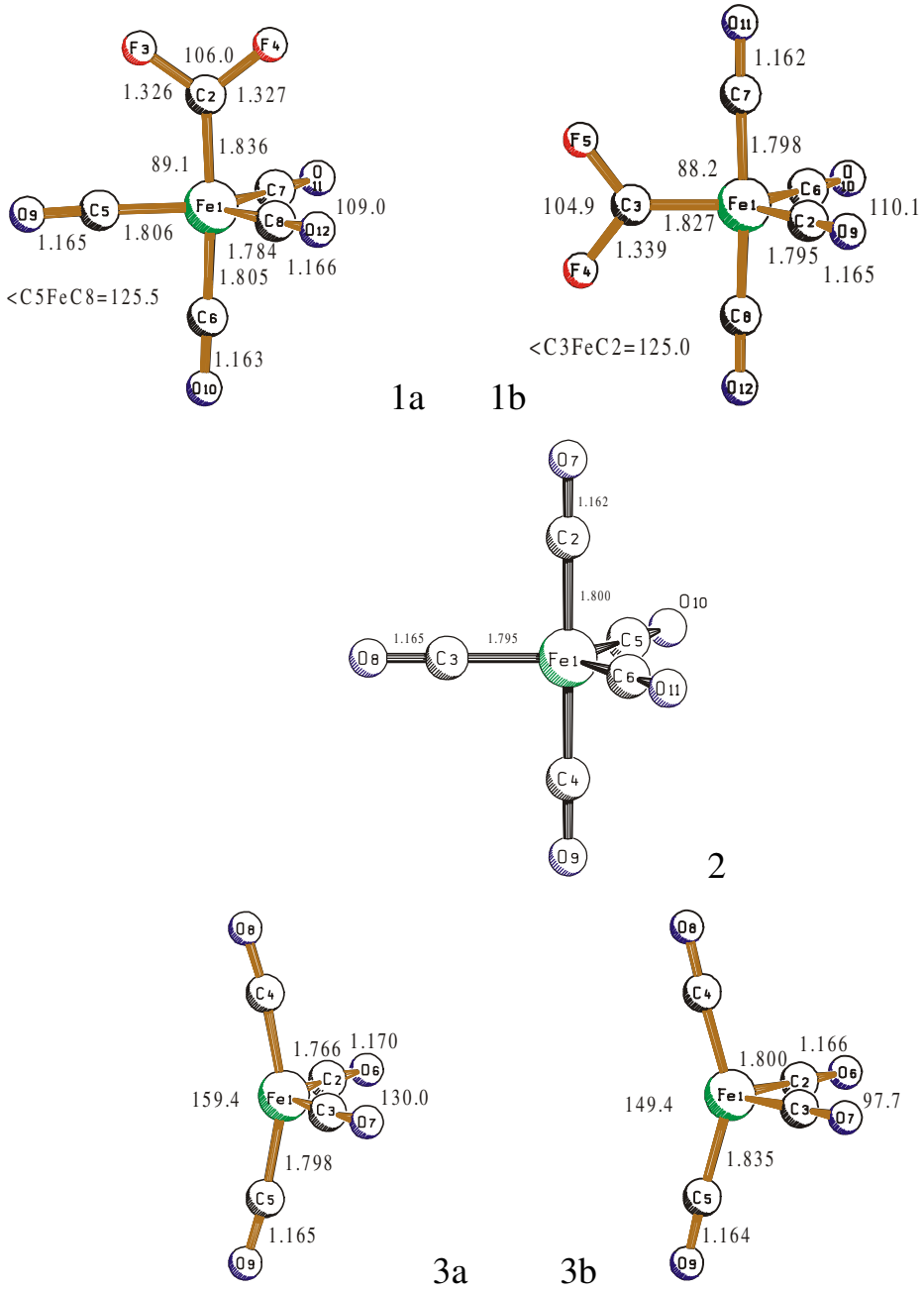

Figure 6.1 Optimized geometries (BP86/BS-A) of $(CO)_4FeCF_2$ (**1**), $Fe(CO)_5$ (**2**), and $Fe(CO)_4$(**3**). Distances in Å , angles in degree.

The optimized geometries of the carbene complex $(CO)_4FeCF_2$ (**1**), the relevant parent complex $Fe(CO)_5$ (**2**) and the dissociation fragment $Fe(CO)_4$ (**3**) are

shown in Figure 6.1. Both the total energies and the relative energies calculated at the BP86/BS-A and CCSD(T)/BS-A levels are presented in Table 6.1. The CF_2 ligand may occupy either an axial or equatorial position in a trigonal bipyramidal iron complex. The only isomer of **1** is the equatorial one in C_{2v} symmetry (**1b**). The axial form where the ligand CF_2 is clipsed to one equatorial CO is a transition state. Further optimization could not locate another stationary point where the ligand CF_2 accepts a staggered form respective to one of the equatorial CO group. Therefore, it is reasonable that **1a** is 2.2 kcal/mol at the BP86/BS-A level and 4.2 kcal/mol at the CCSD(T)/BS-A level less stable than **1b**, which means that the potential energy surface of **1** is very flat.

Table 6.1 Calculated total energies E_{tot} (au.), relative energies E_{rel} (kcal/mol) , zero point vibrational energies ZPE (kcal/mol), number of imaginary frequencies *i*, theoretically predicted bond dissociation energy D_e and D_o (kcal/mol) [a, b, c] at BP86/BS-A and at CCSD(T)/BS-A.

		BP86 [d]						CCSD(T)			
Molecule	No.	Sym.	E_{rel}	ZPE	*i*	D_e	D_o	E_{tot}	E_{rel}	D_e	D_o
$(CO)_4Fe=CF_2$	**1a**	C_s	0.0	27.4	*1*	61.0	58.0	-812.25479	0.0	62.7	59.7
$(CO)_4Fe=CF_2$	**1b**	C_{2v}	-2.2	27.5	*0*	63.2	60.1	-812.26154	-4.2	66.9	63.8
$(CO)_4Fe$-CO	**2**	D_{3h}		26.2	*0*	48.7	45.8	-688.13594		47.8	44.9
$Fe(CO)_4$ ($^1A_1$)	**3a**	C_{2v}	0.0	20.3	*0*			-575.02598			
$Fe(CO)_4$ ($^3B_2$)	**3b**	C_{2v}	-0.2	18.9	*0*			nc [e]			
CF_2 ($^1A_1$)		C_{2v}	0.0	4.1	*0*			-237.12890	0.0		
CF_2 ($^3B_1$)		C_{2v}	52.9	4.1	*0*			-237.04258	54.2		
CO		$C_{\infty v}$		3.0	*0*			-113.03377			

[a] using BP86/BS-A optimized geometries
[b] using ZPE values at BP86/BS-A
[c] with respect to singlet $Fe(CO)_4$ and CF_2 or CO
[d] BP86 total energies are omitted for clarity
[e] SCF not converged

A previous theoretical study [154] using the SCF-MO method showed that the barrier to rotation around the Fe-$C_{carbene}$ is very low, only 2.9 kcal/mol for $(CO)_4FeCH(OH)$. What should be noted is that an assumed geometry was used in the work. By using a fully optimized geometry of **1b,** this work can give a more reliable answer about the barrier to rotation of the carbene ligand group in the iron carbene complex.

Unfortunately, the stationary point which is symmetry equivalent (C_{2v}) to **1b** could not be located by means of optimization and other standard methods for finding a transition state. By varying only the rotational angle 90° around the Fe-$C_{carbene}$ bond an unstable isomer **1c** is obtained, which is 14.1 kcal/mol higher in energy than **1b** (Scheme 6.1). Further optimization led to a second order saddle point **1d** which corresponds to simultaneous (1) rotation around the Fe-$C_{carbene}$ axis and (2) changes of the axial and equatorial (OC)Fe(CO) angle. **1d** is 10.3 kcal/mol at the BP86/BS-A level less stable than **1b**. Therefore, it can be concluded that the barrier to rotation should be lower than 14.1 kcal/mol.

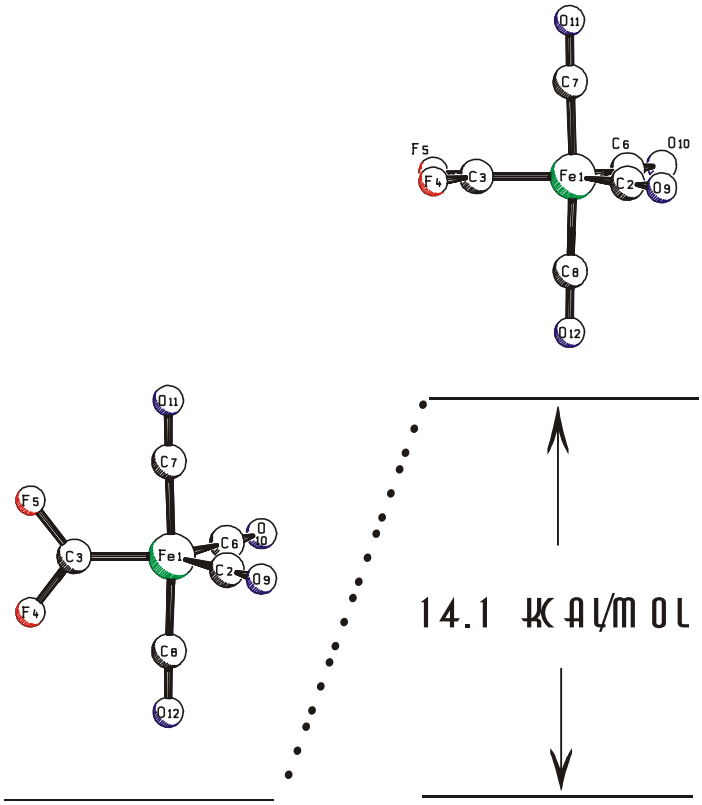

Scheme 6.1 Schematic representation of the rotation barrier of CF_2 group around Fe-$C_{carbene}$ axis for $(CO)_4FeCF_2$ (eq) complex. Barrier height is obtained at BP86/BS-A approximately (see text fro detail)

The calculated Fe-$C_{carbene}$ dissociation energy with respect to singlet $Fe(CO)_4$ (**3a**) is D_o = 60.1 kcal/mol at BP86/BS-A and D_o = 63.8 kcal/mol at CCSD(T)/BS-A

(both using ZPE-correction at the BP86/BS-A level), respectively, which is about 14-19 kcal/mol stronger than that of Fe-C in its parent complex $Fe(CO)_5$ (**2**) (Table 6.1) for which the D_o value at the CCSD(T)/BS-A level is comparable with experimental data.[74] It is reasonable to deduce that D_o is slightly overestimated (~ 3 kcal/mol) for the carbene complex **1b** at the highest theoretical level of the work, CCSD(T). The energy difference between singlet (**3a**) and triplet iron tetracarbonyl (**3b**) is negligible as it is only 0.2 kcal/mol at the BP86/A level.

The geometry of the fragment $Fe(CO)_4$ in the complex is more similar to singlet **3a** than to triplet **3b** . The geometries of the free ligand CF_2 is calculated to be 1.330 Å for the C-F bond length and 104.0 ° for the F-C-F angle. These values are in good agreement with experimental results of 1.3 Å /104.8° [152] or 1.3035 Å /104.8° [156]. The calculated geometry of the CF_2 group changes only little (0.009 Å and 0.9°) on going from the free ligand to complex **1b**. Hence, $(CO)_4FeCF_2$ (**1b**) may be explained as a combination of singlets $Fe(CO)_4$ and CF_2.

There are no experimental results available to make a direct comparison of the Fe-carbene distance with the theoretical value. One can compare the calculated value of **1b** with the complex $(CO)_4Fe=C=C=C[C(tBu)_2OC(O)O]$,[87b] where the ligand is equatorial. A rather short bond distance (1.80 Å) was observed in experiment. The calculated Fe-C bond length of **1b** is 1.827 Å.

Table 6.2 lists the calculated vibrational frequencies and IR intensities of **1b**, which may help to characterize the possible monomer complex experimentally.

Table 6.2 Calculated vibrational frequencies (cm^{-1}) and IR intensity (km $mole^{-1}$) of $(CO)_4FeCF_2$(eq) at BP86/II level

symm.	mode	frequencies	intensity
A_1	[CO]	2097	80
	[CO]	2034	266
	[CF] + $[FeC]_F$	1196	628
	[δFeCO] + [δFCF]	678	76
	[δFCF] + [δFeCO]	633	23
	[FeC]	485	2
	[δFeCO]	476	15
	[FeC]	451	0
	[FeC] + [δFCF]	359	2
	[δCFeC]	112	0
	[δCFC]	66	0
A_2	[δFeCO]	559	0
	[δFeCO]	388	0
	[δCFeC]	93	0
	[δFCF]	64	0
B_1	[CO]	2017	881
	[δFCF] + [δFeCO]	707	144
	[δFCF] + [FeC]	536	4
	[δFeCO] + [δFCF]	469	1
	[δFeCO]	378	2
	[δCFeC]	104	0
	[δFCF] + [δCFeC]	23	0
B_2	[CO]	2032	1131
	[CF]	1145	208
	[δFeCO]	620	104
	[δFeCO]	532	3
	[δFeCO]	452	0
	[δFCF]	296	1
	[δFCF]	126	0
	[δCFeC]	102	0

6.3.2 Bonding Analysis

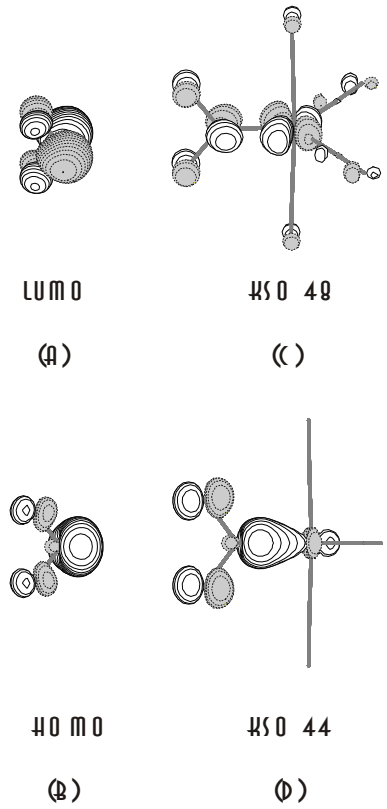

Figure 6.2 Schematic representation of the most important Kohn-Sham (KS) orbitals of the free ligand and the carbene complex **1b** for F_2C-$Fe(CO)_4$ interactions as revealed by CDA. LUMO(a) and HOMO(b) of free carbene (left) and donation-back donation interaction of **1b** (right). d ≈ 0, b = 0.232, r = -0.046 for KSO 48 and d = 0.178, b = 0.018, r = -0.003 for KSO 44.

The CDA results at BP86/A show that the complex **1b** can be reasonably interpreted as a complex between the closed-shell fragments $Fe(CO)_4$ and CF_2 since the residue term is ≈ 0. The CDA data for **1b** indicate also that the carbene ligand CF_2 is a stronger electron donor (d = 0.544) than acceptor (b = 0.291) which is similar to the situation in carbene complexes of group 6.[37,38c] The most important Kohn-Sham (KS) orbitals of the free ligand CF_2 and the carbene complex **1b** are schematically shown in Figure 6.2. The HOMO (Figure 6.2, b) is antibonding in character while the LUMO (Figure 6.2, a) is strongly antibonding for the free ligand. These orbitals interact with those of $Fe(CO)_4$ fragment of the same symmetry.

A previous study (see chapter 2) using the NBO partitioning scheme at the B3LYP/BS-A level predicted that the donation $F_2C \rightarrow Fe(CO)_4$ and the back donation $F_2C \leftarrow Fe(CO)_4$ are almost the same amount and the back donation is slightly stronger (0.01e) than the donation which correlates well with the ligand equatorial site preference. Here the distinction in energy between **1a** and **1b** at the BP86/A level is even subtle. Consequently, the ligand CF_2 should have even weaker site preference to coordinate equatorially. More interesting, the NBO results obtained at the BP86 level show that the CF_2 ligand is a somewhat stronger donor than acceptor, which indicates a weak dependence of NBO values on the computational method.

6.3.3 ^{13}C and ^{19}F NMR Chemical Shifts

Table 6.3 Calculated ^{13}C NMR and ^{19}F NMR chemical shifts of $(CO)_4FeCF_2$(eq) and $Fe(CO)_5$ at the DFT (BP86, B3LYP) level (in ppm). [a, b, c]

		BP86/			B3LYP/			
No.	Atom	BS-A	BS-B	BS-C	BS-A	BS-B	BS-C	exp
1b	C_{ax}	208.3	229.1	234.4	224.9	250.4	254.1	
	C_{eq}	197.6	221.5	222.0	210.1	234.8	237.7	
	$C_{aver.(ax,eq)}$	203.0	225.3	228.2 (208.9[d])	217.5	242.6	245.9 (210.5[d])	208[e1] 206[e4]
	$C_{carbene}$	244.7	264.7	271.3 (252.3[d])	261.2	286.5	290.3 (254.9[d])	258[e1] 243[e4]
	F	125.8 (162.5)	126.7(168.0)	129.7 (179.9)	138.3(146.8)	136.8 (151.6)	139.4 (162.8)	
2	C_{ax}	210.7	234.2	238.0	226.8	254.6	257.0	
	C_{eq}	198.6	221.1	223.5	210.2	235.1	237.7	
	$C_{aver.(ax,eq)}$	203.4	226.3	229.3 (210.0)	216.8	242.9	245.4 (210.0)	211.9±0.2[f]

[a] using the optimized geometry at the BP86/BS-A level.
[b] respective to CH_4 for ^{13}C.
[c] using CCl_3F as primary reference (using HF as secondary reference with a correction of 214 ppm experimentally determined difference between HF and CCl_3F given in parentheses) for ^{19}F.
[d] using experimental ^{13}C value of secondary reference $Fe(CO)_5$ as standard one.
[e] see Berke, H.; Größmann, U.; Huttner, G.; Zsolnai, L. *Chem. Ber.,* **1984**, *117*, 3423
[e1] $(CO)_4Fe{=}C{=}C{=}C(tBu)_2$ (**1**) in $CDCl_3$, -50 °C
[e4] $(CO)_4Fe{=}C{=}C{=}C[C(tBu)_2OC(O)O]$ (**4**) in $CDCl_3$, 0 °C.
[f] see Mann, B. E. *J. Chem. Soc*., *D,* **1971**, 1173.

The calculated ^{13}C and ^{19}F NMR chemical shifts of **1b** are given in Table 6.3. The relevant data of **2** are also collected for comparison.

Due to the dynamical rearrangement of the axial and equatorial carbonyl groups only one signal is recorded for **2** in ^{13}C NMR experiment. The calculated GIAO values (average of axial and equatorial ones) at the DFT level with the biggest

basis set (BS-C) are ~ 20 (BP86//BP86/BS-A) and 35 (B3LYP//BP86/BS-A) ppm higher than the experimental value [157] (Table 6.3). Similar results were obtained in Simion and Sorensen's quantum mechanical study [151a]. The computational error in this work is acceptable because of the moderate basis set. By enlarging the basis set on going from BS-A to BS-C, the calculated GIAO-NMR values converge well. With **2** as a reference (assigned to 210 ppm), the estimated ^{13}C NMR values of **1b** with BS-C are given in parentheses (Table 6.3), which is in better agreement with experiment. The chemical shift of the carbonyl carbon is predicted to be at 208.9 (BP86) and 210.5 (B3LYP) ppm. Most iron complexes with a formal Fe=C bond have low-field ^{13}C resonance[158]. For complex $[(MeO)_3P]_2(CO)_2Fe=C=CHCHO$, in which the two trimethyl phosphite ligands were axial, even lower field ^{13}C resonances (above 300 ppm) than the values given in Table 6.3 were reported. [159] Note that, the experimental values of carbene compounds cited in Table 6.3 (column 8) have different ligands.

Table 6.4 Calculated DFT-GIAO Anisotropies of ^{13}C Chemical Shifts for Carbenic Carbon Atom in $(CO)_4Fe\text{-}CF_2$ (**1b**) . [a, b]

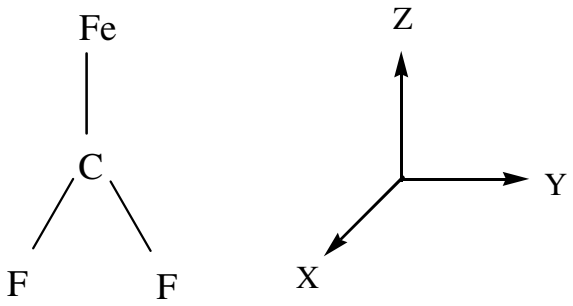

Method	Basis set	δ(YY)	δ(XX)	δ(ZZ)	Δ(YY-XX)	Δ(XX-ZZ)
BP86	BS-A	436.1	171.5	126.7	264.6	44.8
	BS-B	476.6	185.6	132.0	291.0	53.5
	BS-C	485.6	190.0	138.3	295.6	51.7
B3LYP	BS-A	489.5	170.9	123.3	318.6	47.6
	BS-B	540.6	186.8	132.0	353.7	54.9
	BS-C	546.6	190.2	134.1	356.4	56.1

[a] respective to CH_4 .
[b] using BP86/BS-A optimized geometry.

Final investigation was made by examining the calculated anisotropies of ^{13}C chemical shifts of carbenic C in **1b .** Table 6.4 shows that the component of the ^{13}C chemical shift tensor, which is parallel to the Fe-$C_{carbene}$ bond of the complex **1b** (ZZ), is shielded more than other components. In the direction of the p(π) orbital of carbenic carbon atom (XX), the shield effect is not as significant as that in the ZZ direction, but it is still ~ 300 (BP86/BS-B and BP86/BS-C) and 350 ppm (B3LYP/BS-B and B3LYP/BS-C) stronger than the YY component where the attack of nucleophilic regents may take place.

The ^{19}F NMR of **1b** was recalculated with the GIAO approach, the improved estimations are given in parentheses in Table 6.3. HF is chosen as secondary reference which was optimized at the same theoretical level as for **1b.** The calculated ^{19}F NMR value of **1b** respective to HF is converted to the standard CCl_3F scale of 214 ppm.[150b, 160]

$$\delta (^{19}F \text{ of } \mathbf{1b}) = \sigma (^{19}F \text{ of } \mathbf{1b}) - \sigma (^{19}F \text{ of HF}) - 214 \text{ ppm} \quad \text{(Eq 6.1)}$$

In this way, the calculated ^{19}F NMR chemical shift for **1b** with BS-C is about δ180 ppm (BP86) and δ163 ppm (B3LYP), respectively.

6.4 Summary and Conclusion

The calculated geometry of **1b** shows that the carbene ligand CF_2 prefers to coordinate equatorially to iron in a trigonal bipyramidal configuration, but the preference is very weak. The Fe-$C_{carbene}$ bond in **1b** is ~20 kcal/mol stronger than the Fe-C bond in the parent complex **2**. The bonding analysis shows that **1b** can be considered as a donor-acceptor complex (Fischer-type carbene complex). The calculated ^{13}C NMR data of **1b** is reliable when **2** is used as secondary reference.

Chapter 7. Summary

In this thesis, equilibrium geometries, bond dissociation energies and relative energies of axial and equatorial iron tetracarbonyls $Fe(CO)_4L$ (L = CO, CS, N_2, NO^+, CN^-, NC^-, η^2-C_2H_4, η^2-C_2H_2, CCH_2, CH_2, CF_2, NH_3, η^2-H_2, NF_3, PH_3, PF_3) are calculated using density functional theory (B3LYP) and effective-core potentials with a valence basis set of DZP quality for iron and 6-31G(d) all-electron basis sets for the other elements. The theoretically predicted structural parameters are in very good agreement with previous theoretical results and with available experimental data. Improved estimates for the $(CO)_4Fe$–L bond dissociation energies (D_o) are obtained using the CCSD(T)/II//B3LYP/II combination of theoretical methods. The strongest Fe–L bonds are found for those complexes involving NO^+, CN^-, CH_2 and CCH_2 with bond dissociation energies of 105.1, 96.5, 87.4 and 83.8 kcal mol^{-1}, respectively. These values decrease to 78.6, 64.3 and 64.2 kcal mol^{-1}, respectively, for NC^-, CF_2 and CS. The $Fe(CO)_4L$ complexes with L = CO, η^2-C_2H_4, η^2-C_2H_2, NH_3, PH_3 and PF_3 have even smaller bond dissociation energies ranging from 45.2 to 37.3 kcal mol^{-1}. Finally, the smallest bond dissociation energies of 23.5, 22.9 and 18.5 kcal mol^{-1}, respectively are found for the ligands NF_3, N_2 and η^2-H_2. A detailed examination of the $(CO)_4Fe$–L bond in terms of a quantitative Dewar-Chatt-Duncanson (DCD) model using the CDA method and NBO analyses reveals a general trend that is consistent with the classical picture of the ligand site preference in trigonal bipyramidal $Fe(d^8)$-complexes. Hence, by comparing relative energies of the axial and the equatorial isomers of $Fe(CO)_4L$ with the relative σ-donor/π-acceptor strengths of the various ligands L, it is found that exclusively π-accepting ligands like NO^+ prefer equatorial coordination sites, whereas the strong σ-donors CN^-, NC^- preferably coordinate axially. Although this behaviour is less obvious for moderately strong σ-donors like NH_3, NF_3, PH_3, and PF_3, a distinct axial preference is noticeable. Ligands like CS and N_2 have σ-donor/π-acceptor ratios close to unity leading to energetically likewise favourable isomers, thus indicating an indifferent attitude towards axial and equatorial coordination sites. However, exception has been found for L= C_2H_4, C_2H_2, CCH_2, CH_2, CF_2, H_2.

Quantum chemical calculations at the NL-DFT (B3LYP) and CCSD(T) levels of theory have also been carried out for the carbon complex $Fe(CO)_4C$. The bonding situation was analyzed with the NBO partitioning scheme and with the topological analysis of the electron density distribution. The results have been compared with the bonding situations in $Fe(CO)_4CH_2$, $I(CO)_3FeCH$ and $Fe(CO)_5$. The trigonal-bipyramidal complex $(CO)_4FeC$ with an axial Fe-C bond is a minimum on the singlet potential energy surface, while the equatorial form is a transition state. The Fe-C bond has a large dissociation energy D_e = 84.1 kcal/mol at B3LYP/II and D_e = 94.5 kcal/mol at CCSD(T)/II. The carbon ligand is a strong π–acceptor and an even stronger σ donor. The analysis of the electronic structure suggests that $(CO)_4FeC$ should behave like a carbon nucleophile. Geometry optimization of the donor-acceptor complex $(CO)_4FeC\text{-}BCl_3$ yielded a strongly bonded compound which has a calculated C-B bond energy of D_e = 25.6 kcal/mol at B3LYP/II and 27.1 kcal/mol at CCSD(T)/II, respectively. Lewis acid stabilized carbon complexes like $(CO)_4FeC\text{-}BCl_3$ might be isolated under appropriate conditions.

Theoretical studies using density functional theory (DFT) at the B3LYP level of theory and at the CCSD(T) level of theory are reported for mononuclear and dinuclear iron carbonyl complexes with the nitrogen-ligands N_2, N_2H_2, N_2H_4, and NH_3 bound to the metal. The reaction enthalpies ($\Delta H°$) for the hydrogenation steps of free N_2 are well reproduced when relative large basis sets like 6-311+G(d,p) are used for N and H. The respective $\Delta H°$-values are 45.3(51.9), -22.4 (-18.3), -44.1(-43.5) kcal mol^{-1} for the formation of N_2H_2, N_2H_4, and NH_3 at the B3LYP(CCSD(T)) level of theory, respectively. For the reaction involving nitrogen coordinated to the $Fe(CO)_4$ complex fragment, activation of N_2 is found for the first reaction step yielding coordinated N_2H_2. The reaction energy is reduced by more than 14 kcal mol^{-1} compared to the analogous reaction of free N_2. This trend is even stronger for the dinuclear iron carbonyl complex $[Fe(CO)_4]_2N_2$ where $\Delta H°$ for the first hydrogenation step is lower by 18.2 kcal mol^{-1}. In contrast to the first reaction step, the last two steps (from N_2H_2 via N_2H_4 to NH_3) show almost no catalytic effect by the iron tetracarbonyl complex fragments.

The structure and NMR chemical shifts of the iron carbene complex $(CO)_4FeCF_2$ were calculated at the NL-DFT (BP86 and B3LYP) level with three

different basis sets. The calculated geometries indicate that the carbene ligand occupies an equatorial position in the trigonal bipyramidal complex, however with a weak site preference. No minimum was found for the axial isomer. The nature of the bonding between iron and carbene ligand in the Fischer-type complex was examined. The Fe-$C_{carbene}$ bond strength (D_o = 63.8 kcal/mol) of $(CO)_4FeCF_2$ (eq) is higher (~20 kcal/mol) than that of Fe-CO in its parent complex $Fe(CO)_5$ at the CCSD(T) level. The barrier to rotation of equatorial CF_2 ligand around Fe-$C_{carbene}$ axis in $(CO)_4FeCF_2$ (eq) was estimated to be lower than 14.1 kcal/mol at the BP86 level. ^{13}C and ^{19}F NMR chemical shifts of $(CO)_4FeCF_2$ (eq) were calculated for the first time using the GIAO method. With theoretical calculations as a guidance, it is suggested that the ^{13}C NMR resonance of the carbonyl carbon atom almost does not change when it goes from the parent complex $Fe(CO)_5$ to substituted $(CO)_4FeCF_2$ (eq). The carbenic C atom is much more deshielded (~ 40 ppm) with respect to the CO ligand at both BP86 and B3LYP. The ^{19}F NMR chemical shift is predicted to be in the range of 160-180 ppm combining the results from DFT-GIAO calculations.

Zusammenfassung

In der vorliegenden Arbeit wurden die Gleichgewichtsstrukturen und relativen Energien von $Fe(CO)_4L$ Komplexen mit den Liganden L = CO, CS, N_2, NO^+, CN^-, NC^-, η^2-C_2H_4, η^2-C_2H_2, CCH_2, CH_2, CF_2, η^2-H_2, NH_3, NF_3, PH_3 und PF_3 mittels DFT-Rechnungen und nichtrelativistischem Pseudopotential (ECP) für Eisen sowie Standard-Basissätzen (DZP) für die Liganden untersucht. Für zuverlässige Dissoziationsenergien (D_o) wurden *single point* CCSD(T)-Energien auf den B3LYP-Geometrien gerechnet. Die stärksten Fe-L-Bindungen ergeben sich für die Komplexe mit den Liganden L = NO^+, CN^-, CH_2 und CCH_2 von 105.1, 96.5, 87.4 und 83.8 kcal mol^{-1}. Es folgen die Komplexe mit L = NC^-, CF_2 und CS, mit D_o-Werten von 78.6, 64.3, und 64.2 kcal mol^{-1}. Die Komplexe mit L = CO, η^2-C_2H_4, η^2-C_2H_2, NH_3, PH_3 und PF_3 haben kleinere Bindungsenergien von 45.2 bis 37.3 kcal mol^{-1}. Die niedrigsten Dissoziationsenergien von 23.5, 22.9 und 18.5 kcal mol^{-1} ergeben sich für die Komplexe mit L = NF_3, N_2 und η^2-H_2. Zur Analyse der Fe-L Donor-Akzeptor-Wechswickung wurden die CDA (*Charge Decomposition Analysis*) und NBO (*Natural Bond Orbital*) Methoden verwendet. Die Ergebnisse zeigen, daß die bevorzugte Stellung eines Liganden L in axialer oder äquatorialer Stellung in einem fünffach koordiniertem Komplex mit trigonal-bipyramidaler Anordnung in guter Übereinstimmung mit klassischen Vorstellungen sind. Ein Vergleichen zwischen der relativen σ-Donor/π-Akzeptor-Starke der Liganden L und der Stabilität von äqutorialen bzw. axialen Isomeren der Komplexe $Fe(CO)_4L$ zeigt, daß NO^+ als π-Akzeptor eine äquatoriale Stellung bevorzugt. Als starke σ-Donor werden CN^- und NC^- in der axialen Position gebunden. Eine klare Bevorzugung der axialen Stellung wird für relativ starke σ-Donor NH_3, NF_3, PH_3, und PF_3 gefunden. Wegen der ähnlich starken σ-Donierung und π-Rückdonierung ergeben sich für die Komplexe mit L = CS und N_2 keine bevorzugte Koordinationsstelle. Ausnahme wird für die Liganden C_2H_4, C_2H_2, CCH_2, CH_2, CF_2 and H_2 gefunden.

Die quantenchemischen Rechnungen von Carbonkomplex $Fe(CO)_4C$ wurden auf dem B3LYP- und CCSD(T)-Niveau durchgeführt. Die Bindungsverhältnisse wurden mittels der NBO und der AIM-Methoden untersucht. Die Ergebnisse wurden mit den

Daten des Carbenkomplexes $Fe(CO)_4CH_2$, des Carbinkomplexes $I(CO)_3FeCH$ und des Carbonylkomplexes $Fe(CO)_5$ verglichen. Der trigonal–bipyramidale Komplex $Fe(CO)_4C$ mit axialer Fe-C_{carbon} Bindung ist ein Minimum auf der Singulett Potential-Energie-Fläche. Die äquatoriale Form ist ein Übergangszustand. Die Bindungsenergie von Fe-C in $(CO)_4FeC(ax)$ ist mit D_e = 94.5 kcal/mol sehr stark. Der Kohlenstoff-Ligand ist ein starker π–Akzeptor und noch stärkerer σ-Donor. Die Analyse der elektronischen Struktur zeigte, daß der Kohlenstoff-Ligand des Komplexes $(CO)_4FeC$ nukleophile Eigenschaft haben sollte. Die Geometrieoptimierung des Donor-Akzeptor-Komplexs $(CO)_4FeC\text{-}BCl_3$ ergibt einen stark gebunden Komplex, der eine C-B-Bindungsenergie von D_e = 27.1 kcal/mol auf CCSD(T)/II-Niveau hat. Der von der Lewis-Säure stabilisierte Carbonkomplex $(CO)_4FeC\text{-}BCl_3$ ist unter günstigen Bedingungen zu isolieren.

Die theoretischen Untersuchungen über die mit Stickstoff-Liganden N_2, N_2H_2, N_2H_4, und NH_3 koordinierten Eisenkomplexe wurden mit der DFT-Methode B3LYP durchgeführt. Die Reaktionsenthalpie ΔH^o wurde auf CCSD(T)-*single-point* Niveau berechnet. Bei Verwendung relativ großer Basissätze (6-311+G(d,p)) sind die berechneten ΔH^o–Werte für die Reaktion von N_2 zu NH_3 in guter Übereinstimmung mit experimentellen Daten. Die ΔH^o-Werte auf B3LYP (CCSD(T))-Niveau sind 45.3 (51.9), -22.4 (-18.3), -44.1 (-43.5) kcal mol^{-1} für die Bildung der Moleküle N_2H_2, N_2H_4, und NH_3. Bei den das mononukleare $Fe(CO)_4$-Fragment erhaltenen Reaktionen ist eine N_2-Aktivierung gefunden worden. Die benötige Energie zur Bildung von koordiniertem N_2H_2 ist 14 kcal mol^{-1} geringer als die analoge nicht-katalysierte Reaktion. Dieser Trend ist noch stärker für die Reaktion mit dem dinuklearen Fe-Fragment. Der ΔH^o-Wert beträgt hier nur 18.2 kcal mol^{-1}. Im Vergleichen zu diesem ersten Schritt zeigt sich, daß die zwei nachfolgenden Schritten keinen Katalyseeffekt der $Fe(CO)_4$-Fragmente aufweisen.

Die Struktur und chemische Verschiebungen des Eisenkomplexes $Fe(CO)_4CF_2$ wurden auf dem NL-DFT-Niveau (BP86 und B3LYP) mit drei verschiedenen Basissätzen untersucht. Im stabilsten Isomer ist CF_2 äquatorial koordiniert. Die Energiedifferenz zwischen axialen und äquatorialen Isomer ist aber sehr gering. Bei der ^{13}C-NMR-Berechnung gibt es keine Änderung für den Carbonyl-Kohlenstoff vom Carbonylkomplex $Fe(CO)_5$ hin zum Carbenkomplex $Fe(CO)_4CF_2$. Dagegen ist der

Carben-Kohlenstoff mehr als 40 ppm abgeschirmt. Aus den berechneten ^{19}F chemischen Verschiebungen kann man abschätzen, daß der Wert im Bereich 160-180 ppm sein sollte.

Chapter 8. References

1 Whitmire, K. H. in "Comprehensive Coordination Chemistry II: A Review of the Literature 1982-1994", Abel, E. W.; Stone, F. G. A.; Wilkinson, G. Eds., Vol. 7, Pergamon Press: Oxford, 1995.

2 Elschenbroich C.; Salzer. A. "Organometallics : A Concise Introduction" 2. Edition, VCH: Weinheim, 1992.

3 (a) Hehre, W. J.; Radom, L.; Schleyer, P. v. R.; Pople, J. A. "Ab initio Molecular Orbital Theory", Wiley, New York, 1986. (b) Levine, I. N. "Quantum Chemistry", Prentice Hall, Englewood Cliffs, 1991. (c) Szabo, A.; Ostlund, N. "Modern Quantum Chemistry: Introduction to Advanced Electronic Structure Theory", Dover Publications, Mineola, New York, 1996. (d) Jensen, F. "Introduction to Computational Chemistry", John Wiley & Sons, Chichester, 1999. (e) Kutzelnigg, W. "Einführung in die Theoretische Chemie", VCH, Weiheim, 1992. (f)Atkins, P. W.; Friedman, R. S. "Molecular Quantum Mechanics", Oxford University Press, Oxford, 3rd Ed. 1997.

4 (a) Schrödinger, E. *Ann. Physik* **1926**, *79*, 361. (b) Schrödinger, E. *Ann. Physik* **1926**, *80*, 437. (c) Schrödinger, E. *Ann. Physik* **1926**, *81*, 109.

5 Born, M.; Oppenheimer, J. R. *Ann. Physik* **1927**, *84*, 457.

6 (a) Hartree, D. R. *Proc. Camb. Phil. Soc*. **1928**, *24*, 89. (b) Fock. V. *Z. Phys.* **1930**, *61*, 161.

7 Pauli, W. *Z. Physik* **1925**, *31*, 765.

8 (a) Slater, J. C. *Phys. Rev.* **1929**, *34*, 1293 (b) Slater, J. C. *Phys. Rev.* **1930**, *35*, 509.

9 Eckart, C. E. *Phys. Rev.* **1930**, *36*, 878.

10 (a) Roothaan, C. C. J. *Rev. Mod. Phys.* **1951**, *23*, 69 (b) Hall, G. G. *Proc. Roy. Soc. London* **1951**, *A205*, 541.

11 Møller, C.; Plesset, M. S. *Phys. Rev.* **1934**, *46*, 618.

12 (a) Thomas, L. H. *Proc. Camb. Phil. Soc.* **1927**, *23*, 542. (b) Fermi, E. *Rend. Accad. Lincei.* **1927**, *6*, 602.

13 Hohenberg, P. ; Kohn, W. *Phys. Rev. B.* **1964**, *136*, 864.

14 Kohn, W. ; Sham, L. J. *Phys. Rev. A.* **1965**, *140*, 1133.

15 Becke, A. D. *Phys. Rev. A.* **1988**, *38*, 3098.

16 Vosko, S. H.; Wilk, L.; Nusair, M. *Can. J. Phys.* **1980**, *58*, 1200.

17 Perdew, J. P. *Phys. Rev. B.* **1986**, *33*, 8822.

18 Lee, C.; Yang, W.; Parr, R. G.; *Phys. Rev. B.* **1988**, *37*, 785.

19 Becke, A. D. *J. Chem. Phys*. **1993**, *98*, 5648.

20 Perdew, J. P.; Wang, Y. *Phys. Rev. B.* **1992**, *45*, 13244.

21 (a) Bartlett, R. J. *J. Phys. Chem.* **1989**, *93*, 1697 (b) Cizek, J. *J. Chem. Phys.* **1966,** *45,* 4256 (c) Cizek, J. *Adv. Chem. Phys.* **1969,** *14*, 35.

22 Slater, J. C. *Phys. Rev.,* **1930**, *36*, 75.

23 Boys, S. F. *Proc. Roy. Soc. London* **1950**, *A200*, 542

24 Phillips, J. C.; Kleinman, L. *Phys. Rev.* **1959**, *116*, 287

25 Huzinaga, S.; Anzelm, J.; Klobukowski, M.; Radzio-Andzelm, E.; Sakai, Y.; Tatewaki, H. "Gaussian Basis Sets for Molecular Calculations", Elsevier, Amsterdam, 1984

26 (a) Dolg, M.; Wedig, U.; Stoll, H.; Preuß, H. *J. Chem. Phys*. **1987**, *86*, 866. (b) Bergner, A.; Dolg, M.; Küchle, W.; Stoll, H.; Preuß, H. *Mol. Phys.* **1993**, *80*, 1431.

27 (a) Hay, P.J.; Wadt, W.R. *J. Chem. Phys*. **1985**, *82*, 270. (b) Hay, P.J.; Wadt, W.R. *J. Chem. Phys*. **1985**, *82*, 284. (c) Hay, P.J.; Wadt, W.R. *J. Chem. Phys*. **1985**, *82*, 299.

28 Bader, R. F. W. "Atoms in Molecules. A Quantum Theory", Oxford Press, 1990.

29 Reed, A. E.; Curtiss, L. A.; Weinhold, F. *Chem. Rev.* **1988**, *88*, 899.

30 Weinhold, F. in *Encyclopedia of Computational Chemistry*, Schleyer, P. v. R.; Allinger, N. L.; Clark, T.; Kollman, P. A.; Schaefer, H. F. III.; Scheiner, P. R.; Eds, Wiley-VCH: Chichester, **1998**, ***3***, 1793-1811

31 Löwdin, P.-O. *Phys. Rev.* **1955**, *97*, 1474

32 Reed, A. E.; Weinhold, F. *J. Chem. Phys.* **1985**, *83*, 1736

33 Dapprich S.; Frenking, G. *J. Phys. Chem*. **1995**, *99*, 9352.

34 (a) Dewar, J. S. *Bull. Soc. Chim. Fr*. **1951**, *18,* C79. (b) Chatt, J.; Duncanson, L. A. *J. Chem. Soc.* **1953**, 2939.

35 See, for example: Cotton, F. A. Wilkinson, G.; Grimes, R. N. "*Advanced Inorganic Chemistry*", 6th ed.; John Wiley and Sons: New York, 1999.

36 See, for example: (a) Hoffmann, R.; Chen, M., M.-L.; Thorn, D. L. *Inorg. Chem.* **1977**, *16*, 506. (b) Hoffmann, R.; Albright, T. A.; Thorn, D. L. *Pure Appl. Chem.* **1978**, *50*, 1 and references cited therein. (c) Schilling, B. E. R.; Hoffmann, R. *J. Am. Chem. Soc.* **1979**, *101*, 3456.

37 Ehlers, A.W.; Dapprich, S.; Vyboishchikov, S.F.; Frenking, G. *Organometallics* **1996**, *15*, 105.

38 (a) Pidun, U.; Frenking, G. *J. Organomet. Chem.* **1996**, *525*, 269. (b) Frenking, G.; Pidun, U. *J. Chem. Soc., Dalton Trans.* **1997**, 1653. (c) Vyboishchikov, S. F.; Frenking, G. *Chem. Eur. J*. **1998**, *4*, 1428; 1439.

39 (a) Szilagyi, R. K.; Frenking, G. *Organometallics* **1997**, *16*, 4807. (b) Diefenbach, A.; Bickelhaupt, F. M.; Frenking, G. *J. Am. Chem. Soc.* **2000**, *122*, 6449

40 (a) Strauss, S. H. *Chemtracts: Inorg. Chem.* **1997**, *10* , 77. (b) Lupinetti, A. J.; Frenking, G.; Strauss, S. H. *Angew. Chem.* **1998**, *110*, 2229; *Angew. Chem., Int. Ed. Engl.* **1998**, *37*, 2113.

41 (a) Goldman, A. S.; Krogh-Jespersen, K. *J. Am. Chem. Soc.* **1996**, *118*, 12159. (b) Lupinetti, A. J.; Fau, S.; Frenking, G.; Strauss, S.H. *J. Phys. Chem. A*. **1997**, *101*, 9551.

42 (a) Bauschlicher, C. W.; Bagus, P. S. *J. Chem. Phys*. **1984**, *81*, 5889. (b) Bauschlicher, C. W.; Petterson, L. G. M.; Siegbahn, P. E. M. *J. Chem. Phys.* **1987**, *87*, 2129. (c) Bauschlicher, C. W.; Langhoff, S. R.; Barnes, L. A. *Chem. Phys.* **1989**, *129*, 431. (d) Bauschlicher, C. W. *J. Chem. Phys.* **1986**, *84*, 260. (e) Bauschlicher, C. W.; Bagus, P. S.; Nelin, C. J.; Roos, B. O. *Chem. Phys.* **1986**, *85*, 354. (f) Barnes, L. A.; Rosi, M.; Bauschlicher, C. W. *J. Chem. Phys.* **1991**, *94*, 2031. (g) Barnes, L. A.; Rosi, M.; Bauschlicher, C. W. *J. Chem. Phys.* **1990**, *93*, 609. (h) Barnes, L. A.; Bauschlicher, C. W. *J. Chem. Phys.* **1989**, *91*, 314. (i) Blomberg, M. R. A.; Brandemark, U. B.; Siegbahn, P. E. M.; Wennerberg, J.; Bauschlicher, C. W. *J. Am. Chem. Soc.* **1988**, *110*, 6650. (j) Hall, M. B.; Fenske, R. F. *Inorg. Chem.* **1972**, *11*, 1620. (k) Sherwood, P. E.; Hall, M. B. *Inorg. Chem.* **1979**, *18*, 2325. (l) Sherwood, P. E.; Hall, M. B. *Inorg. Chem.* **1980**, *19*, 1805. (m) Williamson, R. L.; Hall, M. B. *Int. J. Quantum Chem.* **1987**, *21S*, 503. (n) Hillier, I. H.; Saunders, V. R. *Mol. Phys.* **1971**, *23*, 1025. (o) Hillier; I. H.; Saunders, V. R. *J. Chem. Soc., Chem. Commun*.

1971, 642. (p) Ford, P. C.; Hillier, I. H. *J. Chem. Phys.* **1984**, *80*, 5664. (q) Ford, P. C.; Hillier, I. H.; Pope, S. A.; Guest, M. F. *Chem. Phys. Lett.* **1983**, *102*, 555. (r) Cooper, G.; Green, J. C.; Payne, M. P.; Dobson, B. R.; Hillier, I. H. *Chem. Phys. Lett.* **1986**, *125*, 97. (s) Cooper, G.; Green, J. C.; Payne, M. P.; Dobson, B. R.; Hillier, I. H.; Vincent, M.; Rosi, M. *J.Chem. Soc., Chem. Commun.* **1986**, 438. (t) Moncrieff, D.; Ford, P. C.; Hillier, I. H.; Saunders, V. R. *J. Chem. Soc., Chem. Commun.* **1983**, 1108. (u) Smith, S.; Hillier, I. H.; von Niessen, W.; Guest, M. C. *Chem. Phys.* **1989**, *135*, 357. (v) Vanquickenborne, L. G.; Verhulst, J. *J. Am. Chem. Soc.* **1987**, *109*, 4825. (w) Pierfoot, K.; Verhulst, J.; Verbeke, P.; Vanquickenborne, L. G. *Inorg. Chem.* **1989**, *28*, 3059. (x) Yamamoto, S.; Kashiwagi, H. *Chem. Phys. Lett.* **1993**, *205*, 306. (y) Blomberg, M. R. A.; Siegbahn, P. E. M.; Lee, T. L.; Rendell, A. P.; Rice, J. E. *J. Chem. Phys.* **1991**, *95*, 5898.

43 (a) Kunze, K.L.; Davidson, E. R. *J. Phys. Chem.* **1992**, *96*, 2129. (b) Davidson, E. R.; Kunze, K. L.; Machado, F. B. C.; Chakravorty, S. J. *Acc. Chem. Res.* **1993**, *26*, 628. (c) Baerends, E. J.; Rozendaal, A. in " *Quantum Chemistry: The Challenge of Transition Metals and Coordination Chemistry*", Veilhard, A. (Ed), Proceedings of the NATO ASI, Reidel: Dordrecht, p. 159, 1986.

44 Ziegler, T.; Tschinke, V.; Ursenbach, C. *J. Amer. Chem. Soc*. **1987**, *109,* 4825.

45 See, for example: (a) Rossi, A. R.; Hoffmann, R. *Inorg. Chem.* **1975**, *14*, 365. (b) Burdett, J. K. *Inorg. Chem.* **1976**, *15*, 212. (c) Favas, M. C.; Kepert, D. L *Porg. Inorg. Chem.* **1980**, *27*, 325. (c) Bauer, D. P.; Ruff, J. K. *Inorg. Chem.* **1983**, 22, 1686. (d) Beach, D. B.; Smit, S. P.; Jolly, W. L. *Organometallics* **1984**, *3*, 556.

46 Albright, T. A.; Burdett, J. K.; Whangbo, M. H. "*Orbital Interactions in Chemistry*", Wiley: New York, 1985, pp 324-325.

47 Radius, U.; Bickelhaupt, F.M.; Ehlers, A.W.; Goldberg, N.; Hoffmann, R. *Inorg. Chem.* **1998**, *37*, 1080.

48 Li, J.; Schreckenbach, G.; Ziegler, T. *Inorg. Chem.* **1995**, *34*, 3245.

49 Torrent, M.; Sola, M.; Frenking, G. *Organometallics* **1999**, *18*, 2801.

50 Gonzalez-Blanco, O.; Branchadell, V. *Organometallics* **1997**, *16*, 5556.

51 Decker, S. A.; Klobukowski, M. *J. Am. Chem. Soc.* **1998**, *120*, 9342.

52 (a) Becke, A. D. *J. Chem. Phys*. **1993**, *98*, 5648. (b) Lee, C.; Yang, W.; Parr, R. G. *Phys. Rev.* **1988**, *B37*, 785.

53 (a) Hehre, W. J.; Ditchfield R.; Pople, J. A. *J. Chem. Phys*. **1972**, *56*, 2257. (b) Hariharan, P. C.; Pople, J.A. *Theoret. Chimica Acta* **1973**, *28*, 213. (c) Gorden, M. S. *Chem. Phys. Lett*., **1980**, *76*, 163.

54 The additional polarization function is taken from the standard 6-31G(d,p) basis set. For details, see Ref 53b.

55 Frenking, G.; Antes, I.; Böhme, M.; Dapprich, S.; Ehlers, A.W.; Jonas, V. ; Neuhaus, A.; Otto, M.; Stegmann, R.; Veldkamp, A.; Vyboishchikov, S. F. in *Reviews in Computational Chemistry*, Vol. 8, Lipkowitz K.B.; Boyd D.B. (Eds), VCH: New York, pp.63-144, 1996.

56 (a) *Gaussian 94*, Revision D.4, M. J. Frisch, G. W. Trucks, H. B. Schlegel, P. M. W. Gill, B. G. Johnson, M. A. Robb, J. R. Cheeseman, T. Keith, G. A. Petersson, J. A. Montgomery, K. Raghavachari, M. A. Al-Laham, V. G. Zakrzewski, J. V. Ortiz, J. B. Foresman, J. Cioslowski, B. B. Stefanov, A. Nanayakkara, M. Challacombe, C. Y. Peng, P. Y. Ayala, W. Chen, M. W. Wong, J. L. Andres, E. S. Replogle, R. Gomperts, R. L. Martin, D. J. Fox, J. S. Binkley, D. J. Defrees, J. Baker, J. P. Stewart, M. Head-Gordon, C. Gonzalez, and J. A. Pople, Gaussian, Inc., Pittsburgh PA, 1995. (b) *Gaussian 98*, Revision A.3, M. J. Frisch, G. W. Trucks, H. B. Schlegel, G. E. Scuseria, M. A. Robb, J. R. Cheeseman, V. G. Zakrzewski, J. A. Montgomery, Jr., R. E. Stratmann, J. C. Burant, S. Dapprich, J. M. Millam, A. D. Daniels, K. N. Kudin, M. C. Strain, O. Farkas, J. Tomasi, V. Barone, M. Cossi, R. Cammi, B. Mennucci, C. Pomelli, C. Adamo, S. Clifford, J. Ochterski, G. A. Petersson, P. Y. Ayala, Q. Cui, K. Morokuma, D. K. Malick, A. D. Rabuck, K. Raghavachari, J. B. Foresman, J. Cioslowski, J. V. Ortiz, B. B. Stefanov, G. Liu, A. Liashenko, P. Piskorz, I. Komaromi, R. Gomperts, R. L. Martin, D. J. Fox, T. Keith, M. A. Al-Laham, C. Y. Peng, A. Nanayakkara, C. Gonzalez, M. Challacombe, P. M. W. Gill, B. Johnson, W. Chen, M. W. Wong, J. L. Andres, C. Gonzalez, M. Head-Gordon, E. S. Replogle, and J. A. Pople, Gaussian, Inc., Pittsburgh PA, 1998.

57 ACES II, an ab initio program system written by J. F. Stanton, J. Gauss, J. D. Watts, W. J. Lauderdale, and R. J. Bartlett, University of Florida, Gainesville, 1991.

58 MOLPRO is a package of ab initio programs written by H.-J. Werner and P. J. Knowles, Universität Stuttgart and University of Birmingham.

59 CDA 2.1, Dapprich S.; Frenking G. Marburg, 1994. The Program is available via anonymous ftp server: ftp.chemie.uni-marburg.de/pub/cda.

60 At the B3LYP/II level of theory, the $^1A_1$ state of $Fe(CO)_4$ is higher in energy than the $^3B_2$ state by 8.3 kcal mol^{-1}. A detailed discussion of singlet *vs*. triplet $Fe(CO)_4$ is given in: (a) Poliakoff, M.; Turner, J. J. *J. Chem. Soc., Dalton Trans*. **1974** 2276. (b) Barton, J.; Grinter, R.; Thomson, A. J.; Davies, B.; Poliakoff, M. *J. Chem. Soc., Chem. Commun.* **1977**, 841. (c) Poliakoff, M. *Chem. Soc. Rev.* **1978**, 527. (d) Poliakoff, M.; Weitz, E. *Acc. Chem. Res*. **1987**, *20,* 408. (e) Lyne, P.D.; Mingos, D. M. P.; Ziegler, T.; Downs, A. J. *Inorg. Chem.* **1993**, *32*, 4785.

61 BSSE and basis set incompletion error (BSIE) have opposite sign and are computational artefacts due to the use of a truncated and incomplete basis set. Approaches like the counterpoise correction [Boys, S. F.; Bernardi, F. *Mol. Phys.* **1970**, 553.] only account for the BSSE and leave the BSIE uncorrected. A more saturated basis set would in principle correct both BSSE and BSIE but would also make such computations quite uneconomical in terms of computational resource usage. We therefore think that for a comparison with experimental data directly calculated results should be used rather than estimated data. A detailed discussion is given in Refs 33 and 37.

62 The residual term Δ is close to zero for all complexes examined in this study thus showing that the Fe–L bond of these complexes can indeed be described in terms of the conventional DCD model. Large Δ-values on the other hand would imply rather covalent bonds, which should not be discussed in terms of donor-acceptor interactions. For a detailed discussion see: Ref. 38 and Fröhlich, N; Frenking, G. in *Solid State Organometallic Chemistry: Methods and Applications*, Gielen, M.; Willem, R.; Wrackmeyer, B. (Eds), John Wiley and Sons: New York, 1999.

63 Braga, D.; Grepioni, F.; Orpen, A.G. *Organometallics* **1993**, *12*, 1481.

64 Beagley, B.; Schmidling, D.G.; *J. Mol. Struct.* **1974**, *22*, 466.

65 Jones, L. H.; McDowell, R. S.; Goldblatt, M.; Swanson, I. *J. Chem. Phys.* **1972**, *57*, 2050.

66 (a) Braterman, P. S. "*Metal Carbonyl Spectra*", Academic: London,1975. (b) Van Rentergem, M.;.Claeys, E. G.; Van Der Kelen, P. G. *J. Mol. Struct.* **1983**, *99*, 207

67 Bigorgne, M. *J. Organomet. Chem.* **1970**, *24*, 211.

68 Jonas, V.; Thiel, W. *J. Chem. Phys*. **1995**, *102*, 8474.

69 Berces, A.; Ziegler, T. *J. Phys. Chem*. **1995**, *99*, 11417.

70 Ehlers, A. W.; Frenking, G. *Organometallics* **1995,** *14*, 423.

71 Li, J.; Schreckenbach, G.; Ziegler, T. *J. Am. Chem. Soc.* **1995,** *117*, 486.

72 Lüthi, H. P.; Siegbahn, P. E. M.; Almlöf, J. *J. Phys. Chem*. **1985,** *89*, 2156.

73 Barnes, L.A.; Rosi, M.; Bauschlicher, C.W. *J. Chem. Phys.* **1991**, *94*, 2031.

74 Lewis, K. E.; Golden, D. M.; Smith, G. P. *J. Am. Chem. Soc.* **1984**, *106*, 3905.

75 (a) Petz,W. *J.Organomet.Chem.* **1978**, *146,* C23 (b) Petz,W. *J. Organomet. Chem.* **1981**, *205*, 203. (c) Böhm, M. C.; Gleiter, R.; Petz, W. *Inorg. Chim. Acta.* **1982**, *59*, 255. (d) Petz, W. *J. Organomet. Chem*. **1984,** *270,* 81. (e) Petz, W. *J. Organomet. Chem*. **1988**, *346*, 397. (f) Petz, W.; Wrackmeyer, B.;Storch, W. *Chem. Ber.* **1989**, *122,* 2261. (g) Petz, W; Weller, F. *Z. Naturforsch.* **1991**, *46(B),* 971. (h) Petz, W. *Inorg. Chim. Acta.* **1992,** *201*, 203. (i) Petz, W.; Weller, F. *Organometallics* **1993**, *12*, 4056.

76 Touchard, D.; Fillaut, J-L.; Dixneuf, P. H.; Toupet, L. *J. Organomet. Chem.* **1986**, *317*, 291.

77 Only one side-on isomer $Fe(CO)_4(\eta^2\text{-}CS)$, with CS occupying an equatorial coordination site is found. Compared to its corresponding end-on counterpart this complex is less stable by 34 kcal mol^{-1}. The linkage isomer $Fe(CO)_4SC$ is even less favourable and this energy difference is increased to 50 kcal mol^{-1}.

78 Corresponding side-on dinitrogen iron tetracarbonyls $Fe(CO)_4(\eta^2\text{-}N_2)$ are found to be at least 10 kcal mol^{-1} less stable than the presented end-on isomers.

79 Cooper, A. I.; Poliakoff, M. *Chem. Phys. Lett.* **1993**, *212*, 611.

80 (a) Morris, R. H.; Schlaf, M. *Inorg.Chem.* **1994**, *33*, 1725. (b) Bancroft, G. M.; Mays, M.; Prater, B. E.; Stefanini, F.P. *J. Chem. Soc., A.* **1970**, 2146.

81 Hedberg, L.; Hedberg, K.; Satijia, S. K.; Swanson, B. I. *Inorg. Chem.* **1985**, *24*, 2766.

82 The analogous isomers $Fe(CO)_4(\eta^2\text{-}NO^+)$ and $Fe(CO)_4ON^+$ are found to be less stable by 37 and 14 kcal mol^{-1}, respectively.

83 Goldfield, S. A.; Raymond, K. N. *Inorg. Chem*. **1974**, *13*, 770.

84 Lewis, K. E.; Golden, D. M.; Smith, G. .P. *J. Am. Chem. Soc.* **1984**, *106,* 3905.

85 Drouin, B. J.; Kukolich, S. G. *J. Am. Chem. Soc* **1999**, *121*, 4023.

86 Meier-Brocks, F.; Albrecht, R.; Weiss, E. *J. Organomet. Chem.* **1992,** *439,* 65.

87 (a) Selegue, J. P. *J. Am. Chem. Soc.* **1982**, *104*, 119. (b) Berke, H.; Größmann, U.; Huttner, G.; Zsolnai, L. *Chem. Ber.* **1984,** *117*, 3432. (c)) Iyer, R. S.; Selegue, J. P. *J. Am. Chem. Soc.* **1987**, *109*, 910. (d) Gamasa, M. P.; Gimeno, J.; Lastra, E.; Martin, B. M. *Organometallics,* **1992**, *11*, 1373.

88 (a) Huttner, G.; Gratzke, W.; *Chem. Ber.* 1972, 105, 2714. (b) Neumüller, B.; Riffel, H.; Fluck, E. *Z. Anorg. Allg. Chem.* **1990**, *588*, 147. (c) Petz, W.; Weller, F.; Schmock, F. *Z. Anorg. Allg. Chem.* **1998**, *624*, 1123.

89 Fischer, E. O.; Schneider, J.; Neugebauer, D. *Angew. Chem.* **1984**, *96*, 814; *Angew. Chem., Int. Ed. Engl*. **1984**, *23,* 820.

90 Fischer, R. A.; Schulte, M. M.; Weiss, J.; Zsolnai, L.; Jacobi, A.; Huttner, G.; Frenking, G.; Boehme, C.; Vyboishchikov, S. F. *J. Am. Chem. Soc.* **1998**, *120*, 1237.

91 The hybridization of the lone-pair donor orbital at carbon of CF_2, CH_2 and CO based on the NBO analysis are 74.1%, 52.9% and 76.8% , respectively.

92 (a) Dapprich, S; Frenking, G. *Angew. Chem.* **1995**, *107*, 383.; *Angew. Chem,. Int. Ed. Engl.***1995**, *34*, 354. (b) Dapprich, S.; Frenking, G. *Organometallics*, **1996**, *15*, 4547.

93 Cotton, F. A; Troup, J. M. *J. Am. Chem. Soc.* **1974***, 96*, 3438.

94 (a) Shubert, E. H.; Sheline, R. K. *Inorg. Chem.* **1966**, *5*, 1071. (b) Cotton, F. A.; Hanson, B. E. *Isr. J. Chem.* **1977**, *15*, 165.

95 Elzinga, J.; Hogeveen, H. *J. Chem. Soc., Chem. Commun.* **1977**, 705. (b) Alper, H.; Edward, J. *Can. J. Chem.* **1970**, *48*, 1543.

96 Frenking, G.; Dapprich, S.; Meisterknecht, T.; Uddin, J. *Metal-Ligand Interactions in Chemistry, Physics and Biology,* Russo, N.; Salahub, D. R. (Eds)**,** Kluwer Academic Press: Netherlands, p 73 – 89, 2000.

97 The authors of Ref. 50 only consider structures of $Fe(CO)_4PH_3$ and $Fe(CO)_4PF_3$ in which the phosphanes are staggered with respect to the three equatorial COs. According to our CCSD(T)/II calculations, the eclipsed conformer is more stable for both complexes. At the B3LYP/II level, the relative energies of these two conformations are, however, very small and only 0.1 and 1.2 kcal mol^{-1} for $Fe(CO)_4PH_3$ and $Fe(CO)_4PF_3$, respectively.

98 Fischer, E. O.; Maasböl, A. *Angew. Chem.* **1964**, *76,* 645.; *Angew. Chem. Int. Ed. Engl.* **1964**, *3,* 580.

99 Schrock, R. R. *J. Am. Chem. Soc.* **1974**, *96,* 6796.

100 Fischer, E. O.; Kreis, G.; Kreiter, C. G.; Müller, J.; Huttner, G.; Lorenz, H. *Angew. Chem.* **1973**, *85,* 618; *Angew. Chem. Int. Ed. Engl.* **1973**, *12,* 564.

101 McLain, S. J.; Wood, C. D.; Messerle, L. W.; Schrock, R. R.; Hollander, F. J.; Youngs, W. J.; Churchill, M. R. *J. Am. Chem. Soc.* **1978**, *100,* 5962.

102 (a) Dötz, K. H.; Fischer, H.; Hofmann, P.; Kreissl, F. R.; Schubert, U.; Weiss, K. "Transition Metal Carbene Complexes" , Verlag Chemie, Weinheim, 1983. (b) Dötz, K. H. *Pure Appl. Chem.* **1983**, *55*, 1689. (c) Dötz, K. H. *Angew. Chem.* **1984**, *96,* 573; *Angew. Chem. Int. Ed. Engl.* **1984**, *23,* 587. (d) Hegedus, L. S. *Pure Appl. Chem.* **1990**, *62*, 691. (e) Fischer, H.; Hofmann, P.; Kreissl, F. R.; Schrock, R. R.; Schubert, U.; Weiss, K. *Carbyne Complexes*, VCH, New York, 1988. (f) *Transition Metal Carbyne Complexes*, Kreissl, F. R.(Ed.), Kluwer Academic Publishers, Dordrecht, The Netherlands, 1993. (g) Mayr, A.; Hoffmeister, H. *Adv. Organomet. Chem.* **1991**, 32, 227. (h) Kim, H. P.; Angelici, R. J. *Adv. Organomet. Chem.* **1987**, *27*, 51. (i) Nugent, W. A.; Mayer, J. M. "Metal-Ligand Multiple Bonds", Wiley, New York, 1988.

103 (a) Taylor, T. E.; Hall, M. B. *J. Am. Chem. Soc.* **1984**, *106*, 1576. (b) Carter, E. A.; Goddard III, W.A. *J. Am. Chem. Soc.* **1986**, *108*, 4746.

104 Hofmann, P. in ref. 102a, p. 59f.

105 (a)Chisholm, M. H.; Hammond, C. E.; Johnston, V. J.; Streib, W. E.; Huffman, J. C. *J. Am. Chem. Soc.* **1992**, *114*, 7056. (b) Caulton, K. G.; Cayton, R. H.; Chisholm, M. H.; Huffman, J. C.; Lobkovsky, E. B.; Xue, Z. *Organometallics* **1992**, *11*, 321. (c) Miller, R. L.; Wolczanski, P. T.; Rheingold, A. L. *J. Am. Chem. Soc.* **1993**, *115*, 10422. (d) Neithamer, D. R.; LaPointe, R. E.; Wheeler, R. A.; Richeson, D. S.; Van Duyne, G. D.; Wolczanski, P. T. *J. Am. Chem. Soc.* **1989**, *111*, 9056. (e) Mansuy, D.; Lecomte, J.-P.; Chottard, J.-C.; Bartoli, J.-F. *Inorg. Chem.* **1981**, *20*, 3119. (f) Goedkin, V. L.; Deakin, M. R.; Bottomley, L. A. *J. Chem. Soc., Chem. Commun.* **1982**, 607. (g) Latesky, S. L.; Selegue, J. P. *J. Am. Chem. Soc.* **1987**, *109*, 4731. (h) Etienne, M.; White, P. S.; Templeton, J. L. *J. Am. Chem. Soc.* **1991**, *113*, 2324.

106 Peters, J. C.; Godom, A. L.; Cummins, C. C. *J. Chem. Soc., Chem. Commun.* **1997**, 1995.

107 Another bonding model for **1a** would be a shared-electron double bond between the unpaired electrons of triplet $Fe(CO)_4$ and the unpaired electrons of carbon in the triplet ground state. This leads to an iron atom in the formal oxidation state +2 and a carbon ligand with the formal charge –2, which is a rather unrealistic views.

108 Stevens, P. J.; Devlin, F. J.; Chablowski, C. F.; Frisch, M. J. *J. Phys. Chem.* **1994**, *98*, 11623.

109 (a) Pople, J. A.; Krishnan, R.; Schlegel, H. B.; Binkley, J. S. *Int. J. Quantum Chem.* **1978**, *14,* 545. (b) Bartlett, R. J.; Purvis, G. D. *Int. J. Quantum Chem.* **1978**, *14,* 561. (c) Purvis, G. D.; Bartlett, R. J. *J. Chem. Phys.* **1982**, *76,* 1910. (d) Purvis, G. D.; Bartlett, R. J. *J. Chem. Phys.* **1987**, *86,* 7041. (e) Pople, J. A.; Head-Gordon, M.; Raghavachari, K. *J. Chem. Phys.* **1987**, *87,* 5968.

110 Beste, A.; Krämer, O.; Gerhard, A.; Frenking, G. *Eur. J. Inorg. Chem.* **1999**, 2037.

111 Hoffmann, R. *Angew. Chem.* **1982**, *94,* 725; *Angew. Chem. Int. Ed. Engl.* **1982**, *21,* 711.

112 The calculated $^3P \rightarrow {}^1D$ excitation energy at B3LYP/II (44.1 kcal/mol) and CCSD(T)/II (37.1 kcal/mol) is too high because of the poor description of the ^1D state at the one-determinant level.

113 Moore, C. E. "Atomic Energy Levels", *Nat. Stand. Ref. Data Ser., Nat. Bur. Stand. (U.S.)* **1971**, 35/V.

114 Wiberg, K. B. *Tatrahedron* **1968**, *24*, 1083

115 The calculated small positive charge of the carbon atom in **1a** does not contradict the classification of the carbon ligand as a nucleophile. Carbon monoxide also reacts as C-nucleophilic agent, although the carbon atom of CO carries a positive charge. The shape of the charge distribution has a stronger influence on the chemical reactivity than the atomic partial charge.

116 Page 290 in reference 28.

117 Cremer, D.; Kraka, E. *Angew. Chem.* **1984**, *96*, 612; *Angew. Chem., Int. Ed. Engl.* **1984**, *23*, 627.

118 The complex **5** may also be considered as the final and yet unknown member of the series L_nFe-CX where X = O, NR, CR_2, BR_3.

119 (a) Kim, J.; Rees, D. C. *Biochemistry* **1994**, *33*, 389. (b) Siegbahn, P. E. M.; Blomberg, M. R. A. *Chem. Rev*. **2000**, *100*, 421

120 Büchel, K. H.; Moretto, H.-H.; Woditsch, P. "Industrielle Anorganische Chemie", 3rd edition, Wiley-VCH, Weinheim, **1999**.

121 See, for example: (a) "Catalytic Ammonia Synthesis: Fundamentals and Practice", Vol. I, J. R. Jennings (Ed.), Plenum, New York, **1991**. (b) Cotton F. A.; Wilkinson, G.; Murillo, C. A.; Bochmann, M. Advanced Inorganic Chemistry 6th edition, Wiley- Interscience, **1999**, 316 – 318.

122 For recent reviews, see: (a) Howard, J. B.; Rees, D. C. C*hem. Rev*. **1996**, *96*, 2965. (b) Burgess, B. K. D.; Lowe, J. *Chem. Rev.* **1996**, *96*, 2983. (c) Eady, R. R. *Chem. Rev.* **1996**, *96*, 3013. (d) Fryzuk, M. D.; Johnson, S. A. *Coord. Chem. Rev.* **2000**, *200-202*, 379.

123 (a) Kim, J. ; Rees, D. C. *Science* **1992**, *257*, 1677. (b) Kim, J.; Rees, D. C. *Nature* **1992**, *360*, 553.

124 (a) Sellmann, D.; Sutter, J. *Acc. Chem. Res.* **1997**, *30*, 460. (b) Sellmann, D.; Utz, J.; Blum, N.; Heinemann, F. W. *Coord. Chem. Rev.* **1999**, *190-192*, 607. (c) Sellmann, D.; Fürsattel, A.; Sutter, J. *Coord. Chem. Rev.* **2000**, *200-202*, 545.

125 (a) Machado, B. C.; Davidson, E. R. *Theor. Chim. Acta* **1995**, *92*, 315. (b) Dance, I. *J. Chem. Soc., Chem. Commun.* **1996**, 165. (c) Dance, I. *J. Chem. Soc., Chem. Commun.* **1998**, 523.

126 Koch, G. E.; Schneider, K. C.; Burris, R. H. *Biochem. Biophys. Acta* **1960**, *37*, 273.

127 Sellman, D.; Hennige, A. *Angew. Chem.* **1997**, *109*, 270.

128 See, for example: (a) Ehlers, A. W.; Frenking, G. *Organometalics* **1995**, *14*, 423 (b) Torrent, M.; Sola, M.; Frenking, G. *Organomeallics* **1999**, *18*, 2801.

129 Sekusak, S.; Frenking, G. *J. Mol. Struct., Theochem*, submitted for publication.

130 Herzberg, H. "Molecular Spectra and Molecular Structure, Part I - Spectra of Diatomic Molecules", 2nd Ed., Krieger Publishing Co., Malabar, Florida, **1989**.

131 Demaison, J.; Hegelund, F.; Bürger, H. *J. Mol. Struct.* **1997**, *413*, 447.

132 "CRC Handbook of Chemistry and Physics", 76th edition., Lide, D. R. Ed., **1995-1996**.

133 (a) Pople, J. A.; Curtiss, L. A. *J. Chem. Phys.* **1991**, *95*, 4385. (b) Mckee, M. L.;Stanbury, D. M. *J. Am. Chem. Soc*. **1992**, *114*, 3214.

134 Experimental data and qualitative molecular orbital considerations imply that strong π-accepting ligands prefer equatorial coordination sites of trigonal bipyramidal complexes of d^8 metals, whereas σ-donor ligands prefer axial coordination sites. See, for example: (a) Rossi, A. R.; Hoffmann, R. *Inorg. Chem.* **1975**, *14*, 365. (b) Burdett, J. K. *Inorg. Chem.* **1976**, *15*, 212. (c) Favas, M. C.; Kepert, D. L. *Prog. Inorg. Chem.* **1980**, *27*, 325. (d) Bauer, D. P.; Ruff, J. K. *Inorg. Chem.* **1983**, 22, 1686. (e) Beach, D. B.; Smit, S. P.; Jolly, W. L. *Organometallics* **1984**, *3*, 556. (f) Albright, T. A.; Burdett, J. K.; Whangbo, M. H. "*Orbital Interactions in Chemistry*", Wiley: New York, **1985**, pp 324-325.

135 Note the levels of theory used for this comparison. Reaction enthalpies of reduction steps following $(CO)_4Fe{-}N_2{-}Fe(CO)_4$ use the B3LYP/{II+6-311+G(d,p)} //B3LYP/II combination of methods.

136 Sellmann, D.; Friedrich, H.; Knoch, F.; Moll, M. *Z. Naturforsch. B* **1994**, *49*, 76.

137 Cardin, D. J.; Cetinkaya, B.; Lappert, M. F. *Chem. Rev.* **1972**, *72,* 545

138 Cotten, F. A.; Wilkinson, G. "*Advanced Inorganic Chemistry*", 4th ed.; Wiley: New York, **1980**

139 For example: Calderon, N.; Lawrence, J. P.; Ofstead, E. A. *Adv. Organomet. Chem.* **1979**, *17,* 449

140 For example: Vannice, M. A. *Catal. Rev. – Sci. Eng.* **1976**, *14,* 15

141 (a) Ziegler, K.; Holzkamp, E.; Breil, H.; Martin, H. *Angew. Chem.* **1955**, *67,* 541 (b) Natta, G. *Macromol. Chem.* **1955**, *16,* 213

142 (a) Schrock, R. R. *Acc. Chem. Res.* **1979**, *12,* 98 (b) Nugent, W. A.; Mayer, J. M. "*Metal-Ligand Multiple Bonds*", Wiley, New York, 1988

143 (a) Gobbi, A.; Frenking, G. *Bull. Chem. Soc. Jpn*. **1993**, *66,* 3153 (b) Gutsev, G. L.; Ziegler, T. *J. Phys. Chem.* **1991**, *95,* 7220

144 Brothers, P. J.; Roper, W. R. *Chem. Rev.* **1988**, *88,* 1293

145 Petz, W. private communication

146 Berces, A.; Ziegler, T. *Topics in Current Chemistry*; Nalewajski, R. F., Ed.; Springer-Verlag: Berlin, **1996**, Vol 182, p41f

147 (a) Kaupp, M.; Malkin, V. G.; Malkina, O. L. "*Encyclopedia of Computational Chemistry"*, Schleyer, P. v. R.; Allinger, N. L.; Clark, T.; Kollman, P. A.; Schaefer, H. F. III.; Scheiner, P. R.; Eds, Wiley-VCH: Chichester, **1998**, ***3***, 1857 (b) Diedenhofen, M.; Wagener, T.; Frenking, G. *submitted for publ.*

148 (a) Wolinsky, K.; Hilton, J. F.; Pulay, P. *J. Am. Chem. Soc,* **1990**, *112,* 8251 (b) Dodds, J. L.; McWeeny R.; Sadlej, A. J. *Mol. Phys.* **1980**, *41*, 1419 (c) Ditchfield, R. *Mol. Phys.* **1974**, 27, 789 (d) McWeeny, R. *Phys. Rev.* **1962**, *126*, 1028 (e) London, F. *J. Phys. Radium, Paris* **1937**, *8*, 397

149 See for example: (a) Wagener, T.; Frenking, G. *Inorg. Chem.* **1998**, *37,* 1805 (b) Wagener, T. *Dissertation*, **1999**, Marburg.

150 (a) Kutzelnigg W. *Isr. Chem.* **1980**, *19,* 193 (b) Kutzelnigg, W.; Fleischer, U.; Schindler, M. *NMR Basic Principles and Progress*, **1990**, *23*, 165

151 (a) Simion, D. V.; Sorensen, T. V. *J. Am. Chem. Soc.* **1996**, *118*, 7435 (b) Dickson, R. M.; Ziegler, T. *J. Phys. Chem.* **1996**, *100*, 5286

152 Dunning, T. H. Jr.; Hay, P. J. in *Modern Theoretical Chemistry*, Ed. Schaefer, H. F. III, Plenum: New York, **1976**, 1-28.

153 see ref 146b Kutzelnigg, W.; Fleischer, U.; Schindler, M. *NMR Basic Principles and Progress*, **1990**, *23*, 165, H: (5s1p) / [3s1p] {311/1} C: (9s5p1d) / [5s4p1d] {51111/2111/1} O: (9s5p1d) / [5s4p1d]

{51111/2111/1} F : (9s5p1d) / [5s4p1d] {51111/2111/1} Cl: 11s7p2d / [7s6p2d] {5111111/211111/11}

154 Nakatsuji, H.; Ushio, J.; Han, S.; Yonezawa, T. *J. Am. Chem. Soc.* **1983**, *105,* 426

155 (a) Powell, F. X.; Lide, D. L., Jr. *J. Chem. Phys.* **1966**, *45,* 1067 (b) Mathews, C. W. *Can. J. Phys.* **1967**, *45,* 2355 (c) Mathews, C. W. *J. Chem. Phys.* **1967**, *45,* 1068

156 Kirchhoff, W. H.; Lide, D. R., Jr.; Powell, F. X. *J. Mol. Spectrosc.* **1973**, *47,* 491

157 Mann, B. E. *J. Chem. Soc*., *D.* **1971**, 1173

158 Robert. C. *Comprehensive Organometallic Chemistry II, A Review of Literature of 1982-1994*, Abel, E. W.; Stone, F. G. A.; Wilkinson, G. Eds. **1995**, Vol 7, p101 Elsevier Science: Pergamon

159 Löwe, C.; Hund, H.-U.; Berke, H. *J. Organomet. Chem.* **1989**, *372*, 295

160 See for example: (a) Jameson, C. J.; Jameson, A. K.; Burrell, P. M. *J. Chem. Phys.* **1980**, *73*, 6013 (b) Onak, T.; Diaz, M.; Barfield, M. J. *J. Am. Chem. Soc.* **1995**, *117*, 1403 (c) Alkorta, I.; Elguero, J. *New J. Chem.* **1998**, *22*, 381

Chapter 9. Appendix

9.1 The Cartesian Coordinates of Iron Carbonyl Complexes and Related Complexes for Chapter 3

1
$Fe(CO)_5$ (D_{3h})

Fe	0.000000	0.000000	0.000000
C	0.000000	0.000000	1.818518
C	0.000000	1.805349	0.000000
C	0.000000	0.000000	-1.818518
C	1.563478	-0.902674	0.000000
C	-1.563478	-0.902674	0.000000
O	0.000000	0.000000	2.965718
O	0.000000	2.956453	0.000000
O	0.000000	0.000000	-2.965718
O	2.560364	-1.478227	0.000000
O	-2.560364	-1.478227	0.000000

2a
$Fe(CO)_4$ (C_{2v})

Fe	0.000000	0.000000	-0.172403
C	1.619672	0.000000	0.572488
C	-1.619672	0.000000	0.572488
C	0.000000	1.772130	-0.562061
C	0.000000	-1.772130	-0.562061
O	2.567322	0.000000	1.231117
O	-2.567322	0.000000	1.231117
O	0.000000	2.851139	-0.958783
O	0.000000	-2.851139	-0.958783

2b
$Fe(CO)_4$ (C_{2v})

Fe	0.000000	0.000000	0.314107
C	0.000000	-1.393989	-0.890228
C	0.000000	1.393989	-0.890228
C	-1.784347	0.000000	0.855318
C	1.784347	0.000000	0.855318
O	0.000000	-2.261318	-1.645798
O	0.000000	2.261318	-1.645798
O	-2.890807	0.000000	1.161556
O	2.890807	0.000000	1.161556

3a
$Fe(CO)_4CS$ (C_{3v})

Fe	0.000000	0.000000	-0.298252
C	0.000000	0.000000	1.488309
C	1.803458	0.000000	-0.277675
C	0.000000	0.000000	-2.133316
C	-0.901729	-1.561840	-0.277675
C	-0.901729	1.561840	-0.277675
S	0.000000	0.000000	3.039523
O	2.953693	0.000000	-0.239815
O	0.000000	0.000000	-3.280082
O	-1.476847	-2.557974	-0.239815
O	-1.476847	2.557974	-0.239815

3b
$Fe(CO)_4CS$ (C_{2v})

Fe	-0.294529	0.000000	0.000000
C	-0.190389	0.000000	1.813421
C	1.484687	0.000000	0.000000
C	-0.190389	0.000000	-1.813421
C	-1.294955	-1.509406	0.000000
C	-1.294955	1.509406	0.000000
O	-0.100798	0.000000	2.957013
S	3.043996	0.000000	0.000000
O	-0.100798	0.000000	-2.957013
O	-1.907339	-2.482992	0.000000
O	-1.907339	2.482992	0.000000

4a
$Fe(CO)_4N_2$ (C_{3v})

Fe	0.000000	0.000000	0.009202
N	0.000000	0.000000	1.921245
C	0.000000	0.000000	-1.784128
C	0.000000	1.816433	-0.004886
C	1.573077	-0.908217	-0.004886
C	-1.573077	-0.908217	-0.004886
N	0.000000	0.000000	3.032587
O	0.000000	0.000000	-2.933137
O	0.000000	2.967597	-0.027428
O	2.570014	-1.483798	-0.027428
O	-2.570014	-1.483798	-0.027428

4b
$Fe(CO)_4N_2$ (C_{2v})

Fe	0.020944	0.000000	0.000000
C	-0.021230	0.000000	1.827046
N	1.927804	0.000000	0.000000
C	-0.021230	0.000000	-1.827046
C	-0.863499	-1.560960	0.000000
C	-0.863499	1.560960	0.000000
O	-0.058810	0.000000	2.973621
N	3.042299	0.000000	0.000000
O	-0.058810	0.000000	-2.973621
O	-1.486097	-2.531741	0.000000
O	-1.486097	2.531741	0.000000

5a
$Fe(CO)_4NO^+$ (C_{3v})

Fe	0.000000	0.000000	0.079383
N	0.000000	0.000000	1.760763
C	0.000000	0.000000	-1.807483
C	0.000000	1.857249	-0.045893
C	1.608425	-0.928624	-0.045893
C	-1.608425	-0.928624	-0.045893
O	0.000000	0.000000	2.896889
O	0.000000	0.000000	-2.941114
O	0.000000	2.992479	-0.098523
O	2.591563	-1.496239	-0.098523
O	-2.591563	-1.496239	-0.098523

5b
$Fe(CO)_4NO^+$ (C_{2v})

Fe	0.094201	0.000000	0.000000
C	0.031247	0.000000	1.878161
N	1.788706	0.000000	0.000000
C	0.031247	0.000000	-1.878161
C	-1.012796	-1.505865	0.000000
C	-1.012796	1.505865	0.000000
O	-0.010622	0.000000	3.010774
O	2.930479	0.000000	0.000000
O	-0.010622	0.000000	-3.010774
O	-1.654090	-2.442981	0.000000
O	-1.654090	2.442981	0.000000

6a
$Fe(CO)_4\ CN^-$ (C_{3v})

Fe	0.000000	0.000000	0.073242
C	0.000000	0.000000	-1.890394
C	0.000000	0.000000	1.849812
C	0.000000	1.780135	-0.047658
C	-1.541642	-0.890068	-0.047658
C	1.541642	-0.890068	-0.047658
N	0.000000	0.000000	-3.060726
O	0.000000	0.000000	3.012173
O	0.000000	2.938104	-0.144803
O	-2.544473	-1.469052	-0.144803
O	2.544473	-1.469052	-0.144803

6b
$Fe(CO)_4\ CN^-$ (C_{2v})

Fe	-0.061584	0.000000	0.000000
C	0.161170	0.000000	1.776340
C	1.897480	0.000000	0.000000
C	0.161170	0.000000	-1.776340
C	-0.996452	-1.499467	0.000000
C	-0.996452	1.499467	0.000000
O	0.339868	0.000000	2.920882
N	3.069030	0.000000	0.000000
O	0.339868	0.000000	-2.920882
O	-1.667587	-2.453538	0.000000
O	-1.667587	2.453538	0.000000

7a

$Fe(CO)_4\ NC^-\ (C_{3v})$

Fe	0.000000	0.000000	0.054764
N	0.000000	0.000000	-1.932891
C	0.000000	0.000000	1.821231
C	0.000000	1.793827	-0.044950
C	-1.553500	-0.896913	-0.044950
C	1.553500	-0.896913	-0.044950
C	0.000000	0.000000	-3.110019
O	0.000000	0.000000	2.983844
O	0.000000	2.950895	-0.134273
O	-2.555550	-1.475448	-0.134273
O	2.555550	-1.475448	-0.134273

7b

$Fe(CO)_4\ NC^-\ (C_{2v})$

Fe	-0.028400	0.000000	0.000000
C	0.144758	0.000000	1.794146
N	1.974762	0.000000	0.000000
C	0.144758	0.000000	-1.794146
C	-0.966364	-1.492499	0.000000
C	-0.966364	1.492499	0.000000
O	0.292845	0.000000	2.940667
C	3.153322	0.000000	0.000000
O	0.292845	0.000000	-2.940667
O	-1.676946	-2.418622	0.000000
O	-1.676946	2.418622	0.000000

8a

$Fe(CO)_4\ (\eta^2\text{-}C_2H_4)\quad (C_s)$

Fe	0.001469	0.008920	0.000000
C	0.885237	1.976125	0.690661
C	0.885237	1.976125	-0.690661
H	0.094932	2.456099	1.256616
H	1.806097	1.791042	1.233017
H	0.094932	2.456099	-1.256616
H	1.806097	1.791042	-1.233017
C	-1.608488	0.848331	0.000000
C	-0.908510	-1.519718	0.000000
C	0.885237	-0.494108	-1.475592
C	0.885237	-0.494108	1.475592
O	-2.621427	1.401755	0.000000
O	-1.500677	-2.506912	0.000000
O	1.437056	-0.852552	-2.424751
O	1.437056	-0.852552	2.424751

8b

$Fe(CO)_4\ (\eta^2\text{-}C_2H_4)\quad (C_{2v})$

Fe	0.000000	0.000000	0.014304
C	1.813122	0.000000	0.092883
C	0.000000	-0.703298	2.040403
C	0.000000	0.703298	2.040403
H	0.911512	-1.254090	2.252334
H	-0.911512	-1.254090	2.252334
H	0.911512	1.254090	2.252334
H	-0.911512	1.254090	2.252334
C	-1.813122	0.000000	0.092883
C	0.000000	1.492858	-0.975369
C	0.000000	-1.492858	-0.975369
O	2.959304	0.000000	0.169108
O	-2.959304	0.000000	0.169108
O	0.000000	2.445860	-1.623874
O	0.000000	-2.445860	-1.623874

9a

$Fe(CO)_4\ (\eta^2\text{-}C_2H_2)\quad (C_s)$

Fe	0.011682	0.035692	0.000000
C	0.912921	1.963359	0.617719
C	0.912921	1.963359	-0.617719
H	1.056374	2.281286	1.630213
H	1.056374	2.281286	-1.630213
C	-1.578944	0.938803	0.000000
C	-0.943281	-1.466355	0.000000
C	0.912921	-0.479962	-1.462293
C	0.912921	-0.479962	1.462293
O	-2.561433	1.541517	0.000000
O	-1.568219	-2.433061	0.000000
O	1.490249	-0.812105	-2.404966
O	1.490249	-0.812105	2.404966

9b

$Fe(CO)_4\ (\eta^2\text{-}C_2H_2)\quad (C_{2v})$

Fe	0.046414	0.000000	0.000000
C	0.183701	0.000000	1.822151
C	2.046519	0.629447	0.000000
C	2.046519	-0.629447	0.000000
H	2.544792	1.583398	0.000000
H	2.544792	-1.583398	0.000000
C	0.183701	0.000000	-1.822151
C	-0.984086	-1.468563	0.000000
C	-0.984086	1.468563	0.000000
O	0.317834	0.000000	2.961356
O	0.317834	0.000000	-2.961356
O	-1.645957	-2.411172	0.000000
O	-1.645957	2.411172	0.000000

10a
$Fe(CO)_4\ CCH_2$ (C_s)

Fe	0.013422	0.000000	-0.056301
C	0.088584	0.000000	1.731070
C	0.170327	0.000000	3.033830
H	0.205774	0.932151	3.596591
H	0.205774	-0.932151	3.596591
C	1.840577	0.000000	0.060698
C	0.183577	0.000000	-1.879868
C	-1.062660	-1.427778	-0.046167
C	-1.062660	1.427778	-0.046167
O	2.986130	0.000000	0.164897
O	0.317870	0.000000	-3.020003
O	-1.758687	-2.343739	-0.000555
O	-1.758687	2.343739	-0.000555

10b
$Fe(CO)_4\ CCH_2$ (C_{2v})

Fe	-0.055889	0.000000	0.000000
C	0.175807	0.000000	1.800157
C	1.723859	0.000000	0.000000
C	3.034059	0.000000	0.000000
H	3.602763	0.930149	0.000000
H	3.602763	-0.930149	0.000000
C	0.175807	0.000000	-1.800157
C	-1.143734	-1.442773	0.000000
C	-1.143734	1.442773	0.000000
O	0.371781	0.000000	2.930538
O	0.371781	0.000000	-2.930538
O	-1.789580	-2.393935	0.000000
O	-1.789580	2.393935	0.000000

11a
$Fe(CO)_4\ CH_2$ (C_s)

Fe	0.046997	0.000000	0.167588
C	0.139703	0.000000	1.985913
H	1.063187	0.000000	2.571409
H	-0.736277	0.000000	2.644249
C	1.893329	0.000000	0.215689
C	0.176256	0.000000	-1.666718
C	-1.067500	-1.384160	0.223585
C	-1.067500	1.384160	0.223585
O	3.041486	0.000000	0.270411
O	0.289632	0.000000	-2.809352
O	-1.790220	-2.277539	0.302891
O	-1.790220	2.277539	0.302891

11b
$Fe(CO)_4\ CH_2$ (C_{2v})

Fe	0.187996	0.000000	0.000000
C	-0.939849	0.000000	1.410666
C	2.014058	0.000000	0.000000
H	2.652738	0.889139	0.000000
H	2.652738	-0.889139	0.000000
C	-0.939849	0.000000	-1.410666
C	0.410344	-1.796815	0.000000
C	0.410344	1.796815	0.000000
O	-1.594432	0.000000	2.355853
O	-1.594432	0.000000	-2.355853
O	0.598864	-2.928876	0.000000
O	0.598864	2.928876	0.000000

12a
$Fe(CO)_4\ CF_2$ (C_s)

Fe	0.017361	0.000000	-0.224375
C	0.069552	0.000000	1.613064
F	1.125707	0.000000	2.394261
F	-0.971336	0.000000	2.415191
C	1.839640	0.000000	-0.230535
C	0.110417	0.000000	-2.048134
C	-1.021306	-1.461682	-0.219951
C	-1.021306	1.461682	-0.219951
O	2.990049	0.000000	-0.256035
O	0.183220	0.000000	-3.193611
O	-1.693054	-2.396880	-0.201318
O	-1.693054	2.396880	-0.201318

12b
$Fe(CO)_4\ CF_2$ (C_{2v})

Fe	0.000000	0.000000	0.203641
C	1.480447	0.000000	1.241789
C	0.000000	0.000000	-1.618148
F	0.000000	1.052101	-2.429513
F	0.000000	-1.052101	-2.429513
C	-1.480447	0.000000	1.241789
C	0.000000	-1.817661	0.135037
C	0.000000	1.817661	0.135037
O	2.440957	0.000000	1.874557
O	-2.440957	0.000000	1.874557
O	0.000000	-2.963218	0.101913
O	0.000000	2.963218	0.101913

13a
$Fe(CO)_4$ (η^2-H_2) (C_s)

Fe	0.000000	0.361682	0.000000
H	0.466897	2.000714	0.000000
H	-0.354311	2.015208	0.000000
C	1.795497	0.199993	0.000000
C	-0.270792	-1.398543	0.000000
C	-0.765683	0.453996	1.638599
C	-0.765683	0.453996	-1.638599
O	2.939435	0.067293	0.000000
O	-0.442783	-2.535420	0.000000
O	-1.252865	0.504294	2.681228
O	-1.252865	0.504294	-2.681228

13b
$Fe(CO)_4$ (η^2-H_2) (C_{2v})

Fe	0.000000	0.000000	0.359905
C	1.817580	0.000000	0.433858
H	0.000000	-0.433616	1.965036
H	0.000000	0.433616	1.965036
C	-1.817580	0.000000	0.433858
C	0.000000	1.524318	-0.577105
C	0.000000	-1.524318	-0.577105
O	2.963159	0.000000	0.494505
O	-2.963159	0.000000	0.494505
O	0.000000	2.482295	-1.217546
O	0.000000	-2.482295	-1.217546

14a
$Fe(CO)_4\ NH_3$ (C_s)

Fe	0.000000	0.104137	0.000000
N	-0.001353	2.201695	0.000000
H	-0.950252	2.572201	0.000000
H	0.472378	2.574049	0.821279
H	0.472378	2.574049	-0.821279
C	1.803346	0.140378	0.000000
C	-0.901333	0.139151	1.562054
C	-0.901333	0.139151	-1.562054
C	0.000112	-1.676271	0.000000
O	0.000119	-2.828915	0.000000
O	2.959873	0.182295	0.000000
O	-1.479358	0.179923	2.563825
O	-1.479358	0.179923	-2.563825

14b
$Fe(CO)_4\ NH_3$ (C_s)

Fe	.000000	.125862	.000000
N	-.039529	2.261365	.000000
C	1.808488	.178200	.000000
C	-1.810141	.133156	.000000
C	.011406	-.765467	1.535684
C	.011406	-.765467	-1.535684
O	2.960038	.244025	.000000
O	-2.963159	.158818	.000000
O	.020596	-1.432433	2.483689
O	.020596	-1.432433	-2.483689
H	.890910	2.674585	.000000
H	-.522860	2.618555	-.821899
H	-.522860	2.618555	.821899

15a
$Fe(CO)_4\ NF_3$ (C_s)

Fe	.000000	.000000	.424130
N	.000000	.000000	-1.621970
F	.000000	1.235277	-2.235839
F	1.069781	-.617639	-2.235839
F	-1.069781	-.617639	-2.235839
C	.000000	1.814340	.454874
C	-1.571264	-.907170	.454874
C	1.571264	-.907170	.454874
C	.000000	.000000	2.209730
O	.000000	.000000	3.359630
O	.000000	2.965046	.515456
O	-2.567805	-1.482523	.515456
O	2.567805	-1.482523	.515456

15b
$Fe(CO)_4\ NF_3$ (C_s)

Fe	.000000	.421165	.000000
N	-.042412	-1.600607	.000000
C	-1.818716	.541381	.000000
C	1.822808	.407164	.000000
C	.029256	1.287632	1.563395
C	.029256	1.287632	-1.563395
O	-2.961870	.644643	.000000
O	2.970717	.421443	.000000
O	.048099	1.917205	2.530987
O	.048099	1.917205	-2.530987
F	-1.277986	-2.219181	.000000
F	.587932	-2.228902	-1.072666
F	.587932	-2.228902	1.072666

16a
$Fe(CO)_4\ PH_3\ (C_{3v})$

Fe	.000000	.000000	.102625
P	.000000	.000000	-2.169703
H	.000000	1.232119	-2.861448
H	1.067047	-.616060	-2.861448
H	-1.067047	-.616060	-2.861448
C	.000000	1.794705	.077439
C	-1.554260	-.897353	.077439
C	1.554260	-.897353	.077439
C	.000000	.000000	1.886682
O	.000000	.000000	3.037700
O	.000000	2.950329	.060253
O	-2.555059	-1.475164	.060253
O	2.555059	-1.475164	.060253

16b
$Fe(CO)_4\ PH_3\ (C_s)$

Fe	.000000	.095655	.000000
P	-.013355	-2.147421	.000000
C	-1.805186	.093875	.000000
C	1.804808	.053726	.000000
C	.008023	.959927	1.562321
C	.008023	.959927	-1.562321
O	-2.956791	.081854	.000000
O	2.956234	.019397	.000000
O	.011363	1.568254	2.544430
O	.011363	1.568254	-2.544430
H	-1.248708	-2.835096	.000000
H	.588842	-2.873714	-1.056978
H	.588842	-2.873714	1.056978

17a
$Fe(CO)_4\ PF_3\ (C_{3v})$

Fe	.000000	.000000	.612882
P	.000000	.000000	-1.542774
F	.000000	1.383094	-2.311056
F	1.197794	-.691547	-2.311056
F	-1.197794	-.691547	-2.311056
C	.000000	1.798735	.617109
C	-1.557750	-.899367	.617109
C	1.557750	-.899367	.617109
C	.000000	.000000	2.409687
O	.000000	.000000	3.557806
O	.000000	2.949945	.649026
O	-2.554727	-1.474972	.649026
O	2.554727	-1.474972	.649026

17b
$Fe(CO)_4\ PF_3\ (C_s)$

Fe	.000000	.611417	.000000
P	-.008010	-1.512967	.000000
C	-1.808250	.614509	.000000
C	1.807814	.602711	.000000
C	.006161	1.503659	1.560811
C	.006161	1.503659	-1.560811
O	-2.955635	.632695	.000000
O	2.956048	.615687	.000000
O	.009498	2.093400	2.549256
O	.009498	2.093400	-2.549256
F	-1.395834	-2.284233	.000000
F	.692004	-2.304052	-1.188888
F	.692004	-2.304052	1.188888

9.2 The Cartesian Coordinates of Iron Carbonyl Complexes and Related Complexes for Chapter 4

($Fe(CO)_4CH_2$ **2**, $Fe(CO)_5$ **4**, and $Fe(CO)_4$ **6** correspond to **11**, **1**, and **2** in Chapter 3, respectively)

1a
$Fe(CO)_4C$ (C_{3v})

Fe	0.000000	0.000000	0.324074
C	0.000000	0.000000	1.938195
C	0.000000	1.818741	0.299402
C	0.000000	0.000000	-1.727862
C	1.575076	-0.909371	0.299402
C	-1.575076	-0.909371	0.299402
O	0.000000	2.966613	0.327810
O	0.000000	0.000000	-2.868075
O	2.569162	-1.483307	0.327810
O	-2.569162	-1.483307	0.327810

1b
$Fe(CO)_4C$ (C_{2v})

Fe	0.000000	0.000000	0.248745
C	0.000000	1.821798	0.437452
C	0.000000	0.000000	1.911982
C	0.000000	-1.821798	0.437452
C	-1.488341	0.000000	-0.843397
C	1.488341	0.000000	-0.843397
O	0.000000	2.963978	0.532964
O	0.000000	-2.963978	0.532964
O	-2.518800	0.000000	-1.349709
O	2.518800	0.000000	-1.349709

3
$I(CO)_3FeCH$ (C_{3v})

Fe	0.000000	0.000000	0.474099
Cl	0.000000	0.000000	-1.941497
C	0.000000	1.807361	0.206676
C	0.000000	0.000000	2.076604
C	-1.565220	-0.903680	0.206676
C	1.565220	-0.903680	0.206676
O	0.000000	2.941296	0.055425
H	0.000000	0.000000	3.168876
O	-2.547237	-1.470648	0.055425
O	2.547237	-1.470648	0.055425

5
$(CO)_4FeCBCl_3$ (C_{3v})

Fe	0.000000	0.000000	1.236579
C	0.000000	0.000000	-0.416762
C	0.000000	1.820920	1.255343
C	0.000000	0.000000	3.157482
C	-1.576963	-0.910460	1.255343
C	1.576963	-0.910460	1.255343
O	0.000000	2.964451	1.251958
O	0.000000	0.000000	4.297293
O	-2.567290	-1.482226	1.251958
O	2.567290	-1.482226	1.251958
B	0.000000	0.000000	-2.003905
Cl	0.000000	1.793135	-2.462693
Cl	1.552901	-0.896568	-2.462693
Cl	-1.552901	-0.896568	-2.462693

7Q

$I(CO)_3Fe$ (C_{3v})

Fe	.000000	.000000	-.905991
I	.000000	.000000	1.665509
C	.000000	1.877123	-1.430775
C	1.625637	-.938562	-1.430775
C	-1.625637	-.938562	-1.430775
O	.000000	3.002350	-1.623427
O	2.600112	-1.501175	-1.623427
O	-2.600112	-1.501175	-1.623427

7D

$I(CO)_3Fe$ (C_1)

Fe	0.180603	0.023679	0.498466
I	2.378047	0.339421	1.633794
C	0.551582	-1.437269	-0.553804
C	-1.604904	-0.228681	0.489958
C	0.123025	1.528017	-0.555702
O	0.843544	-2.303756	-1.244260
O	-2.743248	-0.374724	0.534169
O	0.155430	2.437579	-1.251749

9.3 The Cartesian Coordinates of Iron Carbonyl Complexes and Related Complexes for Chapter 5

($Fe(CO)_4N_2$ **5** and $Fe(CO)_4NH_3$ **8** correspond to **4** and **14** in Chapter 3, respectively)

1
N_2 ($C_{\infty v}$)

N	0.000000	0.000000	0.552649
N	0.000000	0.000000	-0.552649

2a
N_2H_2 (trans, C_{2h})

N	0.000000	0.622779	0.000000
N	0.000000	-0.622779	0.000000
H	0.998348	0.913291	0.000000
H	-0.998348	-0.913291	0.000000

2b
N_2H_2 (cis, C_{2v})

N	0.000000	0.620229	-0.120241
N	0.000000	-0.620229	-0.120241
H	0.000000	1.030674	0.841686
H	0.000000	-1.030674	0.841686

3a
N_2H_4 (C_2)

N	0.000000	0.717476	-0.078302
N	0.000000	-0.717476	-0.078302
H	0.932869	1.054863	-0.309549
H	-0.218374	1.054863	0.857664
H	-0.932869	-1.054863	-0.309549
H	0.218374	-1.054863	0.857664

3b
N_2H_4 (trans, C_{2h})

N	0.000000	0.744075	0.000000
N	0.000000	-0.744075	0.000000
H	-0.597686	0.977368	0.796945
H	-0.597686	0.977368	-0.796945
H	0.597686	-0.977368	0.796945
H	0.597686	-0.977368	-0.796945

3c
N_2H_4 (cis, C_{2v})

N	0.000000	0.740556	-0.121138
N	0.000000	-0.740556	-0.121138
H	0.805292	1.053467	0.423982
H	-0.805292	1.053467	0.423982
H	-0.805292	-1.053467	0.423982
H	0.805292	-1.053467	0.423982

4
NH_3 (C_{3v})

N	0.000000	0.000000	0.118684
H	0.000000	0.939287	-0.276928
H	0.813446	-0.469643	-0.276928
H	-0.813446	-0.469643	-0.276928

6a
$(CO)_4FeN_2H_2$ (C_s)

Fe	0.000000	0.084446	0.000000
N	-1.657400	-0.960051	0.000000
N	-1.906069	-2.183995	0.000000
C	-0.998737	1.601535	0.000000
C	1.483816	1.103953	0.000000
C	0.508070	-0.704144	1.541326
C	0.508070	-0.704144	-1.541326
O	-1.637442	2.563054	0.000000
O	2.431990	1.754621	0.000000
O	0.820135	-1.212115	2.529509
O	0.820135	-1.212115	-2.529509
H	-2.543039	-0.438868	0.000000
H	-0.998526	-2.679161	0.000000

6b
$(CO)_4FeN_2H_2$ (C_s)

Fe	0.000000	0.066223	0.000000
C	0.629030	-1.633294	0.000000
N	-1.838817	-0.614422	0.000000
N	-2.434573	-1.725289	0.000000
C	-0.665521	1.760909	0.000000
C	0.902066	0.413588	1.507558
C	0.902066	0.413588	-1.507558
O	1.002428	-2.721549	0.000000
O	-1.091310	2.828817	0.000000
O	1.518785	0.651553	2.453819
O	1.518785	0.651553	-2.453819
H	-2.562827	0.112712	0.000000
H	-1.718805	-2.468268	0.000000

7a
$(CO)_4FeN_2H_4$ (C_s)

Fe	0.000000	0.183531	0.000000
N	-1.327854	-1.414380	0.000000
N	-0.859354	-2.805475	0.000000
C	-1.410523	1.304016	0.000000
C	1.142508	1.557553	0.000000
C	0.655201	-0.405818	1.571107
C	0.655201	-0.405818	-1.571107
O	-2.322499	2.015733	0.000000
O	1.882318	2.440577	0.000000
O	1.058669	-0.807679	2.579538
O	1.058669	-0.807679	-2.579538
H	-1.949716	-1.349389	-0.806099
H	-1.949716	-1.349389	0.806099
H	-0.230847	-2.862970	0.803534
H	-0.230847	-2.862970	-0.803534

7b
$(CO)_4FeN_2H_4$ (C_1)

Fe	0.135280	0.066088	-0.029288
C	-1.277528	1.211406	0.035830
N	-1.048479	-1.221665	-1.230872
N	-2.301782	-1.609045	-0.623832
C	1.505261	-1.105021	-0.153331
C	1.142787	1.342578	-0.743086
C	0.112033	-0.105740	1.736559
O	-2.162566	1.945450	0.076074
O	2.362334	-1.871293	-0.252301
O	1.826174	2.196681	-1.125703
O	0.165801	-0.143313	2.894048
H	-1.277316	-0.702644	-2.075584
H	-0.497473	-2.031023	-1.521880
H	-2.104591	-1.750499	0.363889
H	-2.615340	-2.498698	-1.014780

9

$[(CO)_4Fe]_2N_2$ (D_3)

N	0.000000	0.000000	0.559378
N	0.000000	0.000000	-0.559378
Fe	0.000000	0.000000	2.464153
Fe	0.000000	0.000000	-2.464153
C	1.025754	-1.500895	-2.480739
C	-1.812690	-0.137881	-2.480739
C	0.786936	1.638777	-2.480739
C	-0.786936	1.638777	2.480739
C	-1.025754	-1.500895	2.480739
C	1.812690	-0.137881	2.480739
C	0.000000	0.000000	4.259293
O	0.000000	0.000000	5.407763
C	0.000000	0.000000	-4.259293
O	0.000000	0.000000	-5.407763
O	1.675036	-2.451029	-2.500504
O	-2.960171	-0.225109	-2.500504
O	1.285135	2.676138	-2.500504
O	-1.285135	2.676138	2.500504
O	-1.675036	-2.451029	2.500504
O	2.960171	-0.225109	2.500504

10

$[(CO)_4Fe]_2N_2H_2$ (C_{2h})

N	-.501199	.385681	.000000
N	.501199	-.385681	.000000
H	-.177177	1.358316	.000000
H	.177177	-1.358316	.000000
Fe	-2.412334	.010048	.000000
Fe	2.412335	-.010048	.000000
C	-2.716578	1.807653	.000000
C	-4.195960	-.239147	.000000
C	-2.260319	-.924409	-1.539004
C	-2.260319	-.924409	1.539004
O	-2.910187	2.944136	.000000
O	-5.334225	-.396079	.000000
O	-2.149774	-1.511982	-2.524913
O	-2.149774	-1.511982	2.524913
C	2.716578	-1.807653	.000000
C	4.195960	.239147	.000000
C	2.260319	.924409	-1.539004
C	2.260319	.924409	1.539004
O	2.910187	-2.944136	.000000
O	5.334225	.396079	.000000
O	2.149774	1.511982	-2.524913
O	2.149774	1.511982	2.524913

11

$[(CO)_4Fe]_2N_2H_4$ (C_{2h})

N	0.000000	0.734156	0.000000
N	0.000000	-0.734156	0.000000
H	-0.565287	0.998029	0.809218
H	-0.565287	0.998029	-0.809218
H	0.565287	-0.998029	0.809218
H	0.565287	-0.998029	-0.809218
Fe	1.827562	1.719489	0.000000
Fe	-1.827562	-1.719489	0.000000
C	0.944019	3.295760	0.000000
C	3.401927	2.566566	0.000000
C	2.224399	0.952600	1.584240
C	2.224399	0.952600	-1.584240
O	0.382131	4.304416	0.000000
O	4.416395	3.109221	0.000000
O	2.464750	0.449110	2.598115
O	2.464750	0.449110	-2.598115
C	-0.944019	-3.295760	0.000000
C	-3.401927	-2.566566	0.000000
C	-2.224399	-0.952600	1.584240
C	-2.224399	-0.952600	-1.584240
O	-0.382131	-4.304416	0.000000
O	-4.416395	-3.109221	0.000000
O	-2.464750	-0.449110	2.598115
O	-2.464750	-0.449110	-2.598115

9.4 The Cartesian Coordinates of Iron Carbonyl Complexes and Related Complexes for Chapter 6

1a
$Fe(CO)_4CF_2$ (C_s)

Fe	.000000	.223201	.000000
C	-.212357	-1.600137	.000000
F	-1.343579	-2.292637	.000000
F	.766001	-2.496148	.000000
C	-1.797356	.402905	.000000
C	.067488	2.027305	.000000
C	1.031839	.128386	1.452176
C	1.031839	.128386	-1.452176
O	-2.953098	.549878	.000000
O	.096632	3.190005	.000000
O	1.707576	.053480	2.399222
O	1.707576	.053480	-2.399222

1b
$Fe(CO)_4CF_2$ (C_{2v})

Fe	.000000	.000000	.199879
C	-1.470655	.000000	1.228680
C	.000000	.000000	-1.627336
F	.000000	-1.061489	-2.443201
F	.000000	1.061489	-2.443201
C	1.470655	.000000	1.228680
C	.000000	1.797009	.144386
C	.000000	-1.797009	.144386
O	-2.440809	.000000	1.873203
O	2.440809	.000000	1.873203
O	.000000	2.958450	.131046
O	.000000	-2.958450	.131046

2
$Fe(CO)_5$ (D_{3h})

Fe	.000000	.000000	.000000
C	.000000	.000000	1.800359
C	.000000	1.794586	.000000
C	.000000	.000000	-1.800359
C	1.554157	-.897293	.000000
C	-1.554157	-.897293	.000000
O	.000000	.000000	2.962629
O	.000000	2.959581	.000000
O	.000000	.000000	-2.962629
O	2.563072	-1.479790	.000000
O	-2.563072	-1.479790	.000000

3a
$Fe(CO)_4$ (C_{2v})

Fe	.000000	.000000	.209562
C	.000000	-1.600765	-.536185
C	.000000	1.600765	-.536185
C	-1.768743	.000000	.530216
C	1.768743	.000000	.530216
O	.000000	-2.561813	-1.203007
O	.000000	2.561813	-1.203007
O	-2.883683	.000000	.866944
O	2.883683	.000000	.866944

3b
$Fe(CO)_4$ (C_{2v})

Fe	.000000	.000000	.340147
C	.000000	-1.355626	-.844517
C	.000000	1.355626	-.844517
C	-1.770248	.000000	.824404
C	1.770248	.000000	.824404
O	.000000	-2.224737	-1.621007
O	.000000	2.224737	-1.621007
O	-2.904802	.000000	1.083352
O	2.904802	.000000	1.083352

9.5 Abbreviations

AIM	atoms in molecules
CC	coupled cluster
CCSD(T)	coupled cluster singles, doubles and estimated triples
CDA	charge decomposition analysis
CI	configuration interaction
CISD	CI with all single and double substitutions from the Hartree-Fock reference determinant
DFT	density functional theory
ECP	effective core potential
HF	Hartree-Fock
GIAO	gauge-independent atomic orbital
KS	Kohn-Sham
KSO	Kohn-Sham orbital
LCAO-MO	linear combination of atomic orbitals-molecular orbitals
LDA	local density approximation
MO	molecular orbital
MP2	Møller-Plesset perturbation theory including second order correction
NAO	natural atomic orbital
NBO	natural bond orbital
NO	natural orbital
RHF	restricted Hartree-Fork
SCF	self consistent field
UHF	unrestricted Hartree-Fork